MEASUREMENT OF THE MAGNETIC MOMENT OF THE Λ^0 HYPERON

A thesis presented

by

Gülsen Önengüt

to

The Faculty of Arts and Sciences
in partial fulfillment of the requirements
for the degree of

DOCTOR OF PHILOSOPHY

in the subject of

PHYSICS

Middle East Technical University
Ankara, Turkey

July, 1972

I certify that this thesis is satisfactory for the award of the degree of Doctor of Science

P. Tolun
(Supervisor)

(Member of Examining Committee)

(Member of Examining Committee)

(Member of Examining Committee)

Certified that this thesis conforms to the formal standards of the Faculty.

(Office of the Dean)

Abstract

This thesis is about an experiment performed in order to measure the magnetic moment of Λ^0 hyperon. The polarization vector of the Λ^0 hyperons produced in the reaction $\bar{\pi}^- p \rightarrow \Lambda^0 \pi^0$ was made to precess around a transverse magnetic field of 200 kG. Their decays were detected in nuclear emulsion, and from the angular distribution of the decay products in the Λ^0 rest frame, the direction of polarization at the time of decay was determined. The magnetic moment is proportional to the angle of precession of the polarization vector.

The exposure was made at CERN, and the scanning and measurements were done in five laboratories(CERN, Athens, Louvain, Wisconsin and Rome). The result of the collaborative effort is $\mu_\Lambda = -0.66 \pm 0.07\ \mu_N$ [33]. The purpose of this thesis is to give the details of the experiment and also to check the various analysis programs of the collaboration by simpler and independent programs. The result obtained is $\mu_\Lambda = -0.59 \pm 0.13\ \mu_N$ using only the events measured in our laboratory, and $\mu_\Lambda = -0.61 \pm 0.07\ \mu_N$ using all of the events measured in the collaboration.

ACKNOWLEDGMENT

I would like to express my thanks to Dr. Perkins Tolbo for her valuable guidance throughout the project. I feel deeply grateful to Prof. Erich Kahl for his continuous encouragement.

I am also thankful to our colleagues in the collaborating laboratories, to NASA because of the research grant which enabled us to take part in the experiment, to U.S.E.R.D.A. who supported the experiment by a research grant and to by a scholarship, to the persons who did the most tedious part of the job and to Mrs. S. Sagar for typing the thesis.

TABLE OF CONTENTS

		Page
ABSTRACT		iv
ACKNOWLEDGMENT		v
TABLE OF CONTENTS		vi
LIST OF APPENDICES		viii
LIST OF TABLES		x
LIST OF FIGURES		xi
LIST OF COMMON PROGRAMS		xiii
CHAPTER I.	Introduction	1
	I.1. Naming of the magnetic moment	1
	I.2. Magnetic moment of the hyperons	3
CHAPTER II.	EXPERIMENTAL METHOD	7
	II.1. Principle of the experiment	7
	II.2. The source of the polarized hyperons	8
	II.3. Precession of the polarization vector.	10
	II.4. Observation of the final polarization direction	13
CHAPTER III.	APPARATUS	16
	III.1. Beam	16
	III.2. Target	17
	III.3. Pulsed Magnet	18
	III.4. Detector	21

Page

CHAPTER IV. EXPOSURE, SCANNING AND MEASUREMENTS . . . 22

IV.1. Exposure 22

IV.2. Scanning 24

IV.3. Measurements 29

CHAPTER V. ANALYSIS 34

V.1. Grain density calibration 34

V.2. Selection of events 36

V.3. Evaluation of the Λ° magnetic moment 40

V.4. Results $\mu_{\Lambda^{\circ}}$, αP and their statistical errors 42

V.5. Systematic errors 44

CHAPTER VI. DISCUSSION AND CONCLUSIONS 49

BIBLIOGRAPHY 105

LIST OF APPENDICES

		Page
A.	Production and decay of the Λ^0 hyperon:	58
	1) Calculation of the initial polarization and angular distribution of the decay products.	58
	2) Kinematics	59
B.	The covariant form of the precession equation	63
C.	The solution of the precession equation	72
D.	The derivation of the exact angular distribution in terms of the angles φ and Ψ	75
E.	Derivation of the statistical error on the angle φ_0 using the asymmetries in the decay	78
F.	Choosing the cut- off for the angle ψ_0	82
G.	Obtaining an analytical curve for the ρ^{2} - β calibration.	83
	1) Fitting of the curve $\rho^2 = a + \frac{b}{\beta c}$ to the experimental points	85
	2) Fitting of the curve $\log \rho^2 = a + b \log \beta + c (\log \beta)^2$ to the experimental points	90
H.	Least squares fitting to the Λ^0 decay kinematics	93

		Page
I.	Estimation of the production point of Λ^0 in the target	99
J.	Effects caused by the curvature of the incident beam on it within the target	104
K.	Calculation of the angle φ	108
L.	Maximum likelihood method	111

LIST OF TABLES

		Page
Table 1	Some theoretical values of the magnetic moments of the Λ^0 hyperon	117
Table 2	The laboratory velocity, momentum, energy and angle of the Λ^0 produced in the reaction $\pi^- + p \longrightarrow \Lambda^0 + \Sigma^0$ as a function of the c.m.s. angle	118
Table 3	The laboratory momenta and angles of the proton and pion from the decay $\Lambda^0 \longrightarrow p + \pi^-$ as a function of the c.m.s. angle	120
Table 4	The results of some of the reconnaissance .	121
Table 5	The $\rho^{-1} - \beta$ calibration data	122
Table 6	Parameters of the fitted $\rho^{-1} - \beta$ curves of the scanners	123
Table 7	The variations in the grain counts of scanner	124
Table 8	The number of events left (in brackets) after each cut-off	125

LIST OF FIGURES

		Page
Fig.1	Diagram showing the definition of angles and vectors in the rest system of the Λ^0	128
Fig.2	Layout of the experiment	130
Fig.3	Diagram of the target	130
Fig.4	Schematic representation of a pulsed-transformer magnet, showing the concentration of magnetic flux in the central bore of the secondary	132
Fig.5	Vertical section through the magnet assembly, showing the steel yoke surrounding the cylindrical copper blocks, the target T, and the dump channels into which the beam was deflected by the magnetic field	132
Fig.6	Horizontal section (A-A in Fig.5) through the magnet and the magnetic field lines. T is the target, D and D' are the detectors. The primary coil with its cooling water tubes was embedded in the copper blocks which constitute the single-turn secondary	133
Fig.7	Diagram showing the dimensions of an emulsion plate	136
Fig.8	Diagram of the reticule placed in the eyepiece	139
Fig.9	Decay chart of Λ^0	139
Fig.10	Range-energy Relationship for π^-	146
Fig.11	Ionization curve	147
Fig.12	Calibration curves of the scanners	150
	12.a) Scanner 5	150
	12.b) Scanner 6	150

		Page
Fig.13	Comparison of the calibration curves of the two runs with the average curve	140
Fig.14	The distribution of the x-coordinate of the production point	141
Fig.15	The distribution of the y-coordinate of the production point	142
Fig.16	The distribution of the z-coordinate of the production point	143
Fig.17	The theoretical and experimental χ^2 distributions	144
Fig.18	The missing-mass distributions for the selected and non-selected events	145
Fig.19	The distribution of the fitted proton momentum	146
Fig.20	The distribution of the fitted pion momentum	147
Fig.21	The distribution of the fitted opening angle in the Λ^0 decay	148
Fig.22	The distribution of the plane angle of Λ^0	149
Fig.23	The distribution of the dip angle of Λ^0	150
Fig.24	The distribution of the Λ^0 momentum .	151
Fig. 25	The distribution of the angle φ . . .	152
Fig.26	The contour diagram of the likelihood function	153
	a) For future events	153
	b) For all events	153
Fig.27	The theoretical distribution of the angle φ	154
Fig.28	Plot of μ_{Λ^0} against μ_{Σ^+}	155
Fig.29	Curvature of initial π^- beam as it strikes the target	156

LIST OF COMMON PROGRAMS

		Page
P301.1	Plane angle distribution	186
P302.2	Dip angle distribution	190
P303.3	Grain density distribution	160
P304.4	Grain density calibration (1)	160
P305.5	Grain density calibration (2)	164
P306.6	χ^2-fit of the measurements and calculation of the production point, initial polarization	169
P308.7	Obtaining and P by the Modified Likelihood Method	190
P309.8	Simulation of Θ production	172
P310.9	Simulation of Θ decay	178

CHAPTER I

INTRODUCTION

1.1. Meaning of the Magnetic Moment[1,2]

Elementary particles are characterized by a set of quantum numbers like mass, electric charge, spin, intrinsic parity. In addition to these there is other information, such as the nature and frequency of its interaction, which is helpful in understanding the structure of the particle. The magnetic moment is also one of such useful characteristics of the particle.

In electromagnetism one can express the external effects of any distribution of charge and currents in terms of a series of "multipole moments". In many cases a few lower order multipoles are sufficient for describing the effects. The energy of interaction, H_{int}, between an applied electromagnetic field and a charge-current system can be written as follows:

$$H_{int} = q\phi_0 - \bar{P}\cdot\bar{E}_0 - \bar{M}\cdot\bar{H}_0 - \frac{1}{6}\sum_{i,j} Q_{ij}\left(\frac{\partial E_j}{\partial x_i}\right)_0 - \cdots \quad (1.1.1)$$

where $\bar{E}$ and $\bar{H}$ are the applied electric and magnetic fields, and ϕ is the electrostatic potential of the applied field. The subscript 0 indicates that the quantity in question is to be evaluated at the origin of coordinates which is taken at some convenient point in the charge-current system. The symbol q denotes the total charge of the system, $\bar{P}$ is the electric dipole vector, $\bar{M}$ is the magnetic dipole vector, and Q_{ij} is the electric quadrupole tensor.

$\bar{M}$, the magnetic dipole vector is the one which interests us. It is given as a function of a current density $\bar{J}$ and the space coordinates $\bar{r}$ by

$$\bar{M} = \frac{1}{2}\int \bar{r}\times\bar{J}\ dV \quad (1.2.2)$$

where dV is the differential volume element and the integral is performed over the volume which includes the current distribution. $\bar{M}$ depends only on the distribution of the current, therefore a knowledge of $\bar{M}$ gives information about the size, shape and motion of the system. This aspect of the question is related to the many experiments such as electron-proton scattering where an attempt is made to express the results in terms of form factors for the electromagnetic structure of the nucleons. These form factors are usually made of two contributing parts, $F_1(q^2)$ and $F_2(q^2)$, where q is the four-momentum transfer. F_1 describes

the distribution of the electric charge and $\bar{r}_p$ the magnetization.

An alternative form of $\bar{\Pi}$ can be obtained if $\bar{J}$ is produced by an electric charge of density ρ, moving with velocity $\bar{v}$. Then $\bar{J} = \rho\bar{v}/c$. If the charge density is actually composed of particles of charge e and mass m, then the angular momentum density is $\bar{L} = (m\rho/e)(\bar{r} \times \bar{v})$, and one can write

$$\bar{\Pi} = \frac{1}{2}\frac{e}{mc}\int \bar{L}\, dV \qquad (1.1.3)$$

In quantum mechanics the energy H_{int}, and the various multipole moments become operators. The magnetic dipole operator will include the contribution $\bar{\Pi}_{orb}$ and $\bar{\Pi}_{spin}$ of both orbital angular momentum corresponding to the expression (1.1.3) and spin magnetic moment.

The total magnetic-moment operator $\bar{\Pi}$ can be written in the general case of a nucleus composed of A nucleons :

$$\bar{\Pi} = \bar{\Pi}_{orb} + \bar{\Pi}_{spin} = \mu_0 \sum_{k=1}^{A} (g_k^{(l)} \bar{l}_k + g_k^{(\sigma)} \bar{\sigma}_k) \qquad (1.1.4)$$

where μ_0 is the quantity $e\hbar/2m_p c$ (m_p = proton mass) called the nuclear magneton; $\bar{l}_k$ and $\bar{\sigma}_k$ are the orbital and the spin angular momentum operators (divided by $\hbar$) respectively of the k th nucleon; $g_k^{(l)}$ is the orbital factor which is equal to one for protons and zero for neutrons; $g_k^{(\sigma)}$ is the spin gyromagnetic ratio.

The magnetic moment μ is defined as the expectation

value of H_z in the state in which $J_z = J$, where H_z obtains its maximum value, i.e.

$$\mu = \mu_0 g_J J = \int \psi^*_{J,J} \, H_z \, \psi_{J,J} \, dV \qquad (I.1.5)$$

This equation also defines g_J, the nuclear g factor. J, the total angular momentum, is the sum of the orbital angular momentum L and of the intrinsic angular momentum or spin σ. The index J in g_J means that it is the total angular momentum J which contributes to the magnetic moment.

If the particles considered are free particles there is no orbital angular momentum contribution. Equation (I.1.5) then becomes

$$\mu = \mu_0 g_\sigma \sigma \qquad (I.1.6)$$

For particles other than nucleons $\mu_0 = eh / 2mc$ where m is the mass of the particle in question. Then μ_0 is called the "intrinsic magneton". For elementary particles usually there is only the spin contribution to the magnetic moment; then subscript σ is dropped from g_σ.

As examples of how magnetic moment measurements give useful information about the fundamental properties of the particles one can mention the cases of proton, neutron and the electron.

If the proton was a uniformly charged classical sphere, its magnetic moment μ_p should 1/2 nuclear magnetons. If the

proton and the neutron were adequately described by the relativistic wave equation of Dirac, μ_p should be 1 n.m. and μ_n, 0. Experimental results are 2.79 n.m. for μ_p and -1.91 n.m. for μ_n. These results show that the nucleons have a complex inner electrical structure.

Dirac's relativistic quantum mechanics predicts a gyromagnetic ratio g equal to 2 for the electron. Precise measurements gave a value slightly higher than this ($g = 2.0023$). Schwinger showed that the interaction energy between electron and an external field must include a radiative correction term representing the interaction of the electron with the quantized electromagnetic field which modifies the value of its magnetic moment. The electron will emit and reabsorb virtual photons as a result of this coupling with the quantized electromagnetic field. The result of the calculations will depend on the number of virtual photons taken into account. Limiting this number to two virtual photons, one finds for the expression of the magnetic moment

$$\mu_e = 1 + 1/2\ \alpha/2\pi - 0.328\ \alpha^2/\pi^2 \qquad (I.1.7)$$

where α is the fine structure constant. $(\mu_e - 1)$ is defined as the anomalous magnetic moment, μ_a. Experiments confirm the theoretical predictions with good accuracy.

I.2. Magnetic Moments of Hyperons

Different theoretical models predict different values for the magnetic moments of the hyperons.[2] A precise knowledge

---

[2] See Table 1

of the magnetic moments would provide a powerful test of the theories. Existing experimental results are very few and have large errors. The only one which has a small enough error to be meaningfully compared with the theory is the magnetic moment of the Λ^0 hyperon. The world average is $\mu_\Lambda = (-0.77 \pm 0.30)$ nuclear magnetons.[3] The experiments from whose results this value was calculated were all based on the same principles, but used different detection techniques. Their results, all quoted in nuclear magnetons are : -1.5 ± 0.5 by Cool et. al. [4] using spark chambers; 0.0 ± 0.6 by Fernan et al.[5] using a diffusion cloud chamber; -1.39 ± 0.72 by Anderson and Crawford[6] using hydrogen bubble chamber -0.50 ± 0.28 by Churiuso et.al.[7] using emulsions and -0.77 ± 0.27 by Hill et. al.[8] using spark chamber.

The purpose of the experiment reported here is to increase the accuracy in the measurement of Λ^0 magnetic moment. This is done mainly by using a stronger magnetic field and increasing statistics by carefully planning the experiment and improving the analysis methods.

CHAPTER II

EXPERIMENTAL METHOD

II.1. Principles of the Experiment

The basic method of the measurement is identical with that used so far in all other experiments to determine the hyperon magnetic moments. This method was proposed by Goldhaber[9] in 1956 and by T.D. Lee and C.N. Yang[30] in 1957. The method consists of producing polarized hyperons whose polarization is made to precess in a magnetic field. The angle of precession which is directly related to the value of the magnetic moment is measured by determining the polarization vector after the action of the field.

At this point it will be appropriate to define the polarization. Consider a beam of particles of spin $\frac{1}{2}$ and a direction defined by a unit vector $\vec{e}$. If the expectation value of the spin component in the direction $\vec{e}$, $\langle \vec{\sigma} \cdot \vec{e} \rangle$, is not zero for all directions, the beam is said to be

polarized, and there is a direction $\vec{e}_o$ for which $\langle \vec{\sigma} \cdot \vec{e} \rangle$ reaches a maximum

$$\langle \vec{\sigma} \cdot \vec{e} \rangle_{max} = \langle \vec{\sigma} \cdot \vec{e}_o \rangle = P \qquad 0 \leq P \leq 1 \qquad \text{(II.1.1)}$$

where P is the degree of polarization and $\vec{P} = P\vec{e}_o$, the polarization vector.

Three conditions have to be fulfilled for the measurement of the magnetic moment:

(i) a beam of polarized particles must be available, and the initial direction of the polarization must be known;

(ii) these particles must be kept for a sufficiently long time in an intense enough magnetic field to obtain an appreciable precession;

(iii) it must be possible to determine the final direction of the polarization.

II.2. The Source of Polarized Hyperons

The hyperons are transversally (normal to the plane of production) polarized in the production reactions of the following type:

$$\pi + \text{nucleon} \longrightarrow \text{hyperon} + \text{kaon}$$

Longitudinal polarization is not allowed because of parity conservation.

In this experiment Λ^o produced in the reaction

$$\pi^- + p \longrightarrow \Lambda^0 + K^0$$

were used. They are polarized in the direction:

$$\frac{\vec{P}_0}{P} = -\frac{\vec{p}_{inc} \times \vec{p}_\Lambda}{|\vec{p}_{inc} \times \vec{p}_\Lambda|} \qquad (II.3.1)$$

where $\vec{P}_0$ is the initial polarization vector, $P = |\vec{P}_0|$, $\vec{p}_{inc}$ and $\vec{p}_\Lambda$ are the momenta of incoming pion and outgoing lambda respectively. The magnitude of the polarization can be calculated using partial wave analysis.*

For this experiment a polyethylene target was exposed to a beam of π^- mesons from the CERN proton synchrotron. π^- beam was preferred to a K^- beam in spite of the larger cross-section of the reaction $K^- + p \longrightarrow \Lambda^0 + K^0$ because K^- beams have much lower intensity and the Λ^0 polarization is smaller. An incident momentum of 1.05 Gev/c was chosen because it was found out experimentally that at this momentum the cross section for the reaction $\pi^- + p \longrightarrow \Lambda^0 + K^0$ goes through a maximum of about 0.8 mb. and the polarization is close to 100 % over a large angular region in the center-of-momentum system of the reaction.(11)(12) At this energy, the maximum angle of production of the Λ^0 in the laboratory is about $32°$.** In order to maximize the Λ^0 to background ratio, it is advantageous to restrict the acceptance of Λ^0 hyperons to a small range of angles just below this kinematical limit. The interval chosen

---

* See Appendix A.1

** See Appendix A.2, Prog. 8, and Table 2.

one 10° to 22°. This corresponds to center of mass angles between 80° and 140°, representing about 30 % of the total cross section. This corresponds to Λ^0 laboratory momenta between 500 Mev/c and 800 Mev/c.*

II.3. Precession of the Polarization Vector

The polarization, being defined in terms of expectation values follows a classical equation of motion. In a uniform magnetic induction field $\vec{B}$, the polarization vector $\vec{P}$ defined in the rest system of Λ^0 particles obeys the equation of motion:

$$\frac{d\vec{P}}{d\tau} = \mu_\Lambda \frac{2}{mc} \vec{P} \times \vec{B}' \qquad \text{(II.3.1)}$$

where $\vec{B}'$ is the magnetic induction field vector in the rest frame of the particle, τ is the proper time of the particle and μ_Λ is the magnetic moment in nuclear magnetons if m is the proton mass, in intrinsic magnetons if the mass of the Λ^0 is used. In order to write this equation in the laboratory frame** one has to consider the two components of $\vec{P}'$ separately, one parallel to $\vec{p}_\Lambda$, the laboratory momentum of the Λ^0 and another third is perpendicular to it :

$$\vec{P}' = \vec{P}'_{//} + \vec{P}'_{\perp} \qquad \text{(II.3.2)}$$

---

* See Appendix A.2, Prog. 8, and Table 2.

** See Appendix B.

where

$$\mathbf{P}'_{\parallel} = \frac{\mathbf{P}' \cdot \mathbf{P}_{\wedge}}{|\mathbf{P}_{\wedge}|^2} \mathbf{P}_{\wedge} \qquad (II.3.4)$$

and

$$\mathbf{P}'_{\perp} = \mathbf{P}' - \frac{\mathbf{P}' \cdot \mathbf{P}_{\wedge}}{|\mathbf{P}_{\wedge}|^2} \mathbf{P}_{\wedge}$$

These two components transform under Lorentz transformations in different ways:

$$\mathbf{B}'_{\perp} = \gamma \mathbf{B}_{\perp}$$

$$\mathbf{B}'_{\parallel} = \mathbf{B}_{\parallel}$$

Using the Eq. (II.3.4) and $dt = \gamma\, dt'$ one can write the Eq. (II.3.1) in the laboratory frame:

$$\gamma \frac{d\mathbf{P}}{dt} = \frac{\mu_{\wedge} e}{m} \mathbf{P} \times (\gamma \mathbf{B}_{\perp} + \mathbf{B}_{\parallel}) \qquad (II.3.5)$$

or

$$\frac{d\mathbf{P}}{dt} = \mu_{\wedge} \frac{e}{m} \mathbf{P} \times \left[\mathbf{B} - \frac{\gamma - 1}{\gamma} \frac{\mathbf{B} \cdot \mathbf{P}}{\mathbf{P}_{\wedge}^2} \mathbf{P}_{\wedge} \right] \qquad (II.3.6)$$

In this equation $\mathbf{B}$ is expressed in the center of mass system, all other quantities are in the laboratory system.

In the present experiment the magnetic field was applied approximately perpendicular to $\mathbf{P}_{\wedge}$ in order to remove background due to charged particles originating in the target. This simplifies the geometry and the Eq. (II.3.6). It takes the approximate form

---

* See Appendix C.

$$\frac{d\vec{S}}{dt} \simeq \mu_{\wedge} \frac{e}{mc} \vec{E} \times \vec{B} \qquad \text{(II.3.7)}$$

Consider the system of reference determined by the three orthogonal unit vectors:

$$\vec{i} = \frac{\vec{P}}{|\vec{P}_{\wedge}|} , \quad \vec{j} = \frac{\vec{E}_o}{|\vec{E}_o|} , \quad \vec{k} = \vec{i} \times \vec{j} \qquad \text{(II.3.8)}$$

Let

$$\vec{E} = n \vec{E} \qquad \text{(II.3.9)}$$

Then the equation of motion (II.3.7), reduces into two component equations:

$$\frac{dS_x(t)}{dt} = \mu_{\wedge} \frac{e\,B}{m\,c} S_y(t) \qquad \text{(II.3.10)}$$

and

$$\frac{dS_y(t)}{dt} = -\mu_{\wedge} \frac{e\,B}{m\,c} S_x(t) \qquad \text{(II.3.11)}$$

The solution of this set of equations subject to the initial condition

$$\vec{S}\,(t = 0) = \vec{S}_o = P_{\vec{j}} \qquad \text{(II.3.12)}$$

is:

$$\vec{S}(t) = P \left[\sin \left(\frac{\mu\, eB}{mc} t \right) \vec{i} + \cos \left(\frac{\mu\, eB}{mc} t \right) \vec{j} \right] \qquad \text{(II.3.13)}$$

This is a vector which is rotating around the magnetic field direction, in the plane defined by $\vec{P}_{\wedge}$ and the initial polarization $\vec{S}_o$. The angular frequency is $\mu\, eB/mc$. Thus after the particle

has spent a time t in the field, and travelled a distance βct, the polarization vector has rotated through an angle:

$$\varphi_0 = \frac{\mu_0 B}{m} t = \frac{\mu_0 m l}{\alpha \beta c^2} \qquad (II.3.14)$$

In the present experiment the magnetic field is not strictly uniform. For this reason instead of Bl one uses $\int Bdl$. This is done by measuring the field at points spaced 5 cm. apart over the whole useful volume and numerically integrating it along the Λ^0 line of flight.

II.4. Observation of the final Polarization Direction

In the rest system of the polarized Λ^0 hyperon, the angular distribution of the decay $\Lambda^0 \longrightarrow p + \pi^-$ is not isotropic but has the form*

$$I(\theta, \xi)\, d\Omega = \frac{1}{4\pi}\left[1 + \alpha P \cos\theta\right] d\cos\theta\, d\xi \qquad (II.4.1)$$

where θ and ξ are the space and azimuthal angles which $\vec{p}_p^{\,*}$, the proton momentum in the center of mass frame make with the polarization vector $\vec{P}$. P is the degree of polarization ($P = |\vec{P}|$) and α, the decay parameter. Its value has been found experimentally to be 0.642 ± 0.016[3] for this decay mode.

Since the rotation of $\vec{P}$ is approximately confined to the $(\vec{p}_{\Lambda^0}, \vec{p}_\Lambda)$ plane, and the information on the magnetic moment is mainly contained in φ_0, it is convenient to project the

---

* See Appendix A.1

distribution onto this plane.* The decay now can be characterized by two angles ψ between the $\vec{P}_p'$ and the plane $(\vec{P}_\Lambda \times \vec{S}_0)$ and φ between the projection of $\vec{P}_p'$ onto that plane and $\vec{P}_0$. From the geometry (for the approximate case $\xi_z = 0$):**

$$\cos\theta = \cos\psi \cos(\varphi - \varphi_0) \qquad \text{(II.4.2)}$$

and

$$d(\cos\theta)\, d\xi = d\sin\psi\, d\varphi \qquad \text{(II.4.3)}$$

In terms of the new angles φ and ψ, the decay probability distribution equation (II.4.1) is given by:

$$W(\varphi,\psi)\, d\varphi\, d\psi = \frac{1}{4\pi}\left[1 + \alpha P \cos\psi \cos(\varphi - \varphi_0)\right] \cos\psi\, d\varphi \qquad \text{(II.4.4)}$$

To obtain the projection of this distribution onto the $(\vec{P}_\Lambda \times \vec{S}_0)$ plane one integrates the Eq. (II.4.4) over ψ between $-\psi_0$ and $+\psi_0$:

$$W(\varphi/\psi_0)\, d\varphi = \frac{\sin\psi_0}{2\pi}\left[1 + \lambda \alpha P \cos(\varphi - \varphi_0)\right] d\varphi \qquad \text{(II.4.5)}$$

where

$$\lambda(\psi_0) = \frac{1}{2}\left(\cos\psi_0 + \psi_0/\sin\psi_0\right) \qquad \text{(II.4.6)}$$

Thus a measurement of the distribution of φ allows the determination of φ_0 and hence μ_Λ. The statistical error on the angle φ_0 can be calculated using the expressions in the

---

* See Figure 1.

** See Appendix B.

decay.* It is given in radians as:

$$\delta\varphi_o \cong \frac{\pi}{2\lambda\alpha P\sqrt{N}} \qquad (II.b.7)$$

which leads to an uncertainty on the magnetic moment in magnetons:

$$\delta\mu \cong \frac{\pi\beta}{2\lambda\alpha P\sqrt{N}\ \frac{e}{mc^2}\ 31} \qquad (II.b.8)$$

where N is the number of observed events.

This formula is useful in the design of the experiment. One sees that in order to decrease the uncertainty; one has to increase B and L as much as possible and also P. One also sees from this formula that there is an optimum distance L such that $L\sqrt{N} \sim L\, e^{-L/2\beta\gamma c\tau}$ reaches a maximum:

$$L_{opt} = 2\beta\gamma c\tau \qquad (II.b.9)$$

In this experiment this corresponded to a length of $\sim$11 centimeters, and the distance between the target and the detector was chosen accordingly.

It can be shown that** $\delta\varphi_o$ is minimized by applying a cut-off at $\sin\psi_o = 0.92$ which excludes events with large ψ.

---

* See Appendix E.

** See Appendix F.

CHAPTER III

APPARATUS*

III.1. Beam

A non-separated high-intensity beam of negative particles produced at 0° K in a platinum target (2 x 2 x 20 mm^3) by an ejected proton beam of 20.6 Gev/c from the CERN PS, was designed for this experiment. Its main characteristics are listed below:

a) a central momentum of 1.050 Gev/c;

b) a momentum distribution falling almost linearly to zero intensity at ± 1.4 % of the central momentum;

c) an angular divergence of ± 1° in the horizontal plane and ± 4° in the vertical plane; (The horizontal plane almost coincides with the plane of production for the Λ^0 hyperons)

d) a burst length of 2 μs allowing precise synchronization with the pulsed magnetic field;

---

* See Fig. 2.

a) a typical flux of about 1.5×10^7 particles per burst;

b) an intensity distribution at the position of the final image (secondary target) characterized by 80 % of the total flux going through an area 6 cm. wide x 4 cm high, allowing the beam to enter the pulsed magnet through a narrow channel.

This beam was found to consist of 70 % π^- mesons, a heavier contamination of about 30 % electrons and muons, and 1 % K^- mesons[13].

III.3. Target*

If liquid hydrogen is used as the secondary target (source of the Λ^0 hyperons) the Λ^0 produced have maximum polarization and have a constant energy for a given angle of production; also their magnetic moment can be measured with greater accuracy. Unfortunately, the use of liquid hydrogen in the presence of coils for the pulsed magnetic field is an extremely difficult problem. Therefore polyethylene, $(CH_2)_n$, was chosen as a target. One disadvantage of this target is that there are more Λ^0 hyperons produced on carbon instead of hydrogen. These hyperons have reduced polarization. Also the recoil motion of the nucleons means that the energy of the Λ^0 emitted at a given angle is not constant. With the kinematic analysis one can get rid of most of the carbon produced Λ^0's and the resulting

---

* See Fig. 3.

contamination reduces the polarization slightly but does not bias the estimate of the magnetic moment. Moreover the polyethylene contains a higher concentration of protons than liquid hydrogen itself, therefore the polyethylene target can be smaller for the same amount of protons.

III.3. The Pulsed Magnet[14]

In the present experiment the target and the detectors had to be located inside the magnet. In order to make a precise measurement of the Λ^0 magnetic moment it was necessary to impose a field in excess of 200 kilogauss in a direction transverse to the flight paths of the hyperons and over a length of 10 to 12 cm. Moreover in order to eliminate the biases and to increase the number of events, a layout which allows the detection of hyperons both to the left and to the right of the primary beam was needed. Finally it was required that the magnet should withstand operation for of the order of 10^4 pulses.

A magnet was specially designed and built to satisfy these requirements. It was of the flux concentrator type. This type of magnets are essentially pulsed transformers combining a single-turn secondary with a multi-turn primary. In general the secondary consists of a single block of conductor containing a central bore which is linked radially to the outside of the block by means of a slot.* The current pulse through the

---

* See figs. 5 & and 6.

primary winding induces a current in the opposite sense in the outer surface of the secondary which is constrained by the skin effect. This current is forced to flow along the face of the slot and round the central bore, producing a magnetic field in it. Alternatively one can say that the magnetic flux produced by the primary current is concentrated in the bore of the secondary, and the slot prevents a short-circuit. This is the reason for the name "flux concentrator".

The advantages of the magnets of this type are the following:

(i) The principal forces are exerted on a single block of metal, thus the magnet does not depend critically on the resistance to stress of relatively weak insulating materials.

(ii) The inductance presented to the external circuit can be adjusted by choosing the number of primary turns.

(iii) A field of a given configuration may be produced by shaping the inside surface of the secondary.

The main disadvantage is the low efficiency with which energy is transferred into high magnetic field in the useful volume of the magnet.

The magnet designed for this experiment represented quite general application of the flux concentration principle. It was essentially a "double" or "twin" flux concentrator built up of two identical halves made of Cu-Cr-Zr alloy.* They were

---

* See Figs. 5 and 6.

in contact in a plane of mirror symmetry and have their primary windings connected in series. Each block was machined out of a thick circular disc. Into the outer surface of the blocks a deep helical groove was turned to receive the primary windings. The insides were turned and milled out to form the corridor through which the magnetic flux threading the coil was concentrated. Cylindrically-shaped cavities in one end of each corridor provided room for the particle detectors. Cooling water was circulated through four holes traversing the secondary blocks.

The primary windings consisted of four spirals of copper, each having four turns and rectangular cross section.

A heavy stainless-steel yoke was necessary to prestress the secondary block so that the forces generated across the plane of the slot during a pulse would be taken up without causing the slot to open permanently and to constrain the primary windings against the radial forces which tend to eject them from the secondary.

The magnets were powered by a 0.07μF capacitor bank. The electrical characteristic of the magnets, when connected to this bank were the following: inductance 8μH, a.c. resistance 4 mΩ, current rise time 1 ms. Averaged over a typical Λ^0 flight path 11 cm. long, the component of the field normal to the track Λ^0 momentum and initial polarization was 395 k Gauss (200 k Gauss) for a discharge voltage of 2.9 kV (3.2 kV).

During the experiment two such magnets were used and withstood a total of about 9000 pulses at 2.9 kV and 1000 at 3.2 kV.

III.4. The Detector

Nuclear emulsion was the only kind of detector which could be made small enough to fit inside a high-field magnet. It has high spatial resolution and it is possible to make direct precise measurements on the tracks as required for this experiment.

Stacks made of 9 pellicles of Ilford K5 nuclear-research emulsion were used as detectors. The pellicles (200 μ m thick) were of circular shape (22 mm diameter) with two segments cut off to provide straight front and back edges.*

Several technical problems had to be solved, connected with the handling of pellicles of such small size exposed to temperatures around 40°C which is a typical temperature for irradiation inside a pulsed magnet of 200 kG.[19]

As a reference system for scanning and measurement, a grid was photographed onto each emulsion pellicle after the exposure. It consisted of lines of polar coordinates originating at the target center, with one line every 2 mm in the radial direction and every degree in azimuth.

---

* See Fig. 7.

CHAPTER IV

EXPOSURE, SCANNING AND MEASUREMENTS

IV.1. Exposure

A total of 72 stacks were exposed to between 50 and 100 neutrino pulses each. 36 of the stacks were exposed with a neutron of 2.9 BV (~ 192 Mu), the remaining with 5.2 BV (~208 Mu). This corresponded to about 10^9 particles on the target per exposure. Tests had shown that higher exposures lead to unacceptable densities of background tracks.

The stacks were exposed in pairs symmetrically situated with respect to the median plane of the coil.* (Odd and even stacks) In this way, in one exposure, two samples of events with opposite initial polarization were obtained to reduce biases. As another precaution against possible asymmetric effects the field direction was reversed after every five or six pairs of stacks. The direction of the precession of the polarization vector is opposite

---

* See Fig. 2.

in odd and even numbered stacks since the magnetic field is in opposite directions. The orientation of the stacks was such that the Λ^0 momentum $\vec{p}_\Lambda$ and the initial polarisation $\vec{P}_0$ lay approximately in the plane of the pellicles.

The timing of the particle burst with respect to the magnetic field pulse was checked continuously by means of the photographic record of oscilloscope traces of the field pulse and particle burst.

The magnetic field just outside the channel transversed by the Λ^0's was monitored by means of a pick up coil for every discharge of the capacitor bank.

For calibration purposes, some pellicles were exposed directly in the beam which had been tuned for positive particles of various momenta between 450 and 1050 MeV/c; they were made from the same emulsion and were processed in the same way as the Λ^0 plates. These plates were used in establishing the relation between the normalised grain density and the velocity, which was needed in the analysis.

The pellicles were processed using a special routine: Pressed in cold (4^0C) distilled water, cold stage development in Ilford developer, dry hot stage (20-24^0C), stop bath at 4^0C, several days of fixing, dilution, washing and alcohol and air drying. In order to decrease the fading at high temperatures reached during the exposure they were protected at 4^0C.[15] After the processing the pellicles were stuck on glass plates.

IV.2. Scanning

Scanning was done by specially trained scanners. The microscopes used were the Leitz Ortholuz and the Zeiss 4000 with the magnification x 53 objective and x 15 ocular. This was the most time-consuming part of the experiment. The purpose was to develop a fast and efficient scanning procedure with least possible biases.

The momenta of the hyperons lie in the 500-300 Mev/c range and in this range the decay protons are emitted within 11° of the Λ^0 line of flight, and have momenta ranging from 326 to 800 Mev/c (ionization between 1.5 and 1.3 times the plateau ionization) in the laboratory system.* Taking into account the finite dimensions of the target and the curvature due to the magnetic field, one obtains that up to 7 cm beyond the decay point the proton track cannot make an angle larger than 30° with the line joining the target center to the point of observation. This line is the mean direction of the Λ^0's at that point.

The scanning was done as follows: a plane was chosen in the emulsion approximately perpendicular to the average line of flight of neutral particles from the target and at some distance from the front edge of the pellicle. The intersection of this plane with the emulsion plane is called the "scan-line". Tracks crossing the scan-line were picked up if they satisfied

---

* See Appendix A.2, Prog. 9, and Table 3.

the criteria which will be described below. All such tracks were followed back over a minimum distance of 7 cm, or to their point of entry into the pellicle, or to their origin inside the emulsion. However a track originated in a two prong event (i.e. was one branch of a "Y") the event was recorded.

For convenience, angular criteria for picking up tracks were defined independently in the plane of the emulsion (plane-angle criterion), and in the plane perpendicular to it (dip angle criterion). To avoid following a very large number of background tracks, it was necessary to choose an interval of plane-angle out of which most of the charged background had been swept by the action of the magnetic field. At a given distance from the target, the limits of this interval were determined by the curvature of the most energetic particles reaching this point. These particles were the elastically scattered π^- mesons on one side and recoil protons from elastic scattering on the other side of the average Λ^0 direction. They made a minimum angle of 15^0 with the mean Λ^0 direction. Particles from inelastic processes crossed the mean line at larger angles since they had smaller momenta. Therefore only a 7^0 interval of plane angle was allowed to both protons from Λ^0 decays and knock on protons from elastic scattering.

The main background within the chosen angular interval consisted of the electrons and positrons coming from the conversion of γ-rays in the emulsion. These made up about 80 % of the tracks. Grain density criteria were used to discriminate against this

background.

An especially designed eyepiece for the microscopes was used as an aid to scanning. This revolved about a point representing the effective target center, so that the plate always moved along radial lines from this point.

As another aid to scanning a graticule was placed into the eyepiece of the microscope*. This helped the scanners in applying the plane-angle criteria.

In each stack which consisted of 9 pellicles, the central 7 pellicles were scanned. In order to determine the exact orientation of each pellicle, the direction of the radial grid lines printed on the pellicle were compared with that of the electron pairs produced by energetic photons from the target. For this purpose 30 electron pairs were found at the beginning of scanning of each plate and their plane angle distribution was drawn. By using these electron pairs also the uniformity in finding pairs at different z, and the existence of a grain density gradient were tested. The local photon grain density was determined by counting grains on these electron tracks.

Two scan lines were taken, situated at 110 m. and 117 m. from the target center (9 mm and 16 mm. from the entrance edge of the pellicles). The tracks which crossed these lines were followed whenever they left

---

* See Fig. 8.

(i) a dip angle with a tangent smaller than 10/100, (this corresponded in the unprocessed emulsion to a dip angle $\pm 19^{\circ}$ with respect to the plane of the pellicles.)

(ii) a plane angle within $\pm 22^{\circ}$ with the axis $\wedge^{\circ}$ direction, (this meant that among the tracks which crossed the upper line of the graticule the ones inside the plane angular filter as defined by the graticule lines[x] were to be followed.)

(iii) a grain density g, greater than 1.3 times that of the electron density g_0, i.e. $\varepsilon^{x} = g/g_0$ 1.3. In order to increase the scanning speed the scanners were trained to estimate the grain density visually rather than by counting except in the borderline cases. They rejected the tracks which they estimated having smaller ε^{x} than 1.1 and accepted the ones with ε^{x} larger than 1.3 and counted only the ones in between. In the γ° interval of plane angle, which can be reached by the knock-on protons, modified grain density criteria were used to discriminate against thin background also. In this region the scanners rejected the tracks with $\varepsilon^{x} < 1.3$ and accepted the ones with $\varepsilon^{x} > 2$ by visual estimation and counted the ones in between to accept the ones with $\varepsilon^{x} > 1.7$; because in this angular region the energy of the decay protons is smaller than the maximum[xx]. Therefore we can increase the lower limit to grain density in order to eliminate the tracks of knock on protons which generally have larger energies than the decay protons in this angular interval.

---

x See Fig. 6.

xx See Table 3.

For the selected tracks the track number, the distance of the pick-up point from the glass surface on which the emulsion was mounted and its fate after being followed were recorded. If the fate was a V event, stop or start, then the plane angle, the x, y, z coordinates of the end point were recorded (the glass surface was taken as z = 0). These tracks were followed back to the pick up point to record g^* and the plane and dip angle. Plane angle, dip angle and grain density distributions[2] were drawn to check the criteria used to choose the tracks to be followed.

For the V-events a drawing of the event was made and the coordinates of the opening angle, grain count of both tracks, the direction of dip, location with respect to the grid were recorded as a help in refinding the event in order to measure.

Some of the plates were circulated among the collaborating laboratories according to a plan and recommend. This plan was as follows:

a) One plate was circulated through all laboratories, to be scanned by one scanner in each laboratory.

b) One plate from each laboratory (with laboratory number n) was sent to the laboratory number n+1.

c) One plate from each laboratory (with laboratory number n) was sent to the laboratory number n+2.

2/ See Programs 1, 2 and 3.

This system of rescan produced a total of 14 rescan results:

5 from the n $\longrightarrow$ (n+1) series

5 from the n $\longrightarrow$ (n+2) series and an additional 4 from the plate which was passed on. This provided a check on the correctness of the visual estimation and helped to maintain the quality of scanning and uniformity between laboratories throughout the experiment. The reasons for missing an event in one laboratory which was found in another were investigated. In this way one could make sure that events with certain characteristics were not being missed systematically i.e. the scanning was not biased.

The scanning yielded a total of 3125 events in the Dubna collaboration and 493 event in Ankara.

IV.3. Measurements

All the V-events recorded in scanning were measured by projectors unless they were obviously incompatible with $\wedge^0$ decay hypothesis. A decay chart* of $\wedge^0$ (proton momenta plotted versus pion momenta for different opening angles) was used to make the decision. The obviously non $\wedge^0$ events were of four types:

1. Proton Contamination: Ionization of both tracks (I_1, I_2) about the same, dip angles of both tracks (δ_1, δ_2) less than 15° and projected opening angle (α_{12}) greater than 150°.

---

* See Fig. 9.

2. Electron pairs: $I_1 \cong I_2 \cong$ minimum ionization $\pm$ 20 %
$|\delta_1| < 15^0$. $|\delta_2| < 15^0$.
$\alpha_{12} \leq 3.0^0$

3. Obvious neutron stars: Star with one fast secondary (the track followed) and one black stopping track, with the conditions:

$$R_2 > 50\mu$$
$$\theta_{12} < 60^0$$

where R_2 is the range of track 2 and θ is the space opening angle.

4. Events obviously not from target: Both tracks on the same side of the grid line, and both at more than 10^0 from the grid line.

The following measurements were made on the other events:

a) the plane angles of both tracks with respect to the grid.

b) the dip angles of both tracks. This was done by measuring the distance from the glass surface, of two points (one of which was usually the decay vertex) which were separated by a known distance on a track. The separation of these two points was taken as $\sim 300\mu$ for proton tracks and $\sim 200\mu$ for pion tracks since they got scattered much more than the protons.

c) the grain densities. When a new plate was started

being measured 300 grains were counted on each track of fast electron pairs and thus the plateau grain density was determined. On proton and pion tracks 1000 grains were counted corresponding to a statistical error of ~ 3.3 %.

d) the range in the emulsion stack of the secondary particle if it stopped and was not clearly a proton. Obtaining the velocity from the range-energy relationship* is more accurate than obtaining it from the normalized grain densities. Therefore range measurements were made whenever it was possible.

e) the x and y coordinates of the event vertex with respect to the grid photographed and z coordinate with respect to the glass surface.

If the secondary tracks left the plate in which they originated, they were followed into the new plate. In spite of their being kept in humid environment the emulsion plates shrink with time. Their thickness had been measured just after the exposure at the center of each plate (monitor point).

In order to find the shrinkage factor and thus correct the dip measurements, everyday the thickness of the plate at the same point was measured.

Some of the plates were remeasured in different intervals according to the plan explained in the measuring part and none of them were remeasured by the first measurer after a

---

* See fig. 10.

long time or by another measurer in the same laboratory[x] . In this way it was possible to check the estimated standard errors in the measurements.

a) the plane angles of the proton and the pion were usually very well measured, the absolute value of each one, due to the uncertainty of the alignment has an error of about 0.1^0.

b) the uncertainty on the dip angles came from an uncertainty of about $\pm 4\,\mu$ in z-measurement and emulsion shrinkage and about $\pm 2\,\mu$ in x-measurement. This corresponded to a standard error of about 1^0 in the dip angles.

c) the uncertainty in the grain densities is due to the statistical fluctuation of the number of grains pointing on a finite length of tracks which was around 3 % assuming a Poisson distribution, since ~ 1000 grains were counted on each track. Another reason for the difference of grain density counts in measurements was the fact that each measurer estimates the number of grains in a blob differently. This was taken care of by drawing a g^{ion}-β calibration curve for each measurer. On the calibration plates which were exposed to proton beams of known momenta between 450 and 950 Mev/c ~ 600 grains were counted on 10 different tracks for each momentum. The counting was done at the central region of the plate, 1 cm from the entrance edge. The proton tracks of known momenta were picked up by plotting the grain density versus the plane angle for a number of tracks counted

---

x See Table 4.

in a plate. In this way beams of different momenta were easily separated because the plates were exposed to the beams of different momenta at certain plane angles. The differentiation between the proton and electron beams at a definite plane angle was done by means of grain counts. This differentiation was more difficult especially for beams with high momenta. In calculating β from the given momenta the energy lost in travelling 1 cm through the emulsion was taken into account. The effect of the distance travelled in the stack holder etc. was considered negligible. To determine the plateau ionisation in these collimation plates $\sim$ 6000 grains were counted on several electron tracks. The statistical error on the grain counts on the protons was 1.3 %. Combined with the error on the plateau grain density (which was also about 1.3 %) this gave about 2 % error. The grain density-velocity data is given for the two measurers in Ankara.*

d) the uncertainty in the range measurements were due to the misalignment of the scale with the track due to the curvature of the track and were of the order of a few microns ($\sim$ 0.5 %).

There was a sharp decrease in sensitivity near the top and bottom surfaces of the emulsion. Because of this reason, V events in the top or bottom 5 % of the plate thickness were discarded.

The total numbers of events measured was 2113 in the whole collaboration and 453 in Ankara.

---

* See Table 3.

CHAPTER V

ANALYSIS

V.1. Grain Density Calibration

Two types of curves were fitted to the experimental points*

$$\sigma^2 = a + b\,\beta^{-c} \qquad (V.1.1)$$

and

$$\log \sigma^2 = a + b \log \beta + c(\log \beta)^2 \qquad (V.1.2)$$

These curves were also forced to go through the point $(\sigma^2, \beta) = (1.00, 0.56)$ of the universal $\sigma^2 - \beta$ curve (Italian curve)** in order to extrapolate it to the high momentum range and get the right curvature in this range.

The parameters of the above curves calculated by the

---

* See Appendix 3 and programs 4 and 5.

** See Fig. 11.

least squares method are given in the form of tables* and the curves obtained are plotted** for the two measurers of Milton laboratory.

The results showed that both types of functions were reasonably suitable to represent the $g^* - \beta$ dependence in the region of the measured points. However, the second function, $\log g^* = a + b \log \beta + c (\log \beta)^2$ gave slightly better fit (smaller χ^2) and had a more realistic shape when extrapolated to higher grain densities, therefore it was chosen as the $g^* - \beta$ calibration curve.

The experimental χ^2 was larger than the theoretical χ^2. This indicated that the only errors on the experimental points were not the statistical errors in counting. The variations in the counting of the same person***, local fluctuations in the sensitivity of the emulsion, fluctuations in the position and energy of the selected tracks, all contributed to the total error. However the actual χ^2 values indicated that these errors are of the same order of magnitude as the statistical errors in counting. As long as they were random there was no need to worry about them much.

The fitted curves of the two measurers were compared****. The variations of these from the "average" curve (i.e. the curve

---

* See Table 6.
** See Figs. 12, 13.
*** See Table 7.
**** See Table 7.

fitted to the experimental points of both of the measures taken together) were not very large. They were of the same order of magnitude as the differences between curves belonging to the two different functions fitted to the same experimental points. Hence it was concluded that the average curve of the two measures from fitting of the function

$$\log p^* = a + b\log\beta + c(\log\beta)^2$$

to all experimental points plus the point $(p^*,\beta) = (2.00, 0.36)$ could be used for all the events measured in future. This had the parameters

$$\begin{aligned} a &= -0.245 \\ b &= -1.663 \\ c &= -0.138 \end{aligned} \qquad \text{(V.1.3)}$$

V.2. Section of the Events

In order to evaluate the magnetic moment, one has to select a sample of events which have a high probability of being decays of Λ^0's produced in hydrogen in the target. For this purpose one compares the measured momenta and angles with those required by the kinematics of the Λ^0 decay.* The goodness of fit was tested by calculating χ^2 for each event.** The fitted momenta and the opening angle were also calculated. From these

---

* See Appendix A.2 and Prog. 6.

** See Appendix B.

the direction and magnitude of the Λ^0 momentum were obtained*.

The "production point" was then estimated as being the point of closest approach of the fitted path of Λ^0 to the central ray of the incident beam. The distributions of the coordinates of the production point were drawn.**

The first cut-off for selection of true Λ^0 events was put on x^2. The theoretical x^2 distribution for one degree of freedom is given by:

$$f_n(x^2)dx^2 = \frac{(x^2)^{-1/2}}{\sqrt{2\pi}} e^{-x^2/2} dx^2 \qquad (V.2.1)$$

where $f_n(x^2)dx^2$ is the probability that x^2 is between x^2 and $x^2 + dx^2$.

The probability that x^2 is greater than or equal to a given value x^2_0 is

$$P_n(x^2 \geq x^2_0) = \int_{x^2_0}^{\infty} f_n(x^2)dx^2 \qquad (V.2.2)$$

The theoretical and experimental P_n versus x^2_0 curves were plotted.*** One sees that the shapes of the two curves are very similar, only the experimental x^2 scale is different by a factor

---

* See Appendix I and Prog. 6.

** See Figures 14, 15, 16.

*** See Figure 17.

of about 4. The similarity indicates that the background event contamination is rather small and the ratios of the several error estimates are realistic. The difference in the χ^2 scales is due to the fact that all the errors were estimated smaller than their actual values.

The cut-off was put at $\chi^2 = 25$ corresponding to a probability of about 2 %.

Another condition for an event to be accepted as a Λ^0 decay from the target was that the estimated production point should lie in the region of the target traversed by the beam. Considering the dimension of the beam and the target and comparing them with the distributions of the production point coordinates the following restrictions were put on the coordinates:

$$|x_{target}| \leq 24 \text{ mm}$$

$$|y_{target}| \leq 8 \text{ mm} \qquad \text{(V.2.3)}$$

$$|z_{target}| \leq 1 \text{ mm}$$

Still another condition to be satisfied for selection was $|\sin \psi_0| \leq 0.91$ as explained in the section (IV.4).

The quantity $\Delta = (m_x^2 - m_{k^0}^2)$ was calculated for each event. m_x is the missing mass at the production vertex and is given by

$$m_x^2 = (E_1 + E_2 - E_\Lambda)^2 - |\vec{P}_1 - \vec{P}_\Lambda|^2 \qquad \text{(V.2.4)}$$

where E refers to total energy, p to mom. $\vec{P}$ to momentum, the subscript i to the incident pions in the reaction creating the hyperons, and the other subscripts to the other particles. For infinite precision in the measured quantities of $E_{p_0}(V,2,4)$, $\Delta^2 = 0$ if production occured on a free proton. If the production occured on a bound proton with Fermi momentum $\vec{P}_F$, Δ^2 is approximately $-2\,\vec{P}_F \cdot \vec{P}_{p_0}$. For infinite measurement precision this again gives a central value of $\Delta^2 = 0$ since $\vec{P}_F$ is randomly orientated with respect to $\vec{P}_{p_0}$, but this time the distribution has a width of about 0.14 $(Gev)^2$. The Δ^2 distributions were drawn for the V-events which satisfy the restrictions explained above in this section and also for those which do not satisfy* these restrictions. The former have a distribution consistent with their being due to Λ^0 hyperons from the reaction on free protons in the target. The shift of the central value from 0 to 0.01 is due to the tilt of the initial π^- beam because of the magnetic field** and the width of the distribution can be completely explained by measurement errors. The second group of events gives a Δ^2 distribution which is very broad and not at all consistent with what would be expected if it consisted of Λ^0 hyperons.

Λ^0 's produced on protons with Fermi momentum have smaller or larger momenta than those produced on free protons

---

* See Fig. 10

** See Appendix J.

depending on the direction of the Fermi momentum. In order to reduce the small no. of Λ^0's produced on carbon in the sample still further the acceptance was restricted to the region 400 Mev/c $< p_n <$ 800 Mev/c .

As a further check the distributions of the fitted pion and proton momenta, opening angle, plane and dip angles and momentum of Λ^0 were drawn to see if they were the expected distributions.* The number of events left (in Ankara) after each restriction are given in the form of a table.** In the whole collaboration, 1355 events survived.

All the distributions drawn in this section are only for the events measured in Ankara.

V.3. Evaluation of the Λ^0 Magnetic Moment

For each event in the selected sample φ, the angle between the projection of P_p' onto the plane (p_n, c_o) and P_o was calculated.*** The distribution of φ-angles is drawn.**** This distribution is not exactly that given in Eq. (II.3.3) but still very similar to a cosine distribution .

---

* See Figures 19, 20, 21, 22, 23, 24.

** See Table 8.

*** See Fig. 1.

**** See Appendix K and Prog. 6.

***** See Fig. 25.

The reasons for the discrepancy between the theoretical and experimental distributions are the following:

1) To each event there corresponds different values of H, β and t and therefore a different value of φ_0.

2) A proton from a Λ^0 decay may leave the surface of a pellicle before it reaches the scan line. The probability that this should happen increases with the angle between the proton and the Λ^0 direction, and φ is related to this angle. This means that the probability of observing values of φ of around $\pm 90^0$ is not the same as that for φ in the region of 0^0 and $\pm 180^0$. This effect is called the "flat chamber" effect".

3) Because of the restrictions imposed on scanning and acceptance of events, some events are lost. This will be discussed in more detail in the coming sections.

The normalized probability density for the observation of an angle φ_i in the decay of a Λ^0 is:[x]

$$\varphi(\varphi_i \mid \mu_\Lambda, \alpha P) = \frac{1 + \lambda \alpha P \cos\left(\varphi_i \pm \frac{\mu_\Lambda}{mc^2} \frac{(mH)_i}{\beta_i}\right)}{\int \left(1 + \lambda \alpha P \cos\left(\varphi_i \pm \frac{\mu_\Lambda}{mc^2} \frac{(mH)_i}{\beta_i}\right)\right) d\varphi} \qquad (V.3.1)$$

The + or - sign corresponds to the two possible orientations of the field. The integral in the denominator can be replaced by a sum over all events. Its value should be approximately equal to 2π.

---

x See Appendix I.

This equation contains two unknown parameters: the magnetic moment μ_Λ and αP. Given a sample of N events, the best estimates of these quantities are the values which maximize the likelihood function* $L(\mu_\Lambda, \alpha P)$

$$L(\mu_\Lambda, \alpha P) = \sum_{i=1}^{N} q(\varphi_i | \mu_\Lambda, \alpha P) \qquad (V.3.2)$$

or its logarithm

$$\ln L(\mu_\Lambda, \alpha P) = \sum_{i=1}^{N} \ln q(\varphi_i | \mu_\Lambda, \alpha P) \qquad (V.3.3)$$

The summation runs over all finally selected events.

V.4. Results $\mu_\Lambda, \alpha P$ and their Statistical Errors

The results will be given both for Antara events and events of all the collaboration. Only the Imanaka events are excluded because of their very low αP and strange looking likelihood contours.

Countour diagram of the likelihood function were drawn both for Antara events and all events** .

For Antara events the maximum likelihood point lies at $\mu_\Lambda = -0.61\ \mu_N$ and $\lambda \alpha P = 0.49$ ($\alpha P = 0.50$). This value of μ_Λ corresponds to an average precession angle of 45°.

---

* See Prop. 7.

** See Fig. 26.

When all of the events are considered the maximum likelihood point is at $\mu_\Lambda = -0.39$ and $\lambda \alpha P = 0.64$ ($\alpha = 0.24$) corresponding to a precession angle of 44°.

To state the statistical uncertainty in this result one uses the following contours which define 68% confidence levels if the likelihood surface is Gaussian:

a) the closed contour $\ln(L/L_{max}) = -1.15$ if μ_Λ and αP are estimated simultaneously, i.e. the true values of both μ_Λ and αP lie inside the region enclosed by this contour with 68 % confidence limit.

From Fig. 25 one deduces the following uncertainties:

For Solaro	For the collaboration
$\delta(\mu_\Lambda) = \pm 0.22\ \mu_N$	$\delta(\mu_\Lambda) = \pm 0.09\ \mu_N$
$\delta(\alpha P) = \pm 0.14$	$\delta(\alpha P) = \pm 0.05$

b) the tangents parallel to the αP axis to the contour $\ln(L/L_{max}) = -0.5$ which correspond to the 68 % confidence limit for μ_Λ alone*.

Again from Fig. 25 one gets $\delta(\mu_\Lambda) = \pm 0.14\ \mu_N$ for Ankara and $\delta(\mu_\Lambda) = \pm 0.06\ \mu_N$ for the collaboration.

In order to check for the consistency of the maximum likelihood values for μ_Λ and αP the theoretical distribution given by Eq. (II.4.5) was drawn[3] using the values of μ_Λ and αP

---

* See Fig. 27.

obtained above and normalising to the number of events used in the analysis and compared with the experimental distribution.

V.5. Systematic errors

Systematic errors which may arise in the estimate of μ_Λ are listed below:

1) Loss of events at the scanning stage:

Events may be lost because of too strict scanning criteria and because of the errors made in angle measurements and grain density measures. The safety regions used were large enough to prevent this.

Some tracks which satisfy the scanning criteria were sometimes not picked up by the scanners. By rescanning part of the material the overall scanning efficiency was found to be of the order of 99 %. The events missed in one of the two scans appear to be a random sample, with no bias in φ or p_Λ. The distributions of momenta and angles of the Λ^0's are consistent with the expected ones. So we can neglect the error due to loss of events.

2) Measurement errors:

Systematic errors in the measurements can affect the final result in three ways:

(i) The value of μ_Λ is directly effected via the decay angle φ or p_Λ.

(ii) The field integral $\int Bdl$ is affected through the determination of the production point.

(iii) By causing the rejection of Λ^0 decays with particular characteristics, the selection is biased.

By using β -vs- g^* calibration curves in calculating the momenta and excluding events near the surfaces of the emulsion where the distortion probability is highest the measurement errors were tried to be minimized.

All of the measurements were made by physicists and about 10 % of the events were remeasured. The remeasurements gave consistent results and the inconsistencies were random.

3) Errors in the field integral:

Errors in the field integral directly affect the magnetic moment since the angle φ_0 is proportional to $\int Bdl$. They may arise from:

(i) errors in the field measurements,

(ii) changes in the field during the experiment that could not be taken into account in the calculation ,

(iii) errors in the determination of the production point,

(iv) approximations in the evaluation of the field integral.

The measurements and control of the field during the exposures, and calculation of the path integral $\int Bdl$ were performed by the other members of the collaboration. In the analysis the average value of the field over the Λ^0 path given by them ($\bar{B}$ = 200 K Gauss) was used. The systematic error they

associated with this value was 2 %.

4) Λ^o - simulating two-prong events

Of the 3123 events accepted for measurement, 2708 were rejected. A large proportion of these are nuclear disintegrations, produced by fast neutrons from the target, in which one of the tracks satisfy the pick-up criteria for a proton from Λ^o decay. Since their number is quite large it is possible that a small number of such events are included in our Λ^o sample. However any bias caused by this inclusion operates in opposite direction in the two stacks of each pair with opposite initial polarizations.

5) Background Λ^o decays

Some Λ^o s produced in the carbon nuclei in the polyethylene target will be included in the selected sample although their number were reduced by the cut off on Λ^o momentum. Any one of these will not be polarised in the direction of $\vec{s}_o$. Because of the spatial isotropy of the Fermi-momentum vectors, their average direction of polarization will be the same as that of the hydrogen-produced ones, so that this background will reduce the average value of αP but not introduce any bias into the estimate of μ_Λ.

6) Errors introduced in the analysis, approximations

Two main effects were neglected in the analysis. The small curvature of the initial π^- beam due to the magnetic field*

---

* See Appendix J.

and flat chamber effect explained in section V.3. Since the experimental distribution of the angle φ is quite similar to the theoretical one we concluded that the effect of this segment is small.

Small changes in the acceptance criteria does not have any significant effect on the estimate of μ_Λ.

To test the existence of any asymmetry between the two sets of stacks exposed on opposite sides of the π^- beam (odd and even numbered stacks) μ_Λ was estimated for the two sets of stacks separately. The result is as follows:

	For Ankara events	For all events
Odd-numbered stacks	-0.44 ± 0.23 n.m.	-0.54 ± 0.09 n.m.
Even-numbered stacks	-0.71 ± 0.20 n.m.	-0.63 ± 0.09 n.m.

It is seen that 68 % confidence interval includes the values of μ_Λ obtained from odd stacks or even stacks alone for both Ankara events and the whole sample and so the statistics increases the values for odd and even stacks get closer, i.e. statistics might explain the discrepancy between the two sets. But the difference might also be due to an unknown asymmetry since it consistently appears in the same direction in all samples of events. Another fact which supports this view is that number of events found in even stacks is always larger than those found in odd stacks by 15-20 %. Allowing 6 % systematic error for this and combining in with the other

systematic errors one obtains that systematic error is less than 7 % or ± 0,06 μ_B.

CHAPTER VI

DISCUSSION AND CONCLUSIONS

Treating both systematic and statistical errors as standard errors one finds $\mu_\Lambda = (-0.59 \pm 0.07)\mu_p$. If only Ankara events are used the result is $\mu_\Lambda = (-0.61 \pm 0.10)\mu_p$. The two results are consistent with each other, with the previous world average which is $(-0.73 \pm 0.20)\mu_p$ and also with the result of the collaboration published earlier.[16] This result is $(-0.66 \pm 0.07)\mu_p$. It was obtained by a very detailed analysis program using the larger computer at CERN. All the effects which could influence the final result were taken into account. Therefore the systematic error is smaller. The value obtained in this thesis is based on only the scanning of the analysis.

When compared with Table I, one sees that this result is in agreement with the predictions of various broken SU_3 models. But one should remember that most of the theoretical

results in Table I are subject to the validity of assumption and depend on the values of adjustable parameters. For example let us review now the pure SU(3) prediction, $\mu_\Lambda = \frac{1}{2}\mu_n = -0.06\mu_n$ is derived.[17, 18, 19] One uses the hypothesis that the electromagnetic properties are represented by operators which are invariant under U-spin, and transform like a combination of scalar and vector in I-spin. Because of invariance under U-spin the elements of a U-spin multiplet have the same magnetic moment

$$\mu_{\Sigma^+} = \mu_p \tag{VI.1}$$

$$\mu_{\Xi^-} = \mu_{\Sigma^-} \tag{VI.2}$$

$$\mu_{\Xi^0} = \mu_{\Sigma_u^0} = \mu_n \tag{VI.3}$$

where Σ_u^0 is an eigenstate of U-spin with the eigen-value 1. The other eigenstate belonging to the eigenvalue -1 is Λ_u^0:

$$\Lambda_u^0 = -\frac{1}{2}\Lambda^0 - \frac{\sqrt{3}}{2}\Sigma^0 \tag{VI.4}$$

$$\Sigma_u^0 = \frac{\sqrt{3}}{2}\Lambda^0 - \frac{1}{2}\Sigma^0 \tag{VI.5}$$

From these two equations one gets:

$$\mu_{\Sigma_u^0} = \frac{3}{4}\mu_{\Lambda^0} + \frac{1}{4}\mu_{\Sigma^0} - \frac{\sqrt{3}}{2}\mu_{\Sigma^0\Lambda^0} \tag{VI.6}$$

$$\mu_{\Lambda_u^0} = \frac{1}{4}\mu_{\Lambda^0} + \frac{3}{4}\mu_{\Sigma^0} + \frac{\sqrt{3}}{2}\mu_{\Lambda^0\Sigma^0} \tag{VI.7}$$

$$\mu_{\Lambda_u^0\Sigma_u^0} = -\frac{\sqrt{3}}{4}\mu_{\Lambda^0} + \frac{\sqrt{3}}{4}\mu_{\Sigma^0} - \frac{1}{2}\mu_{\Lambda^0\Sigma^0} \tag{VI.8}$$

The transition moment $\mu_{\Lambda\,\Sigma^0_0}$ has to vanish again because of invariance under U-spin

$$\mu_{\Lambda_0 \Sigma_0} = 0 \qquad \text{(VI.9)}$$

Since the operators representing the electromagnetic properties are scalar-vector combinations in I-spin they have the form $a + b\vec{I}$ and only I_3 has expectation values different from zero, in the states of an isotopic multiplet. The operator O has a certain element $\langle\alpha|O|\beta\rangle = \delta_{\alpha\beta}(a + cb)$ between two eigenstates α, β of I_3 where a is such that $I_3|\beta\rangle = a|\beta\rangle$. Since for a multiplet, m takes the $(2n + 1)$ integer values, $-n, \ldots 0, \ldots n$, it follows that

$$\mu_{\Sigma^+} - \mu_{\Sigma^0} = \mu_{\Sigma^0} - \mu_{\Sigma^-} \qquad \text{(VI.10)}$$

From the fact that the charge operator Q may be written as $Q = -\frac{2}{3}(2I_3 + U_3)$ one can assume that the current operator j has the same transformation properties under SU(3) and can be written as:

$$j = j_1(x) I_3 + j_2(x)\, U_3 \qquad \text{(VI.11)}$$

Since summing over the whole baryon octet the expectation values of the operators I_3 and U_3 are zero, one obtains a further relation:

$$\mu_{\Sigma^+} + \mu_{\Sigma^-} + \mu_{\Sigma^0} + \mu_\Lambda + \mu_p + \mu_n + \mu_{\Xi^-} + \mu_{\Xi^0} = 0 \qquad \text{(VI.12)}$$

From the nine equations (VI.1), (VI.2), (VI.5), (VI.6), (VI.7), (VI.8), (VI.9), (VI.10), (VI.12) one can solve for the nine

unknowns $\mu_{\Sigma^+}, \mu_{\Sigma^-}, \mu_{\Sigma^0}, \mu_{\Lambda^0}, \mu_{\Xi^-}, \mu_{\Xi^0}, \mu_{\Lambda^0_u}, \mu_{\Sigma^0_u}, \mu_{\Lambda^0_u}, \Sigma^0_u$ in terms of the other two μ_p and μ_n. In this way one gets for μ_Λ :

$$\mu_\Lambda = \frac{\mu_n}{2} \qquad \text{(VI.13)}$$

It is seen that this result depends on the assumption that the electromagnetic current operator j_μ transforms as a member of an octet under SU(3). But in the real world SU(3) symmetry is broken Several models of symmetry breaking have been introduced up to now. For example T.P. Cheng and L. Fayolo[20] have started with the SU(2) invariance assumption. They used a dynamical model of symmetry breaking, and with the additional assumption of the absence of the 27-dimensional piece of the electromagnetic current they obtained a relationship between Σ^+ and Λ^0 magnetic moments:

$$\mathcal{H}_{\Sigma^+} + \tfrac{1}{2}\mathcal{H}_\Lambda = \mathcal{H}_n \qquad \text{(VI.14)}$$

where the $\mathcal{H}$'s are the anomalous moments in Bohr magnetons.

If one uses the quark model[21] with the assumption of no orbital angular momentum contribution, the baryon magnetic moments are given as the sum of the individual quark moments. In this way one can get another relationship between the magnetic moments of Σ^+ and Λ^0 :

$$3\,\mu_{\Sigma^+} + \mu_\Lambda = \frac{4}{3}(4\mu_p + \mu_n) \qquad \text{(VI.15)}$$

Schwinger[22] obtained the same relationship using partial symmetry which is a phenomenological method making use

of a partial symmetry group. A partial symmetry group is a set of transformations under which a significant portion of an effective Lagrangian, referring to specific physical circumstances remains invariant.

Equations (VI.14) and (VI.15) have been plotted.* The experimental value of μ_Λ presented here and the present world average for μ_{Σ^+} which is[23]

$$\mu_{\Sigma^+} = 2.50 \pm 0.46\ \mu_n$$

are shown on the graph. One sees that our result is in good agreement with Franklin's or Schwinger's results. Using this one can predict $\mu_{\Sigma^+} = 2.68 \pm 0.03\ \mu_n$ which is in agreement with the present world average, but due to the large error of the present μ_{Σ^+} value one cannot conclude much.

---

* See Fig. 2b.

APPENDIX A

PRODUCTION AND DECAY OF THE Λ^0 HYPERON

A.1. Calculation of the initial polarization and angular distribution of the decay products

Λ^0 is produced in the reaction

$$\pi^- + p \longrightarrow \Lambda^0 + K^0 \qquad (A.1.1)$$

when a π^- beam is sent to a proton target.

Assume that the incoming particle is in the z-direction and choose the y-z plane as the production plane, i.e. the outgoing particle is in the direction $(0, \sin\theta, \cos\theta)$.

Since parity transformation changes positive helicity into negative helicity, longitudinal polarization of Λ^0 is not allowed because it violates parity conservation. Therefore the only non-zero polarization component will be P_y which will be calculated below.

The spin up and down states of the scattered wave

(taking $\alpha=0$) given by[24],

$$\psi^{+}_{\infty} = \frac{e^{2ikr}}{2ir}\left\{\left[a_3 + (2a_{33}+a_{31})\cos\theta\right]\chi_{+1} - \left[(a_{33}-a_{31})\sin\theta\right]\chi_{-}\right\} \tag{A.1.2}$$

$$\psi^{-}_{\infty} = \frac{e^{2ikr}}{2ir}\left\{\left[a_3 + (2a_{33}+a_{31})\cos\theta\right]\chi_{-1} - \left[(a_{33}-a_{31})\sin\theta\right]\chi_{+}\right\} \tag{A.1.3}$$

where a's are the partial wave amplitudes. The notation used is:

a_{33}, a_{31} for p-wave

a_{33} for s-wave

where T is the isospin and J is the total angular momentum of the final state.

χ_+ and χ_- are the spin eigenfunctions of Λ^0. $\chi_+=\begin{pmatrix}1\\0\end{pmatrix}$ represents a spin up state and $\chi_- = \begin{pmatrix}0\\1\end{pmatrix}$ represents a spin down state.

To simplify the notation introduce:

$$a = a_3 + (2a_{33}+a_{31})\cos\theta$$

$$b = (a_{33}-a_{31})\sin\theta \tag{A.1.4}$$

$$\alpha = \chi_+ , \quad \beta = \chi_-$$

Then (A.1.2) and (A.1.3) take the form

$$\psi^{+}_{\infty} = a\alpha - ib\beta \tag{A.1.5}$$

$$\psi_{xx}^{-} = -ib\alpha + a\beta \qquad (A.2.6)$$

The polarization in the x direction is the expectation value of σ_x :

$$P_x = \frac{\psi^{\dagger}\sigma_x\psi}{\psi^{\dagger}\psi} \qquad (A.2.7)$$

Since the initial state was unpolarized atoms may enter the two possible states:

$$P_x = \frac{1}{2}\frac{(a^*\alpha^* + ib^*\beta^*)\sigma_x(a\alpha - ib\beta)}{(a^*\alpha^* + ib^*\beta^*)(a\alpha - ib\beta)}$$

$$+ \frac{1}{2}\frac{(ib^*\alpha^* + a^*\beta^*)\sigma_x(-ib\alpha + a\beta)}{(-ib^*\alpha^* + a^*\beta^*)(-ib\alpha + a\beta)} \qquad (A.2.8)$$

Since $\sigma_x\alpha = \beta$; $\sigma_x\beta = \alpha$; $\alpha^*\beta = 0$, $\alpha^*\alpha = 1$ etc.

$$P_x = \frac{1}{2}\frac{ia|b|^2 - ia^*b^2}{aa^* + bb^*} + \frac{1}{2}\frac{-ia^*b + ib^*a}{aa^* + bb^*} = i\frac{ab^* - a^*b}{|a|^2 + |b|^2}$$

(A.2.9)

or

$$P_x = -2\frac{\mathrm{Im}(ab^*)}{|a|^2 + |b|^2} \qquad (A.2.10)$$

Substitute (A.2.4) into (A.2.10) to get

$$P_x = -\frac{\mathrm{Im}\left[a_{11}^*(ia_{11} + a_{21})\cos\theta\right]\left[(a_{11}^* - a_{21}^*)\sin\theta\right]}{\left|a_{11}^*(ia_{11} + a_{21})\cos\theta\right|^2 \left|(a_{11} - a_{21})\sin\theta\right|^2} \qquad (A.2.11)$$

As it is seen from this formula, magnitude of the polarization depends on the direction of the outgoing particle and also on the phase shifts since a' s are dependent on the phase shifts (δ) as :

$$a = e^{i\delta} \sin\delta \qquad (4.3.12)$$

One can show that $P_y = P_z = 0$ as follows :

$$P_y = \frac{1}{2} \frac{(a^2\alpha^2 + ib^2\beta^2)\,\sigma_y(a\alpha - ib\beta)}{(a^2\alpha^2 + ib^2\beta^2)(a\alpha - ib\beta)}$$

$$+ \frac{1}{2} \frac{(ib^2\alpha^2 + a^2\beta^2)\,\sigma_y(-ib\alpha + a\beta)}{(ib^2\alpha^2 + a^2\beta^2)(-ib\alpha + a\beta)} \qquad (4.3.13)$$

Since $\sigma_y\alpha = i\beta$; $\sigma_y\beta = -i\alpha$; $\alpha^2\beta = 0$; $\alpha^2\alpha = 1$ etc.

$$P_y = \frac{1}{2} \frac{a^2b - ab^2}{|a|^2 + |b|^2} + \frac{1}{2} \frac{ab^2 + a^2b}{|a|^2 + |b|^2} = 0 \qquad (4.3.14)$$

Similarly

$$P_z = \frac{1}{2} \frac{(a^2\alpha^2 + ib^2\beta^2)\,\sigma_z(a\alpha - ib\beta)}{(a^2\alpha^2 + ib^2\beta^2)(a\alpha - ib\beta)}$$

$$+ \frac{1}{2} \frac{(ib^2\alpha^2 + a^2\beta^2)\,\sigma_z(-ib\alpha + a\beta)}{(ib^2\alpha^2 + a^2\beta^2)(-ib\alpha + a\beta)}$$

$$(4.3.15)$$

Since $\sigma_z\alpha = \alpha$; $\sigma_z\beta = -\beta$; $\alpha^2\beta = 0$, $\alpha^2\alpha = 1$ etc.

$$P_n = \frac{1}{2}\,\frac{aa^* - bb^*}{|a|^2+|b|^2} + \frac{1}{2}\,\frac{bb^* - aa^*}{|a|^2+|b|^2} = 0 \qquad (4.3.16)$$

Angular distribution of the proton from the decay

$$\Lambda^0 \longrightarrow p + \pi^- \ :$$

Since the parity is not conserved in this decay one expects both $S_{1/2}$ and $P_{1/2}$ states of the decay products. The decay can then be described by a matrix

$$M(\Lambda^0 \longrightarrow \pi^- + p) = a + p\ \vec{\sigma}\cdot\hat{q} \qquad (4.3.17)$$

where a and p indicate the amplitude of S-wave and P-wave proton emission respectively and $q = (\sin\theta\cos\varphi\ ,\ \sin\theta\sin\varphi\ ,\ \cos\theta)$ is the direction of proton emission.

The cross-section is :

$$\frac{d\sigma}{d\Omega} = \psi_f^{*}\, M^{*} M\, \psi_i \qquad (4.3.18)$$

where ψ_f and ψ_i are the initial and final states.

$$\frac{d\sigma}{d\Omega} = |a|^2 + |p|^2 + 2\,\mathrm{Re}\,(a^{*}p)\,\langle\vec{\sigma}\rangle\cdot\hat{q} \qquad (4.3.19)$$

Let

$$\alpha = \frac{2\,\mathrm{Re}(a^{*}p)}{|a|^2+|p|^2} \qquad (4.3.20)$$

Then

$$\frac{d\sigma}{d\Omega} = (\,|a|^2 + |p|^2)\,(1 + \alpha\langle\vec{\sigma}\rangle\cdot\hat{q}) \qquad (4.3.21)$$

If the Λ^0 is polarized along the n-direction

$$\frac{d\sigma}{d\Omega} = (|a|^2 + |b|^2)(1 + \alpha P \cos\theta)$$

where P is the magnitude of the polarization calculated earlier.

4.2 Kinematics

(i) Production

Consider the reaction $p + \pi^- \longrightarrow \Lambda^0 + K^0$ in the laboratory frame and c.m.s. frame:

Lab

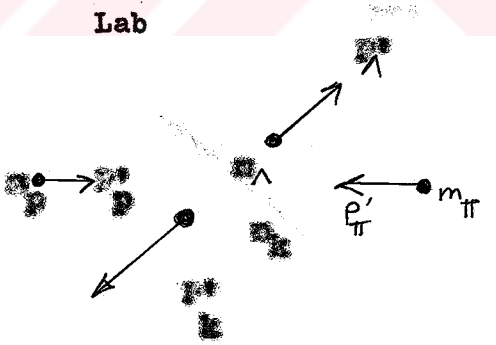

c.m.s.

One obtains the velocity β of the c.m.s. frame with respect to the laboratory frame as follows :

In the c.m.s. frame the momenta of p^0 and π^- are equal :

$$p'_\pi = -p'_p \qquad (4.2.1)$$

Writing this equation in the laboratory frame:

$$\gamma(p_\pi - \beta E_\pi) = -\gamma(-\beta m_p) \qquad (A.3.2)$$

where

$$\gamma = 1/(1-\beta^2)^{1/2} \quad \text{and} \quad E_\pi = \sqrt{p_\pi^2 + m_\pi^2}$$

Solving from this equation one obtains

$$\beta = \frac{p_\pi}{E_\pi + m_p} \qquad (A.3.3)$$

Converting the available laboratory energy into the c.m.s. frame we get

$$E'_{cm} = (E_\pi + m_p - \beta p)_\pi \qquad (A.3.4)$$

This energy is the sum of Λ^0 and K^0 energies in this frame :

$$E'_{cm} = E'_{\Lambda^0} + E'_{K^0} \qquad (A.3.5)$$

or

$$p'^2_{K^0} = (E'_{cm} - E'_{\Lambda^0})^2 \qquad (A.3.6)$$

$$p'^2_{K^0} + m^2_{K^0} = E'^2_{cm} - 2E'_{\Lambda^0} E'_{cm} + p'^2_{\Lambda^0} + m^2_{\Lambda^0} \qquad (A.3.7)$$

since $p'_{\Lambda^0} = -p'_{K^0}$ we can solve for the c.m.s. energy of Λ^0

$$E'_{\Lambda^0} = \frac{E'^2_{cm} + m^2_{\Lambda^0} - m^2_{K^0}}{2E'_{cm}} \qquad (A.3.8)$$

The c.m.s. momentum of Λ^0 is :

$$p^*_{\Lambda^0} = \sqrt{E^{*2}_{\Lambda^0} - m^2_{\Lambda^0}} \qquad (4.2.9)$$

We can find the laboratory momentum and angle of Λ^0 as follows

$$\tan\theta = \frac{p_{\Lambda^0 y}}{p_{\Lambda^0 x}} = \frac{p^*_{\Lambda^0 y}}{\gamma(p^*_{\Lambda^0 x} + \beta E^*_{\Lambda^0})} = \frac{p^*_{\Lambda^0}\sin\alpha}{\gamma(p^*_{\Lambda^0}\cos\alpha + \beta E^*_{\Lambda^0})}$$

$$(4.2.10)$$

In the above equations the unprimed quantities are in the laboratory frame and the primed ones in the cms frame. α, the cms emission angle of Λ^0 changes from 0^0 to 180^0. As calculated in Prog. 6 during this change the maximum value θ attains is $\sim 21^0$.

$$p_{\Lambda^0} = \frac{\gamma(p^*_{\Lambda^0}\cos\alpha + \beta E^*_{\Lambda^0})}{\cos\theta} \qquad (4.2.11)$$

From the output of Prog. 6 we see that p_{Λ^0} changes between 304 and 320 Mev/c (both values for $\theta = 15^0$) for $21^0 > \theta > 15^0$ as in the case in the actual experiment

(ii) Decay

Consider the reaction $\Lambda^0 \longrightarrow p + \pi^-$ in the laboratory frame and c.m.s. frame :

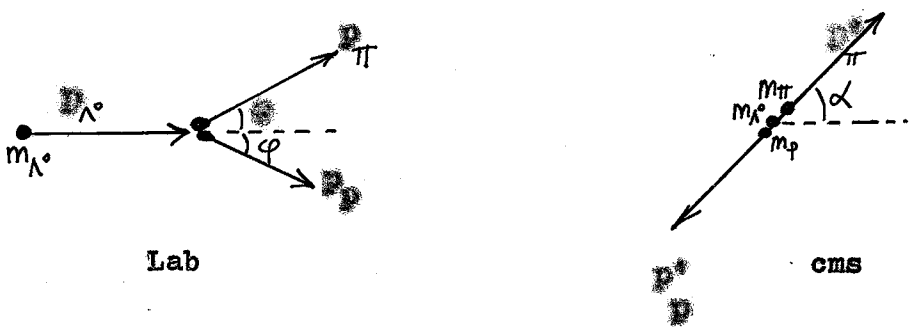

The energy available in the c.m.s. frame is just the rest mass of Λ^0 and it is equal to the sum of proton and pion energies in this frame :

$$E^*_{cm} = m_{\Lambda^0} = E^*_\pi + E^*_p \qquad (A.2.14)$$

or

$$E^*_\pi = m_{\Lambda^0} - E^*_p \qquad (A.2.15)$$

squaring both sides one gets

$$m^2_\pi + p^{*2}_\pi = m^2_{\Lambda^0} - 2m_{\Lambda^0}E^*_p + m^2_p + p^{*2}_p \qquad (A.2.16)$$

since $p^*_p = - p^*_\pi$

we get

$$E^*_p = \frac{m^2_{\Lambda^0} + m^2_p - m^2_\pi}{2m_{\Lambda^0}} \qquad (A.2.17)$$

and

$$E^*_\pi = m_{\Lambda^0} - E^*_p \qquad (A.2.18)$$

The c.m. momenta are

$$p^*_p = \sqrt{E^{*2}_p - m^2_p} \qquad (A.2.19)$$

$$p^*_\pi = \sqrt{E^{*2}_\pi - m^2_\pi} \qquad (A.2.20)$$

The laboratory angles and momenta of the proton and pion are obtained as follows

$$\tan\theta = \frac{p_{\pi_y}}{p_{\pi_x}} = \frac{p^*_{\pi_y}}{\gamma(p^*_{\pi_x} + \beta E^*_\pi)} = \frac{p^*_\pi \sin\alpha}{\gamma(p^*_\pi \cos\alpha + \beta E^*_\pi)} \qquad (A.2.21)$$

$$\tan\varphi = \frac{P'_p \sin\alpha}{\gamma\,(P'_p \cos\alpha + \beta E'_p)} \qquad (A.2.30)$$

$$P_\pi = \frac{\gamma(P'_\pi \cos\alpha + \beta E'_\pi)}{\cos\theta} \qquad (A.2.31)$$

$$P_p = \frac{(P'_p \cos\alpha + \beta E'_p)}{\cos\varphi} \qquad (A.2.32)$$

β and γ occuring in these equations are those of the Λ^0 frame (c.m.s. frame) and given by

$$\beta = \frac{P_{\Lambda^0}}{E_{\Lambda^0}} \qquad (A.2.33)$$

$$\gamma = \frac{1}{\sqrt{1-\beta^2}} \qquad (A.2.34)$$

Prog. 3 calculates the limits between which these quantities change :

$$0.112 < \beta < 0.583 \qquad (A.2.35)$$

$$1.007 < \gamma < 1.231$$

$\tan\theta$, $\tan\varphi$, P_π and P_p are all monotonicly increasing or decreasing functions of β. Therefore in order to find the values between which they change it is sufficient to look at how they change with α for the extremum values of β and γ.

Range 9 calculates the following limits :

$0 < \theta <$ [illegible]°

$0 < \varphi <$ [illegible]° ;

[illegible] $< p_{\pi} <$ [illegible] MeV/c

[illegible] $<$ [illegible] $<$ [illegible]

APPENDIX B

THE COVARIANT FORM OF THE PRECESSION EQUATION

The problem of the precession of the polarization vector of particles moving in an electromagnetic field has been treated by several authors.

Fradkin and Case[29] used a quantum mechanical approach. They considered the Hamiltonian for a particle with an anomalous moment of magnitude $a\mu_0$ (μ_0 is the Bohr magneton) in a constant homogeneous magnetic field $\bar{H}$, in the Foldy - Wouthuysen representation. Restricting themselves only to positive-energy solutions of the wave equation, up to terms of first order in μ_0 the Hamiltonian is

$$\mathcal{H} = \mathcal{E}_\pi - \mu_0 \bar{\sigma}\cdot\bar{H}\left[\frac{1}{\gamma} + a\right] + a\mu_0 \frac{(\bar{\sigma}\cdot\bar{v})(\bar{v}\cdot\bar{H})}{v^2}\left[1 - \frac{1}{\gamma}\right] \qquad (B.1)$$

where $\mathcal{E}_\pi = (m_0^2c^4 + c^2p^2)^{1/2}$ for an uncharged particle. $\bar{\sigma}$ is the spin operator, $\bar{v}$ is the velocity, $\bar{p}$ momentum, m_0 rest mass

of the particle and $\gamma = (1 - v^2/c^2)^{-1/2}$.

The equation of motion for the spin operator is :

$$\dot{\bar{\sigma}} = \frac{1}{i\hbar} [\bar{\sigma}, H] \qquad (2.2)$$

For the two orientations of the magnetic field with respect to the particle velocity one gets :

$$B \parallel \bar{v} \qquad : \qquad d\bar{\sigma}/dt = \frac{e}{m_0 c \gamma} \bar{\sigma} \times B \qquad (2.3)$$

$$B \perp \bar{v} \qquad : \qquad d\bar{\sigma}/dt = \frac{e}{m_0 c} \bar{\sigma} \times B \qquad (2.4)$$

These equations are equivalent to the equation (II.3.6) which we have used in our calculations.

Later other authors[26,27,28] obtained a covariant classical equation of motion for the polarization four-vector. Since polarization is the expectation value of the spin operator it should obey classical laws (Ehrenfest theorem). They start with the classical equation of motion in the rest system (R) of the particles :

$$\frac{d\bar{S}}{d\tau} = \frac{\mu^*}{m_0} \bar{S} \times B \qquad (2.5)$$

where $\bar{S}$ is the polarization vector, and τ is the proper time of the particle. In order to generalize this equation, a polarization four-vector (axial) is introduced :

$$S = (S_0, \bar{S}) \quad , S = (0, \bar{S}) \text{ in } (R) \qquad (2.6)$$

Also the particle motion is expressed by a velocity four-vector:

$$V = (v^0, \bar{v}) = \gamma (1, \bar{\beta}) \quad , V = (1,0) \text{ in } (R) \qquad (2.7)$$

One has the relationship :

$$S.V = S^0 v^0 - \bar{S} . \bar{v} = 0 \qquad (2.8)$$

Therefore

$$S^0 v^0 = \bar{S} . \bar{v} \qquad (2.9)$$

Since $\bar{v} = 0$ in (R) one has :

$$\frac{dS^0}{d\tau} = \bar{S} . \frac{d\bar{v}}{d\tau} \qquad (2.10)$$

If the particle is neutral $\frac{d\bar{v}}{d\tau} = 0$ and consequently one has :

$$\frac{dS^0}{d\tau} = 0 \qquad (2.11)$$

or

$$\frac{dS}{d\tau} = (0, \frac{\mu e}{mc} \bar{S} \times \bar{B}) \quad \text{in } (R) \qquad (2.12)$$

In terms of the skew-symmetric electromagnetic field tensor F and polarization four-vector, $\bar{S} \times \bar{B}$ can be written as :

$$(S \times B)_R = (SF)_R = (\bar{S}_R . \bar{E}, \bar{S}_R \times \bar{B}) \qquad (2.13)$$

i.e. $$\frac{dS}{d\tau} = (0, \frac{\mu e}{mc} (SF)_R) \equiv Z_R \qquad (2.14)$$

To obtain a general expression for Z one uses the properties of S_B : It is linear in both S and F . The only four-vectors with these properties which one can form from S, V and F are SF, V(SFV). Therefore one can write Z as follows

$$Z = a\,SF + b\,V(SFV) \tag{2.15}$$

or

$$S_B = \left\{ a(SF)^0_B + b(SF)^0_B,\ a(\overline{SF})_B \right\} \tag{2.16}$$

Comparing the equations (2.16) and (2.14) one gets :

$$a = \mu e / mc \qquad b = -\mu e / mc$$

Therefore the equation for $\dot{S}$ is :

$$\dot{S} = \frac{\mu e}{mc} \left[SF - V(SFV) \right] \tag{2.17}$$

This is the covariant equation of motion for an uncharged particle with an anomalous magnetic moment μ, in an electromagnetic field. To see that this equation leads to the equation (II.3.6) one first writes the covariant equation in the laboratory frame :

$$\dot{S}_L = \frac{\mu e}{mc} \left(SF \right)_L - V_L(SFV) \tag{2.18}$$

The polarization 4-vec-vector should always be considered in the rest frame, because its magnitude and direction depends on the frame. Therefore in order to obtain an equation with a physical meaning one expresses S_L in terms of $S_B = (0, \vec{S}_B)$ using the Lorentz transformation :

$$S_L = (a^0_L, S_L) = \left(\gamma\bar{\beta}\cdot S_R,\ S_R + \bar{\beta}\,\frac{\gamma^2}{\gamma+1}\,\bar{\beta}\cdot S_R\right) \qquad (D.19)$$

and

$$\dot{S}_L = (\dot{a}^0_L, \dot{a}^0_L) = \left(\gamma\bar{\beta}\cdot\dot{S}_R,\ \dot{S}_R + \bar{\beta}\,\frac{\gamma^2}{\gamma+1}\,\bar{\beta}\cdot\dot{S}_R\right) \qquad (D.20)$$

Also one has for zero electric field :

$$(\Omega V)_L = (0, S_L\times B) = \left\{0,\ \left(S_R + \bar{\beta}\,\frac{\gamma^2}{\gamma+1}\,\bar{\beta}\cdot S_R\right)\times B\right\} \qquad (D.21)$$

and

$$S\Omega V = \gamma(\bar{\beta}, B, S_L) = \gamma(\bar{\beta}, B, S_R) \qquad (D.22)$$

The last equation is written using equation (D.19). Substitution (D.20), (D.21), and (D.22) into the equation (D.18) one gets :

$$\left(\gamma\bar{\beta}\cdot\dot{S}_R,\ \dot{S}_R + \bar{\beta}\,\frac{\gamma^2}{\gamma+1}\,\bar{\beta}\cdot\dot{S}_R\right) = \frac{\mu e}{mc}\Big[-\gamma^2(\bar{\beta}, B, S_R),\ S_R\times B$$

$$+ \frac{\gamma^2}{\gamma+1}(\bar{\beta}\cdot S_R)\,\bar{\beta}\times B$$

$$- \gamma^2\bar{\beta}(\bar{\beta}, B, S_R)\Big] \qquad (D.23)$$

or

$$\dot{S}_R = \frac{\mu e}{mc}\left[S_R\times B + \frac{\gamma^2}{\gamma+1}(\bar{\beta}\cdot S_R)\,\bar{\beta}\times B - \frac{\gamma^2}{\gamma+1}\,\bar{\beta}(\bar{\beta}, B, S_R)\right] \qquad (D.24)$$

Using $\beta^2\gamma^2 = \gamma^2 - 1$ one obtains

$$\dot{S}_R = \frac{\mu e}{mc}\left[S_R\times B + \frac{\gamma-1}{\beta^2}(\bar{\beta}\cdot S_R)\,\bar{\beta}\times B - \frac{\gamma-1}{\beta^2}\,\bar{\beta}(\bar{\beta}, B, S_R)\right] \qquad (D.25)$$

Let $\bar{\beta} \times \bar{B} = \bar{A}$

Then

$$(\bar{\beta} \cdot \bar{E}_{\parallel})\bar{\beta} \times \bar{B} - \bar{\beta}(\bar{\beta} \cdot \bar{B}, \bar{E}_{\parallel}) = (\bar{\beta} \cdot \bar{E}_{\parallel})\bar{A} - (\bar{A} \cdot \bar{E}_{\parallel})\bar{\beta}$$

$$= \bar{E}_{\parallel} \times (\bar{A} \times \bar{\beta})$$

$$= \bar{E}_{\parallel} \times [(\bar{\beta} \times \bar{B}) \times \bar{\beta}]$$

$$= \bar{E}_{\parallel} \times [\beta^2 \bar{B} - (\bar{\beta} \cdot \bar{B})\bar{\beta}] \qquad (B.26)$$

Using the equation (B.26) equation (B.24) is put into the form :

$$\dot{\bar{\epsilon}}_{\parallel} = \frac{d\bar{p}_{\parallel}}{dT} = \frac{Mc}{ec} \bar{E}_{\parallel} \times \left[\gamma \bar{B} - (\gamma - 1)\frac{(\bar{\beta} \cdot \bar{B})}{\beta^2}\bar{\beta}\right] \qquad (B.27)$$

or

$$\frac{d\bar{p}_{\parallel}}{dt} = \frac{Mc}{ec} \bar{E}_{\parallel} \times \left[\bar{B} - \frac{\gamma - 1}{\gamma}\frac{\bar{\beta} \cdot \bar{B}}{\beta^2}\bar{\beta}\right] \qquad (B.28)$$

This is the same equation as the equation (II.3.6) which we have derived earlier in a simple way.

APPENDIX C

The solution of the precession equation

The equation to be solved is:

$$\frac{d\bar{S}}{dt} = \bar{S} \times \bar{\Omega} \qquad (C.1)$$

where

$$\bar{\Omega} = \frac{\mu_0}{2\rho} \left[\bar{S} - \frac{\gamma - 1}{\gamma} \frac{\bar{S} \cdot \bar{P}_{\lambda^0}}{P^2_{\lambda^0}} \bar{P}_{\lambda^0} \right] \qquad (C.2)$$

subject to the initial condition $\bar{S} = (0, P, 0)$ in the coordinate system defined by the equation (II.38). Writing the equation (C.1) in terms of the components one gets:

$$\frac{dS_1}{dt} = \Omega_3 S_2 - \Omega_2 S_3$$

$$\frac{dS_2}{dt} = \Omega_1 S_3 - \Omega_3 S_1 \qquad (C.3)$$

$$\frac{dS_3}{dt} = \Omega_2 S_1 - \Omega_1 S_2$$

This set of equations is very easy to solve in a coordinate system (primed) whose z-axis is along the direction $\vec{\Omega}$. In such a system they take the form:

$$\frac{dx_1'}{dt} = \Omega x_2'$$

$$\frac{dx_2'}{dt} = -\Omega x_1' \qquad (C.4)$$

$$\frac{dx_3'}{dt} = 0$$

The solutions are :

$$x_1' = A \cos \Omega t + B \sin \Omega t$$

$$x_2' = -A \sin \Omega t + B \cos \Omega t \qquad (C.5)$$

$$x_3' = C$$

The constants A, B, C are to be determined from the initial conditions.

One has to transform these components of the vector $\vec{x}$ into a general coordinate system in which the vector $\vec{\Omega}$ has components $\Omega_1, \Omega_2, \Omega_3$. The transformed components of $\vec{x}$ will be solutions of the equation (C.3).

In order to rotate the unprimed system to the primed system one first performs a rotation around the z-axis by an angle φ, and then another rotation around the new y-axis by

an angle Φ. The transformation matrix is :

$$\begin{matrix} \cos\Phi & 0 & -\sin\Phi \\ 0 & 1 & 0 \\ \sin\Phi & 0 & \cos\Phi \end{matrix} \quad \begin{matrix} \cos\varphi & \sin\varphi & 0 \\ -\sin\varphi & \cos\varphi & 0 \\ 0 & 0 & 1 \end{matrix} \quad = \quad \begin{matrix} \cos\Phi\cos\varphi & -\cos\Phi\sin\varphi & -\sin\Phi \\ -\sin\varphi & \cos\varphi & 0 \\ \sin\Phi\cos\varphi & -\sin\Phi\sin\varphi & \cos\Phi \end{matrix} \qquad (C.6)$$

The angles Φ and φ are related to the components of $\overline{\Omega}$ in the unprimed system as follows:

$$\varphi = \cos^{-1}(\Omega_1 / (\Omega^2_1 + \Omega^2_2)^{1/2})$$

$$\Phi = \cos^{-1}(\Omega_3 / \Omega) \qquad (C.7)$$

where

$$\Omega = (\Omega^2_1 + \Omega^2_2 + \Omega^2_3)^{1/2}$$

Therefore the initial condition in the unprimed system $(\bar{\Omega} = (t=0) = (0,0,\Omega))$ corresponds in the primed system to

$$\overline{\Omega}(t=0) = \begin{pmatrix} \frac{\Omega_3\Omega_1}{(\Omega^2_1+\Omega^2_2)^{1/2}\Omega} & \frac{\Omega_3\Omega_2}{\Omega(\Omega^2_1+\Omega^2_2)^{1/2}} & -\frac{(\Omega^2_1+\Omega^2_2)^{1/2}}{\Omega} \\ -\frac{\Omega_2}{(\Omega^2_1+\Omega^2_2)^{1/2}} & \frac{\Omega_1}{(\Omega^2_1+\Omega^2_2)^{1/2}} & 0 \\ \frac{\Omega_1}{\Omega} & \frac{\Omega_2}{\Omega} & \frac{\Omega_3}{\Omega} \end{pmatrix} \begin{pmatrix} 0 \\ 0 \\ \Omega \end{pmatrix} = \begin{pmatrix} \frac{\Omega_3\Omega_1}{(\Omega^2_1+\Omega^2_2)^{1/2}} \\ -\frac{\Omega_2}{(\Omega^2_1+\Omega^2_2)^{1/2}} \\ \frac{\Omega_3}{\Omega} \end{pmatrix}$$

Comparing this with the Equation (C.5) one obtains the constants as follows:

$$A = P\Omega_3\Omega_2\Omega^{-1}(\Omega_1^2+\Omega_2^2)^{1/2}$$

$$B = P\Omega_1(\Omega_1^2+\Omega_2^2)^{-1/2} \qquad (6.6)$$

$$C = \Omega_2\Omega^{-1}$$

The transpose of the matrix of the equation (6.6) will transform the components of $\vec{S}$ from the plane to the unperturbed system

$$\vec{S}(t) = \begin{pmatrix} \frac{\Omega_3\Omega_1}{(\Omega_1^2+\Omega_2^2)^{1/2}\Omega} & \frac{-\Omega_2}{(\Omega_1^2+\Omega_2^2)^{1/2}} & \frac{\Omega_1}{\Omega} \\ \frac{\Omega_3\Omega_2}{(\Omega_1^2+\Omega_2^2)^{1/2}\Omega} & \frac{\Omega_1}{(\Omega_1^2+\Omega_2^2)^{1/2}} & \frac{\Omega_2}{\Omega} \\ \frac{(\Omega_1^2+\Omega_2^2)^{1/2}}{\Omega} & 0 & \frac{\Omega_3}{\Omega} \end{pmatrix} \begin{pmatrix} \frac{\Omega_3\Omega_2}{(\Omega_1^2+\Omega_2^2)^{1/2}\Omega}\cos\Omega t + \frac{\Omega_1}{(\Omega_1^2+\Omega_2^2)^{1/2}}\sin\Omega t \\ \frac{\Omega_3\Omega_2}{(\Omega_1^2+\Omega_2^2)^{1/2}\Omega}\sin\Omega t - \frac{\Omega}{(\Omega_1^2+\Omega_2^2)^{1/2}}\cos\Omega t \\ \frac{\Omega_2}{\Omega} \end{pmatrix}$$

$$= \begin{pmatrix} -\frac{\Omega_3\Omega_2}{\Omega^2}\cos\Omega t + \frac{\Omega_1}{\Omega}\sin\Omega t + \frac{\Omega_1\Omega_2}{\Omega^2} \\ \frac{\Omega_1^2+\Omega_3^2}{\Omega^2}\cos\Omega t + \frac{\Omega_2^2}{\Omega^2} \\ -\frac{\Omega_3\Omega_2}{\Omega^2}\cos\Omega t - \frac{\Omega_1}{\Omega}\sin\Omega t + \frac{\Omega_1\Omega_2}{\Omega^2} \end{pmatrix}$$

$$= \frac{1}{\Omega^2} \begin{pmatrix} \Omega_1\Omega_2(1-\cos\Omega t) + \Omega\Omega_3\sin\Omega t \\ (\Omega_3^2 + \Omega_1^2)\cos\Omega t + \Omega_2^2 \\ \Omega_3\Omega_2(1-\cos\Omega t) - \Omega\Omega_1\sin\Omega t \end{pmatrix} \qquad (C.10)$$

In the coordinate system we have chosen $\bar{\Omega}$ is given as:

$$\bar{\Omega} = \frac{\mu_B}{\hbar} \left[\frac{1}{\gamma} B_1, B_2, B_3\right] \qquad (C.11)$$

It is seen that if $\bar{B}$ is perpendicular to $\bar{p}_\wedge$ and $\bar{B}_0$ which are approximately the case in this experiment, then one has

$$\bar{\Omega} = \frac{\mu_B}{\hbar} (0, 0, B) \qquad (C.12)$$

and

$$\bar{B}(t) = B \begin{bmatrix} \sin\Omega t \\ \cos\Omega t \\ 0 \end{bmatrix} \qquad (C.13)$$

which is the same as the equation (II.3.13).

APPENDIX D

The determination of the exact angular distribution in terms of the angles φ and ψ

One can write equation (II.4.2) in the following form:

$$d\sigma = \frac{1}{4\pi}\left(1+\alpha\frac{\vec{P}\cdot\vec{P}_D'}{P_D'^2}\right)d\Omega \qquad (D.1)$$

where $\vec{P}$ is the polarization vector and $\vec{P}_D'$ is the proton recoil vector in the center of mass $d\Omega$ is the differential solid angle element. The scalar product can be written using the components in the reference system defined by equation (II.3.6)[2] :

$$N(\varphi,\psi)\sin\varphi\,d\varphi\,d\psi = \frac{1}{4\pi}\left[1+\alpha(P_1\cos\psi\sin\varphi+P_2\cos\psi\cos\varphi+P_y\sin\psi)\right]d\varphi\,d\sin\psi \qquad (D.2)$$

One can put this equation into the following form:

$$N(\varphi,\psi)\sin\varphi\,d\varphi\,d\psi = \frac{1}{4\pi}\left[1+\alpha P_y\sin\psi+\alpha\cos\psi(P_1\sin\varphi+P_2\cos\varphi)\right]d\varphi\,d\sin\psi$$

$$= \frac{1}{4\pi}\left[1+\alpha P_y\sin\psi+\alpha\cos\psi P_2(\tan\varphi_0\sin\varphi+\cos\varphi)\right]d\varphi\,d\sin\psi$$

---

[2]

$$= \frac{1}{4\pi}\left[1+\alpha_3\sin\psi+\alpha\cos\beta\frac{\delta_2}{\cos\varphi_0}\cos(\varphi-\varphi_0)\right]\sin\psi\,d\varphi\,d\psi$$

$$= \frac{1}{4\pi}\left[1+\alpha_3\sin\psi+\alpha P\cos(\varphi-\varphi_0)\cos\psi\right]d\varphi\,d\sin\psi \qquad (D.3)$$

where

$$P = \frac{\delta_2}{P\cos\varphi_0}\cdot\frac{\sqrt{\delta_1^2+\delta_3^2}}{P}\cdot\frac{\sqrt{P^2-\delta_3^2}}{P} = \sqrt{1-\left(\frac{\delta_3}{P}\right)^2}\left\{1-\left[\beta_1\sin\theta-\beta_2(\beta_3-\cos\theta)\right]^2\right\}^{1/2} \qquad (D.4)$$

This is the generalized form of the equation (II.4.4) and reduces to it for $\alpha_3 = 0$.

APPENDIX B

DERIVATION OF THE STATISTICAL ERROR ON THE ANGLE φ_o USING THE ASYMMETRIES IN THE DECAY

The final direction of polarization of Λ^0 can be determined by measuring the decay asymmetry with respect to three planes which are perpendicular to each other, in the center of mass system of the particle. Considering an arbitrary plane, defined by a unit vector $\hat{\mathbf{i}}$ normal to the plane, $A(\hat{\mathbf{i}})$, the asymmetry with respect to this plane is defined as follows:

$$A(\hat{\mathbf{i}}) = \frac{N(+) - N(-)}{N(+) + N(-)} \qquad (B.1)$$

where $N(\pm)$ is the number of decays in the half-space corresponding to the direction $\pm\,\hat{\mathbf{i}}$.

Using the equations (II.4.4) and (B.1) one can obtain the angle of precession φ_o in terms of the asymmetries A_x, A_z and A_y:

$$\tan\varphi_0 = \frac{\sqrt{A_1^2 + A_3^2}}{A_2} \tag{2.6}$$

where:

A_1 = forward - backward asymmetry

A_2 = left-right asymmetry

A_3 = up-down asymmetry

Let $u = \tan\varphi_0$, $\delta\varphi_0$, the error in φ_0 is given in terms of δu, the error in u, as follows:

$$\delta\varphi_0 = \frac{\partial\varphi_0}{\partial u}\,\delta u \tag{2.5}$$

One has

$$\frac{\partial\varphi_0}{\partial u} = \frac{1}{1+u^2} \tag{2.4}$$

and

$$(\delta u)^2 = \left(\frac{\partial u}{\partial A_1}\right)^2(\delta A_1)^2 + \left(\frac{\partial u}{\partial A_2}\right)^2(\delta A_2)^2 + \left(\frac{\partial u}{\partial A_3}\right)^2(\delta A_3)^2 \tag{2.3}$$

One obtains the derivatives of u as follows:

$$\frac{\partial u}{\partial A_1} = \frac{A_1}{A_2\left(A_1^2 + A_3^2\right)^{1/2}} \tag{2.8}$$

$$\frac{\partial u}{\partial A_2} = -\frac{\left(A_1^2 + A_3^2\right)^{1/2}}{A_2^2} \tag{2.7}$$

$$\frac{\partial u}{\partial A_3} = \frac{A_3}{A_2\left(A_1^2 + A_3^2\right)^{1/2}} \tag{2.9}$$

The statistical errors δA_1, δA_2 and δA_3 are

$$(\delta A_1)^2 = \left(\frac{\partial A_1}{\partial N_1(+)}\right)^2 (\delta N_1(+))^2 + \left(\frac{\partial A_1}{\partial N_1(-)}\right)^2 (\delta N_1(-))^2 \qquad (3.9)$$

Since $N_1(+) = N_1 - N_1(-)$ the derivatives are

$$\frac{\partial A_1}{\partial N_1(+)} = -\frac{\partial A_1}{\partial N_1(-)} = \frac{1}{N_1} \qquad (3.10)$$

The statistical errors on $N_1(+)$ and $N_1(-)$ are

$$\delta N_1(+) = \sqrt{N_1(+)} \qquad (3.11)$$

$$\delta N_1(-) = \sqrt{N_1(-)}$$

Substituting these into (3.9) we get :

$$(\delta A_1)^2 = \frac{1}{N_1^2} N_1(+) + \frac{1}{N_1^2} N_1(-) \qquad (3.12)$$

or

$$(\delta A_1)^2 = \frac{1}{N_1} \qquad (3.13)$$

The error in u is from equation (3.5)

$$\delta u = \left[\frac{A_1^2}{A_3^2(A_1^2 + A_3^2)} + \frac{A_1^2 + A_2^2}{A_2^4} + \frac{A_2^2}{A_3^2(A_1^2 + A_3^2)}\right]^{1/2} \frac{1}{n^{1/2}} \qquad (3.14)$$

Simplifying this we get:

$$\delta u = \frac{(A_1^2 + A_2^2 + A_3^2)^{1/2}}{n^{1/2} A_3^2} \qquad (3.15)$$

The error in φ_0 is from Eqs. (3.3) and (3.4)

$$\delta\varphi_0 = \frac{1}{1+\frac{A_1^2+A_2^2}{4\xi_2^2}} \frac{(A_1^2+A_2^2+A_3^2)^{1/2}}{n^{1/2}\xi_2^2} = \frac{1}{n^{1/2}(A_1^2+A_2^2+A_3^2)^{1/2}} \tag{11.26}$$

Using the definition $A(\bar{1}) = \frac{\Pi(+)-\Pi(-)}{\Pi(+)+\Pi(-)}$ and the formula (10.4.4) to calculate

$$\Pi(+) \text{ and } \Pi(-)$$

one obtains:

$$A(\bar{1}) = \frac{2}{\pi}\lambda\propto S_0\bar{1} \tag{11.27}$$

If A is measured with respect to three planes defined by the three mutually perpendicular unit vectors $\bar{1}$, $\bar{j}$, $\bar{k}$, $A(\bar{1})$, $A(\bar{j})$ $A(\bar{k})$ are the components of a vector $\bar{A}$ such that

Hence $$\bar{A} = \frac{2}{\pi}\lambda\propto\bar{S} \tag{11.28}$$

$$\delta\varphi_0 \simeq \frac{1}{n^{1/2}\frac{2}{\pi}\lambda\propto P} \tag{11.29}$$

i.e. the error in φ_0 decreases with increasing number of events and increasing polarisation.

APPENDIX F

CHOOSING THE CUT-OFF FOR THE ANGLE ψ_o

The statistical error on the angle φ_o is given by the equation (XI.3.7):

$$\delta\varphi_o \simeq \frac{2}{\lambda \alpha P B^{1/2}}$$

We want to find the cut-off angle ψ_o for which $\delta\varphi_o$ will be minimum. $\delta\varphi_o$ is a function of ψ_o through λ and B. To minimize $\delta\varphi_o$ we equate its derivative with respect to ψ_o to zero:

$$\frac{\partial \delta\varphi_o}{\partial \psi_o} = \frac{\partial \delta\varphi_o}{\partial B} \frac{\partial B}{\partial \psi_o} + \frac{\partial \delta\varphi_o}{\partial \lambda} \frac{\partial \lambda}{\partial \psi_o} = 0 \qquad (F.1)$$

One has

$$\frac{\partial \delta\varphi_o}{\partial B} = -\frac{1}{\lambda \alpha P B^{3/2}} \qquad (F.2)$$

and

$$\frac{\partial \delta\varphi_o}{\partial\lambda} = -\frac{2}{\alpha P \sqrt{N}\, \lambda^2} \qquad \text{(F.3)}$$

N and λ are given by the equations (II.4.5) and (II.4.6) respectively:

$$N(\varphi/\psi_o)d\varphi = \frac{1}{2\pi}\, \sin\psi_o \left\{1 - \alpha P \lambda \sin(\varphi - \varphi_o)\right\} d\varphi$$

$$\lambda = \frac{1}{2}\left(\cos\psi_o + \frac{\psi_o}{\sin\psi_o}\right)$$

Integrating the first equation over φ one gets the total N :

$$N(\psi_o) = \frac{1}{2\pi}\, \sin\psi_o \left[\varphi + \frac{1}{\lambda\alpha P}\, \cos(\varphi - \varphi_o)\right]_0^{2\pi}$$

$$= \sin\psi_o \qquad \text{(F.4)}$$

Differentiating N and λ with respect to ψ_o one obtains the following :

$$\frac{dN}{d\psi_o} = \cos\psi_o \qquad \text{(F.5)}$$

$$\frac{d\lambda}{d\psi_o} = \frac{1}{2}\left(-\sin\psi_o + \frac{\sin\psi_o - \psi_o\cos\psi_o}{\sin^2\psi_o}\right) \qquad \text{(F.6)}$$

Substituting (F.2), (F.3), (F.5) and (F.6) into (F.1) one gets

$$-\frac{\cos\psi_o}{\sin\psi_o} = \frac{2}{\cos\psi_o + \frac{\psi_o}{\sin\psi_o}}\left(\frac{1}{\sin\psi_o} - \sin\psi_o - \psi_o\frac{\cos\psi_o}{\sin^2\psi_o}\right) \qquad \text{(F.7)}$$

APPENDIX A

OBTAINING AN ANALYTICAL CURVE FOR THE σ^2- β CALIBRATION

A.1. Fitting of the curve $\sigma^2 = a + b/\beta^c$ to the experimental points:

One has to minimize the sum of the weighed squares of the deviations between the fitted and measured quantities:

$$\chi^2 = \sum_i \frac{(\sigma_i^2 - a - b/\beta_i^c)^2}{(\delta \sigma_i^2)^2} \qquad (A.1.1)$$

where σ_i^2 and β_i are the measured quantities and $(\delta \sigma_i^2)^2$ is the error in the σ_i^2 measurement. Minimization should be done with respect to the 3 parameters a, b, and c. But the derivative with respect to c is such that it becomes too complicated to solve for a, b, c simultaneously. Therefore what one does is the following:

First χ^2 of the logarithm of the above equation is minimized with respect to b and c, assuming a constant. Let:

$$y = \beta^c = a = b/\beta^c \qquad (3.1.2)$$

Take the logarithm:

$$\log y = \log b - c \log \beta \qquad (3.1.3)$$

Let:

$$\chi^2_{\log} = \sum_i \frac{(\log y_i - \log b + c \log \beta_i)^2}{(\delta \log y_i)^2} \qquad (3.1.4)$$

The derivatives of $\chi^2_{\log}$ with respect to the parameters log b and c are equated to zero:

$$\frac{\partial \chi^2}{\partial (\log b)} = \sum_i - \frac{2(\log y_i - \log b + c \log \beta_i)}{(\delta \log y_i)^2} = 0 \qquad (3.1.5)$$

or

$$\sum_i \frac{\log b}{(\delta \log y_i)^2} - c \sum_i \frac{\log \beta_i}{(\delta \log y_i)^2} = \sum_i \frac{\log y_i}{(\delta \log y_i)^2} \qquad (3.1.6)$$

$$\frac{\partial \chi^2}{\partial c} = \sum_i \frac{2 \log \beta_i (\log y_i - \log b + c \log \beta_i)}{(\delta \log y_i)^2} = 0 \qquad (3.1.7)$$

or

$$\log b \sum_i \frac{\log \beta_i}{(\delta \log y_i)^2} - c \sum_i \frac{(\log \beta_i)^2}{(\delta \log y_i)^2} = \sum_i \frac{(\log \beta_i)(\log y_i)}{(\delta \log y_i)^2} \qquad (3.1.8)$$

One can write (3.1.6) and (3.1.8) as a matrix equation:

$$\begin{pmatrix} \sum_i \frac{1}{(\delta \log y_i)^2} & -\sum_i \frac{\log \beta_i}{(\delta \log y_i)^2} \\ \sum_i \frac{\log \beta_i}{(\delta \log y_i)^2} & -\sum_i \frac{(\log \beta_i)^2}{(\delta \log y_i)^2} \end{pmatrix} \begin{pmatrix} \log b \\ a \end{pmatrix} = \begin{pmatrix} \sum_i \frac{\log y_i}{(\delta \log y_i)^2} \\ \sum_i \frac{(\log \beta_i)(\log y_i)}{(\delta \log y_i)^2} \end{pmatrix}$$

(6.1.9)

Define

$$S_1 = \sum_i \frac{\log \beta_i}{(\delta \log y_i)^2}$$

$$S_2 = \sum_i \frac{(\log \beta_i)^2}{(\delta \log y_i)^2} \qquad (6.1.10)$$

$$S_3 = \sum_i \frac{1}{(\delta \log y_i)^2}$$

$$S_4 = \sum_i \frac{(\log \beta_i)(\log y_i)}{(\delta \log y_i)^2}$$

$$S_5 = \sum_i \frac{\log y_i}{(\delta \log y_i)^2}$$

(6.1.9) takes the form

$$\begin{bmatrix} S_3 & -S_1 \\ S_1 & -S_2 \end{bmatrix} \begin{bmatrix} \log b \\ a \end{bmatrix} = \begin{bmatrix} S_5 \\ S_4 \end{bmatrix} \qquad (6.1.11)$$

Solution of this matrix equation is :

$$\log b = \frac{\begin{vmatrix} s_3 & -s_1 \\ c_4 & -s_2 \end{vmatrix}}{\begin{vmatrix} c_3 & -s_1 \\ c_2 & -s_2 \end{vmatrix}} \qquad (3.1.12)$$

$$a = \frac{\begin{vmatrix} c_3 & -s_3 \\ c_2 & -s_4 \end{vmatrix}}{\begin{vmatrix} c_3 & -s_1 \\ c_2 & -s_2 \end{vmatrix}}$$

Now taking the value of c calculated from (3.1.12) as a constant, χ^2 is minimised with respect to a and b :

$$\frac{\partial \chi^2}{\partial a} = \sum_i \frac{-2(c_i^m - a - b/\beta_i^o)}{(\delta c_i^m)^2} = 0 \qquad (3.1.13)$$

$$\frac{\partial \chi^2}{\partial b} = \sum_i \frac{-\frac{2}{\beta_i^o}(c_i^m - a - b/\beta_i^o)}{(\delta c_i^m)^2} = 0 \qquad (3.1.14)$$

or :

$$a\sum_i \frac{1}{(\delta c_i^m)^2} + b\sum_i \frac{1}{\beta_i^o(\delta c_i^m)^2} = \sum_i \frac{g_i^*}{(\delta c_i^m)^2} \qquad (3.1.15)$$

$$a\sum_i \frac{1}{\beta_i^o(\delta c_i^m)^2} + b\sum_i \frac{1}{\beta_i^{2o}(\delta c_i^m)^2} = \sum_i \frac{c_i^m}{\beta_i^o(\delta c_i^m)^2} \qquad (3.1.16)$$

These two equations are equivalent to :

$$\begin{pmatrix} \sum_i \frac{1}{(\delta c_i^x)^2} & \sum_i \frac{1}{\beta_i^o (\delta c_i^x)^2} \\ \sum_i \frac{1}{\beta_i^o (\delta c_i^x)^2} & \sum_i \frac{1}{\beta_i^{2o} (\delta c_i^x)^2} \end{pmatrix} \begin{pmatrix} a \\ b \end{pmatrix} = \begin{pmatrix} \sum_i \frac{c_i^x}{(\delta c_i^x)^2} \\ \sum_i \frac{c_i^x}{\beta_i^o (\delta c_i^x)^2} \end{pmatrix} \tag{4.2.27}$$

Define:

$$a_6 = \sum_i \frac{1}{\beta_i^{2o} (\delta c_i^x)^2}$$

$$a_7 = \sum_i \frac{1}{(\delta c_i^x)^2}$$

$$a_8 = \sum_i \frac{1}{\beta_i^o (\delta c_i^x)^2} \tag{4.2.28}$$

$$a_9 = \sum_i \frac{c_i^x}{(\delta c_i^x)^2}$$

$$a_{10} = \sum_i \frac{c_i^x}{\beta_i^o (\delta c_i^x)^2}$$

(4.2.27) takes the form:

$$\begin{bmatrix} s_7 & s_8 \\ s_8 & s_6 \end{bmatrix} \begin{bmatrix} a \\ b \end{bmatrix} = \begin{bmatrix} s_9 \\ s_{10} \end{bmatrix} \qquad (3.1.3)$$

The solution is :

$$a = \frac{\begin{vmatrix} s_9 & s_8 \\ s_{10} & s_6 \end{vmatrix}}{\begin{vmatrix} s_7 & s_8 \\ s_8 & s_6 \end{vmatrix}}, \qquad b = \frac{\begin{vmatrix} s_7 & s_9 \\ s_8 & s_{10} \end{vmatrix}}{\begin{vmatrix} s_7 & s_8 \\ s_8 & s_6 \end{vmatrix}} \qquad (3.1.30)$$

The value of a calculated here is substituted as the constant a in (3.1.2) and this procedure is repeated until a small enough χ^2 is obtained.

3.2. Fitting of the curve $\log \varepsilon^2 = a + b \log\beta + c(\log\beta)^2$ to the experimental points:

The sum of the weighted squares of deviations is :

$$\chi^2 = \sum_i \frac{\left(\log \varepsilon_i^2 - a - b \log\beta_i - c(\log\beta_i)^2\right)^2}{(\delta \log \varepsilon_i)^2} \qquad (3.2.1)$$

One minimizes this with respect to the parameters a, b and c :

$$\frac{\partial \chi^2}{\partial a} = \sum_i \frac{-(\log G_i^E - a - b \log \beta_i - c(\log \beta_i)^2)}{(\delta \log G_i^E)^2} = 0 \qquad (3.2.2)$$

$$\frac{\partial \chi^2}{\partial b} = \sum_i \frac{-\log \beta_i (\log G_i^E - a - b \log \beta_i - c(\log \beta_i)^2}{(\delta \log G_i^E)^2} = 0 \qquad (3.2.3)$$

$$\frac{\partial \chi^2}{\partial c} = \sum_i \frac{-(\log \beta_i)^2 (\log G_i^E - a - b \log \beta_i - c(\log \beta_i)^2)}{(\delta \log G_i^E)^2} = 0 \qquad (3.2.4)$$

These three equations are equivalent to the matrix equation:

$$\begin{pmatrix} \sum_i \frac{1}{(\delta \log G_i^E)^2} & \sum_i \frac{\log \beta_i}{(\delta \log G_i^E)^2} & \sum_i \frac{(\log \beta_i)^2}{(\delta \log G_i^E)^2} \\ \sum_i \frac{\log \beta_i}{(\delta \log G_i^E)^2} & \sum_i \frac{(\log \beta_i)^2}{(\delta \log G_i^E)^2} & \sum_i \frac{(\log \beta_i)^3}{(\delta \log G_i^E)^2} \\ \sum_i \frac{(\log \beta_i)^2}{(\delta \log G_i^E)^2} & \sum_i \frac{(\log \beta_i)^3}{(\delta \log G_i^E)^2} & \sum_i \frac{(\log \beta_i)^4}{(\delta \log G_i^E)^2} \end{pmatrix} \begin{pmatrix} a \\ b \\ c \end{pmatrix}$$

$$= \begin{pmatrix} \sum_i \frac{\log G_i^E}{(\delta \log G_i^E)^2} \\ \sum_i \frac{(\log G_i^E)(\log \beta_i)}{(\delta \log G_i^E)^2} \\ \sum_i \frac{(\log G_i^E)(\log \beta_i)^2}{(\delta \log G_i^E)^2} \end{pmatrix} \qquad (3.2.5)$$

Definition

$$S_1 = \sum_i \frac{1}{(\delta \log \sigma_i^2)^2} \qquad (4.2.6)$$

$$S_2 = \sum_i \frac{\log \beta_i}{(\delta \log \sigma_i^2)^2}$$

$$S_3 = \sum_i \frac{(\log \beta_i)^2}{(\delta \log \sigma_i^2)^2}$$

$$S_4 = \sum_i \frac{(\log \beta_i)^3}{(\delta \log \sigma_i^2)^2} \qquad (4.$$

$$S_5 = \sum_i \frac{(\log \beta_i)^4}{(\delta \log \sigma_i^2)^2}$$

$$S_6 = \sum_i \frac{\log \sigma_i^2}{(\delta \log \sigma_i^2)^2}$$

$$S_7 = \sum_i \frac{(\log \sigma_i^2)(\log \beta_i)}{(\delta \log \sigma_i^2)^2}$$

$$S_8 = \sum_i \frac{(\log \sigma_i^2)(\log \beta_i)^2}{(\delta \log \sigma_i^2)^2}$$

(4.2.5) takes the form :

$$\begin{bmatrix} S_1 & S_2 & S_3 \\ S_2 & S_3 & S_4 \\ S_3 & S_4 & S_5 \end{bmatrix} \begin{bmatrix} a \\ b \\ c \end{bmatrix} = \begin{bmatrix} S_6 \\ S_7 \\ S_8 \end{bmatrix} \qquad (4.2.7)$$

The solution is :

$$a = \frac{\begin{vmatrix} s_0 & s_2 & s_3 \\ s_1 & s_3 & s_4 \\ s_2 & s_4 & s_5 \end{vmatrix}}{\begin{vmatrix} s_1 & s_2 & s_3 \\ s_2 & s_3 & s_4 \\ s_3 & s_4 & s_5 \end{vmatrix}}$$

$$b = \frac{\begin{vmatrix} s_1 & s_0 & s_3 \\ s_2 & s_1 & s_4 \\ s_3 & s_2 & s_5 \end{vmatrix}}{\begin{vmatrix} s_1 & s_2 & s_3 \\ s_2 & s_3 & s_4 \\ s_3 & s_4 & s_5 \end{vmatrix}} \qquad (4.2.8)$$

$$c = \frac{\begin{vmatrix} s_1 & s_2 & s_0 \\ s_2 & s_3 & s_1 \\ s_3 & s_4 & s_2 \end{vmatrix}}{\begin{vmatrix} s_1 & s_2 & s_3 \\ s_2 & s_3 & s_4 \\ s_3 & s_4 & s_5 \end{vmatrix}}$$

The errors $(\delta c_1^*)^2$ and $(\delta \log c_1^*)^2$ are calculated as follows:

The normalised grain density, g^N, is defined as:

$$g^N = \frac{n}{n^0} \qquad (6.7.9)$$

where n and n^0 are the number of grains counted on equal length of particle and relativistic electron tracks. The error in g^N will be due to the errors on n and n^0. These errors are quadratically combined to give the error in g :

$$\frac{\delta g^N}{g^N} = \left(\left(\frac{\delta n^0}{n^0} \right)^2 + \left(\frac{\delta n}{n} \right)^2 \right)^{1/2}$$

or

$$\delta g^N = g^N \left(\left(\frac{\delta n^0}{n^0} \right)^2 + \left(\frac{\delta n}{n} \right)^2 \right)^{1/2} \qquad (6.7.10)$$

Assuming a Poisson distribution for the grain counts δn^0 and δn will be proportional to the square root of the number of grains counted. $\delta \log g_1^N$ is obtained as follows :

$$\frac{\delta \log g_1^N}{\delta g_1^N} = \frac{1}{g_1^N}$$

or

$$\delta \log g_1^N = \frac{\delta g_1^N}{g_1^N} \qquad (6.7.11)$$

APPENDIX E

LEAST SQUARES FITTING TO THE Λ^0 DECAY KINEMATICS

For each event which we suspect of being a Λ^0 decay we measure the plane and dip angles and momenta of both tracks. From the plane and dip angles one can calculate the space opening angle. If Θ is the space, δ is the dip and α is the plane opening angle, it can be easily shown that:

$$\cos\Theta = \sin\delta_p \sin\delta_\pi + \cos\delta_p \cos\delta_\pi \cos\alpha \qquad (E.1)$$

In a Λ^0 decay we therefore have only one unknown momentum of the Λ^0. The number of constraint equations is two: Conservation of momentum and conservation of energy:

$$p^2_{\Lambda^0} = p^2_p + p^2_\pi + 2\, p_p p_\pi \cos\Theta \qquad (E.2)$$

$$\left(p^2_{\Lambda^0} + m^2_{\Lambda^0}\right)^{1/2} = \left(p^2_p + m^2_p\right)^{1/2} + \left(p^2_\pi + m^2_\pi\right)^2 \qquad (E.3)$$

One unknown and two constraints mean a 1-C fit. We can

eliminate P_{Λ^0}. From the two equations above and get the only constraint equation:

$$(P_p, P_\pi, \theta) = A + P_p P_\pi \cos\theta - \left((P_p^2 + m_p^2)(P_\pi^2 + m_\pi^2)\right)^{1/2} = 0 \quad (II.4)$$

where $$A = \frac{m_{\Lambda^0}^2 - m_p^2 - m_\pi^2}{2}$$

We want to minimize

$$\chi^2(P_p, P_\pi, \theta) = \frac{(P_p - P_p^0)^2}{(\delta P_p)^2} + \frac{(P_\pi - P_\pi^0)^2}{(\delta P_\pi)^2} + \frac{(\theta - \theta^0)^2}{(\delta\theta)^2} \quad (II.5)$$

subject to the constraint given by (II.4).

In (II.5) the superscript 0 refers to the measured quantities.

One way to do the minimization as well as satisfying the constraint is to multiply (II.4) by a Lagrange multiplier α, to be determined in the process and add to (II.5); we then minimize

$$\chi^2 (P_p, P_\pi, \theta,) = \frac{(P_p - P_p^0)^2}{(\delta P_p)^2} + \frac{(P_\pi - P_\pi^0)^2}{(\delta P_\pi)^2} + \frac{(\theta - \theta^0)^2}{\delta\theta^2}$$

$$+ 2\alpha(A + P_p P_\pi \cos\theta - \left((P_p^2 + m_p^2)(P^2 + m^2)\right)^{1/2}) \quad / \quad (II.6)$$

Equate the derivatives with respect to P_p, P_π, θ to zero:

$$\frac{\partial \chi^2}{\partial P_p} = 2\left[\frac{P_p - P_p^0}{(\delta P_p)^2} + \alpha P_\pi \cos\theta - \frac{\alpha P_p \left(P^2 + m^2\right)^{1/2}}{\left(P_p^2 + m_p^2\right)^{1/2}}\right] = 0 \quad (II.7)$$

$$\frac{\partial \chi^2}{\partial p_\pi} = 2\left[\frac{p_\pi - p_\pi^0}{(\delta p_\pi)^2} + \alpha p_p \cos\theta - \frac{p_\pi (p_p^2 + m_p^2)^{1/2}}{(p_\pi^2 + m_\pi^2)^{1/2}}\right] = 0 \qquad (4.8)$$

$$\frac{\partial \chi^2}{\partial \theta} = 2\left[\frac{\theta - \theta^0}{(\delta\theta)^2} - p_p p_\pi \sin\theta\right] = 0 \qquad (4.9)$$

From the three equations above we can solve for p_p, p_π and θ. In order to reduce χ^2 further we have to repeat the calculations. A superscript ν means that this value has been derived in the ν-th iteration.

$$p_p^{\nu+1} = p_p^0 + (\delta p_p)^2 (p_p^\nu - p_\pi^\nu (E_p^\nu)^{-1} - p_\pi^\nu \cos\theta^\nu)\alpha^{\nu+1} \qquad (4.10)$$

$$p_\pi^{\nu+1} = p_\pi^0 + (\delta p_\pi)^2 (p_\pi^\nu - p_p^\nu (E_\pi^\nu)^{-1} - p_p^\nu \cos\theta^\nu)\alpha^{\nu+1} \qquad (4.11)$$

$$\theta^{\nu+1} = \theta^0 + (\delta\theta)^2 p_p^\nu p_\pi^\nu \sin\theta^\nu \alpha^{\nu+1} \qquad (4.12)$$

where $E = (m^2 + p^2)^{1/2}$ is the energy of each particle.

In order to eliminate $\alpha^{\nu+1}$ we expand the constraint equation :

$$f(p_p^{\nu+1}, p_\pi^{\nu+1}, \theta^{\nu+1}) = f(p_p^\nu, p_\pi^\nu, \theta^\nu) + \frac{\partial f(p_p^\nu, p_\pi^\nu, \theta^\nu)}{\partial p_p^\nu}(p_p^{\nu+1} - p_p^\nu)$$

$$+ \frac{\partial f(p_p^\nu, p_\pi^\nu, \theta^\nu)}{\partial p_\pi^\nu}(p_\pi^{\nu+1} - p_\pi^\nu)$$

$$+ \frac{\partial f(p_p^\nu, p_\pi^\nu, \theta^\nu)}{\partial \theta^\nu}(\theta^{\nu+1} - \theta^\nu) \qquad (4.13)$$

or

$$A+p_p^{\nu}p_\pi^{\nu}\cos\theta^{\nu}-\alpha^{\nu}p_p^{\nu}E_\pi^{\nu}+(p_\pi^{\nu}\cos\theta^{\nu}-p_p^{\nu}\frac{E_\pi^{\nu}}{E_p^{\nu}})(p_p^{\nu+2}-p_p^{\nu})+(p_p^{\nu}\cos\theta^{\nu}-p_\pi^{\nu}\frac{E_p^{\nu}}{E_\pi^{\nu}})(p_\pi^{\nu+2}-p_\pi^{\nu})$$

$$-p_p^{\nu}p_\pi^{\nu}\sin\theta^{\nu}(\theta^{\nu+2}-\theta^{\nu})=0 \qquad (II.14)$$

Substituting for $p_p^{\nu+2}$, $p_\pi^{\nu+2}$, $\theta^{\nu+2}$ from the equations (II.10), (II.11), (II.12) respectively we get :

$$A+p_p^{\nu}p_\pi^{\nu}\cos\theta^{\nu}-\alpha^{\nu}p_p^{\nu}E_\pi^{\nu}+(p_\pi^{\nu}\cos\theta^{\nu}-p_\pi^{\nu}\frac{E_\pi^{\nu}}{E_p^{\nu}})(p_p^{0}-p_p^{\nu}+(\delta p_p)^2(p_p^{\nu}\frac{E_\pi^{\nu}}{E_p^{\nu}}-p_\pi^{\nu}\cos\theta^{\nu})\alpha^{\nu+1}$$

$$+(p_p^{\nu}\cos\theta^{\nu}-p_\pi^{\nu}\frac{E_p^{\nu}}{E_\pi^{\nu}})(p_\pi^{0}-p_\pi^{\nu}+(\frac{\delta}{\delta p_\pi})^2(p_\pi^{\nu}\frac{E_p^{\nu}}{E_\pi^{\nu}}-p_p^{\nu}\cos\theta^{\nu})\alpha^{\nu+1})$$

$$-p_p^{\nu}p_\pi^{\nu}\sin\theta^{\nu}(\theta^{0}-\theta^{\nu}+(\delta\theta)^2p_p^{\nu}p_\pi^{\nu}\sin\theta^{\nu}\alpha^{\nu+2})=0 \qquad (II.15)$$

From (II.13) we can solve for $\alpha^{\nu+1}$:

$$\alpha^{\nu+1}=\Big[A+p_p^{\nu}p_\pi^{\nu}\cos\theta^{\nu}-\alpha^{\nu}p_p^{\nu}E_\pi^{\nu}+(p_\pi^{\nu}\cos\theta^{\nu}-p_p^{\nu}E_\pi^{\nu}/E_p^{\nu})(p_p^{0}-p_p^{\nu})$$

$$+(p_p^{\nu}\cos\theta^{\nu}-p_\pi^{\nu}E_p^{\nu}/E_\pi^{\nu})(p_\pi^{0}-p_\pi^{\nu})-p_p^{\nu}p_\pi^{\nu}\sin\theta^{\nu}(\theta^{0}-\theta)\Big]\Big/$$

$$\Big[(p_p^{\nu}E_\pi^{\nu}/E_p^{\nu}-p_\pi^{\nu}\cos\theta^{\nu})^2(\delta p_p)^2+(p_\pi^{\nu}E_p^{\nu}/E_\pi^{\nu}-p_p^{\nu}\cos\theta^{\nu})^2(\delta p_\pi)^2$$

$$+p_p^{\nu 2}p_\pi^{\nu 2}\sin^2\theta^{\nu}(\delta\theta)^2\Big] \qquad (II.16)$$

By substituting $\alpha^{\nu+1}$ back into the equations (II.10), (II.11) and (II.12), $p_p^{\nu+2}$, $p_\pi^{\nu+2}$ and $\theta^{\nu+1}$ can be calculated.

APPENDIX I

DETERMINATION OF THE PRODUCTION POINT OF Λ^0 IN THE CHAMBER

The coordinates of the decay vertex of Λ^0 were measured in a coordinate system[x] whose x' - y' plane is the emulsion plane and z' is the direction perpendicular to it. Let the measurements in such a system whose origin is at the center of the stack be x', y' and z' (y' is measured in degrees). In another coordinate system whose origin is at the center of the target and x'' axis along the symmetry axis of the experiment the coordinates of the decay vertex can be written as follows

$$x'' = (110 + x') \cos 20^0 - z \sin 20^0 \qquad (I.1)$$

$$y'' = (210 + x') y' \pi/180 \qquad (I.2)$$

$$z'' = (110 + x') \sin 20^0 + z' \cos 20^0 \qquad (I.3)$$

y'' is measured along a circular arc whose center is at the target center. The last expression is correct for only the set of

---

x See Figure 2.

stack), placed at one side of the initial π^- beam(positive x' side). For the other set x' is equal to the negative of the expression. In the calculations x' was taken always positive. This means rotating the second stack around x' by 180^0. Thus the magnetic field in this stack becomes opposite in the direction, which makes the polarization rotate in the opposite direction. Therefore in order to combine the angular distributions of odd and even numbered stacks one has to subtract the angles in one set of stacks from 2π .

The magnitude of the Λ^0-momentum at the decay vertex is calculated from the conservation of momentum:

$$P_{\Lambda^0} = (P_\pi^2 + P_p^2 - 2 P_p P_\pi \cos\theta)^{1/2} \qquad (I.4)$$

where θ is the space opening angle.

From the conservation of momentum in the x' direction one gets:

$$P_{\Lambda^0} \sin\delta_{\Lambda^0} = P_p \sin\delta_p + P_\pi \sin\delta_\pi \qquad (I.5)$$

where δ's are the dip angles and from which one can calculate δ_{Λ^0} , the dip angle of Λ^0.

The projection of Λ^0-momentum into the x'-y' plane is given by:

$$P'_{\Lambda^0} = (P_\pi^2 \cos^2\delta_\pi + P_p^2 \cos^2\delta_p - 2P_p P_\pi \cos\alpha \cos\delta_p \cos\delta_\pi)^{1/2} \qquad (I.6)$$

where α is the plane opening angle. The total momentum in the x' direction is:

$$P'_x = P_p \cos\delta_p \cos\theta_p + P_\pi \cos\delta_\pi \cos\theta_\pi \qquad (2.7)$$

where θ's are the plane angles. The plane angle of Λ° with respect to the grid line closest to the vertex is:

$$\theta' = \cos^{-1}(P'_x / P'_{\Lambda^\circ}) \qquad (2.8)$$

Since the angle between adjacent grid lines is 1°, the plane angle with respect to the central grid line is:

$$\theta_{\Lambda^\circ} = y' \frac{\pi}{120} + \theta' \qquad (2.9)$$

We can write a unit vector in the Λ° direction in the double polar system as follows:

$$\hat{u}_{\Lambda^\circ} = (\cos\delta_{\Lambda^\circ} \cos\theta_{\Lambda^\circ} \cos 20^\circ - \sin\delta_{\Lambda^\circ} \sin 20^\circ)\,\hat{i}'' + (\cos\delta_{\Lambda^\circ} \sin\theta_{\Lambda^\circ})\,\hat{j}''$$
$$+ (\sin\delta_{\Lambda^\circ} \cos 20^\circ + \cos\delta_{\Lambda^\circ} \cos\theta_{\Lambda^\circ} \sin 20^\circ)\,\hat{k}'' \qquad (2.10)$$

Let

$$u_{\Lambda^\circ x} = \cos\delta_{\Lambda^\circ} \cos\theta_{\Lambda^\circ} \cos 20^\circ - \sin\delta_{\Lambda^\circ} \sin 20^\circ$$
$$u_{\Lambda^\circ y} = \cos\delta_{\Lambda^\circ} \sin\theta_{\Lambda^\circ} \qquad (2.11)$$
$$u_{\Lambda^\circ z} = \cos\delta_{\Lambda^\circ} \cos\theta_{\Lambda^\circ} \sin 20^\circ + \sin\delta_{\Lambda^\circ} \cos 20^\circ$$

Equation of the Λ° direction is given by :

$$x - x'' = \frac{u_{\Lambda^\circ z}}{u_{\Lambda^\circ x}} (z - z'')$$
$$y - y'' = \frac{u_{\Lambda^\circ y}}{u_{\Lambda^\circ x}} (x - x'') \qquad (2.12)$$

The production point (x_0, y_0, z_0) is estimated as being the point of closest approach of the Λ^0 path to the central ray of the incident π^- beam. The distance of a point on the Λ^0 path, (x, y, z) to the central π^- ray (x-axis) is given by :

$$d = (y^2+z^2)^{1/2} = (y'^2 + z'^2 + \frac{u_{\Lambda^0_y}^2 + u_{\Lambda^0_z}^2}{u_{\Lambda^0_x}^2}(x - x')^2$$

$$+ \frac{2}{u_{\Lambda^0_x}}(u_{\Lambda^0_z} z' + u_{\Lambda^0_y} y')(x - x'))^{1/2} \qquad (I.13)$$

We want this distance to be a minimum :

$$\frac{d}{dx} d^2 = 2(x - x') \frac{u_{\Lambda^0_y}^2 + u_{\Lambda^0_z}^2}{u_{\Lambda^0_x}^2} + \frac{2}{u_{\Lambda^0_x}} (u_{\Lambda^0_z} z' + u_{\Lambda^0_y} y') = 0$$

(I.14)

The solution of this equation is:

$$x_0 = x' - \frac{u_{\Lambda^0_x}}{u_{\Lambda^0_y}^2 + u_{\Lambda^0_z}^2}(u_{\Lambda^0_z} z' + u_{\Lambda^0_y} y') \qquad (I.15)$$

From (I.12) we get y_0 and z_0 :

$$y_0 = y' - \frac{u_{\Lambda^0_x}}{u_{\Lambda^0_y}^2 + u_{\Lambda^0_z}^2}(u_{\Lambda^0_z} z' + u_{\Lambda^0_y} y')$$

(I.16)

$$z_0 = z' - \frac{u_{\Lambda^0_z}}{u_{\Lambda^0_y}^2 + u_{\Lambda^0_z}^2}(u_{\Lambda^0_z} z' + u_{\Lambda^0_y} y')$$

Since we now have the coordinates of the production and decay vertices we can calculate the length l of the path travelled in the field :

$$[illegible] \quad [illegible]$$

$$[illegible] \quad [illegible]$$

APPENDIX J

EFFECTS CAUSED BY THE CURVATURE OF THE INCIDENT BEAM AS IT STRIKES THE TARGET*

Let d be the vertical displacement of the beam with respect to the axis of the beam channel and x the variable distance along the axis (x = 0 at the front end of the target) d is given by :

$$d = \frac{1}{2} a t^2 \qquad (J.1)$$

where a is the acceleration of the particle due to the magnetic field and t is the time spent in the field. Since incoming pions have a momentum of 1.05 Gev/c they are relativistic and the force on them is given in the laboratory frame by:

$$F = \frac{-dE}{e} \quad (\gamma \approx 1) \qquad (J.2)$$

and their acceleration is :

---

* See Figure 29.

$$n = \frac{B}{n_0} = \frac{pr}{n_0 e} \quad (\gamma \gg 1) \tag{J.3}$$

The distance travelled by the particles in the magnetic field is x/γ therefore the time spent is :

$$t = \frac{x}{\gamma v} \tag{J.4}$$

Substituting (J.3) and (J.4) into (J.1) we get:

$$d = \frac{1}{2} \frac{ex}{n_0 e} \left(\frac{x}{\gamma v}\right)^2 \simeq \frac{eB}{2\gamma n_0 c^2} x^2 \tag{J.5}$$

γ is given by :

$$\gamma = \frac{(m^2c^4 + p^2c^2)^{1/2}}{mc^2} \simeq \frac{1052}{140} = 7.5 \tag{J.6}$$

Therefore d is :

$$d = \frac{4.8 \times 10^{-10} \times 200 \times 10^3}{2 \times 7.5 \times 140 \times 1.6 \times 10^{-6}} x^2 = 0.0285\, x^2 \text{ cm} \tag{J.7}$$

The beam was adjusted such that d was zero at the centre of the target. Therefore we have :

$$d = 0.0285\,(x^2 - 1.6^2) \text{ cm} \tag{J.8}$$

i.e. d changes between -0.073 cm and +0.32 cm.

Since an incident π^- now has the direction θ' instead of θ the production angle of the Λ^0 produced by the π^- is changed by $\Delta\theta = \theta_1 - \theta_0 = \theta_0$ is taken to be 20^0. θ_1 is given by :

$$\theta_1 = \sin^{-1} \frac{1}{d} \qquad (3.7)$$

The maximum value θ_1 takes is therefore $22^0 40'$.

The production plane ACB' (defined by $\overline{P}_{\Lambda^0}$ and $\overline{P}_{\pi^-_{lab}}$) is inclined with respect to the horizontal median plane of the coil ACB by the angle ψ. From Fig. 29 we see that

$$B'C = \frac{BC}{\cos\psi} = AC \tan\theta_1 = BC \frac{\tan\theta_1}{\tan\theta_0} \qquad (3.10)$$

Therefore

$$\cos\psi = \tan\theta_0 / \tan\theta_1 \qquad (3.11)$$

$\cos\psi$ changes between 0.87 and 1.

The direction of the Λ^0 polarization vector is inclined by the same angle ψ with respect to the plane of the emulsion pellicles. The effect of this on the φ distribution is to reduce the observed value of αP by the factor $\cos\psi$. This introduces an error of $\sim 3\%$ into the estimate of μ_{Λ^0}.

Another effect the beam tilt has is on the matching cone distribution. This effect depends on the angle δ which measures the angle of deviation of the beam in the vertical plane. It is equal to :

$$\delta = \sin^{-1} (\sin\theta_1 \cdot \sin\psi) \qquad (3.12)$$

The maximum value it takes is 10^0.

In calculating the missing mass we had assumed $\delta = 0$ neglecting the perpendicular component of $\overline{P}_{inc}$. The error this introduces into the missing mass is :

$$\delta\Delta = (P_{inc} \sin\delta)^2 \cong (1050 \times \sin 10^0)^2 = 0.02\ (Gev/c^2)^2$$

This is in agreement with our missing mass distribution.[2]

---

x See Figure 12.

APPENDIX K

CALCULATION OF THE ANGLE φ

φ is the angle between $\bar{a}_0$, the initial polarization vector of Λ^0 and the projection of the proton momentum vector onto the $(\bar{p}_{\Lambda^0}, \bar{a}_0)$ plane, in the c.m.s. system of Λ^0. The analysis is done in the coordinate system given by the Eq. (II.3.8) :

$$\bar{I} = \frac{\bar{p}_{\Lambda^0}}{|\bar{p}_{\Lambda^0}|} \quad , \quad \bar{J} = \frac{\bar{a}_0}{|\bar{a}_0|} \quad , \bar{K} = \bar{I} \times \bar{J} \qquad \text{(II.3.8)}$$

In terms of the double primed coordinate system defined in Appendix F, $\bar{I}$, $\bar{J}$, $\bar{K}$ is given as:

$$\bar{I} = u_{\Lambda^0 x}\bar{I}'' + u_{\Lambda^0 y}\bar{J}'' + u_{\Lambda^0 z}\bar{K}'' \qquad \text{(K.1)}$$

$$\bar{J} = -\frac{\bar{I}'' \times \bar{p}_{\Lambda^0}}{|\bar{I}'' \times \bar{p}_{\Lambda^0}|} = (u_{\Lambda^0 y}^2 + u_{\Lambda^0 z}^2)^{-1/2}(u_{\Lambda^0 z}\bar{J}'' - u_{\Lambda^0 y}\bar{K}'') \qquad \text{(K.2)}$$

$$\bar{K} = \bar{I} \times \bar{J} = (u_{\Lambda^0 y}^2 + u_{\Lambda^0 z}^2)^{-1/2}\left[-(u_{\Lambda^0 y}^2 + u_{\Lambda^0 z}^2)\bar{I}'' + u_{\Lambda^0 x}u_{\Lambda^0 y}\bar{J}'' + u_{\Lambda^0 x}u_{\Lambda^0 z}\bar{K}''\right] \qquad \text{(K.3)}$$

$\bar{P}_{p'}$, the proton laboratory momentum vector, in the double primed system is given in terms of the measured quantities as follows :

$$\bar{P}_p = P''_{p_x}\bar{i}'' + P''_{p_y}\bar{j}'' + P''_{p_z}\bar{k}'' \qquad (X.4)$$

where $P''_{p_x} = (\cos\delta_p \cos\theta_p \cos 20^\circ - \sin\delta_p \sin 20^\circ)P_p$

$$P''_{p_y} = (\cos\delta_p \sin\theta_p)P_p \qquad (X.5)$$

$$P''_{p_z} = (\cos\delta_p \cos\theta_p \sin 20^\circ + \sin\delta_p \cos 20^\circ)P_p$$

δ_p is the dip angle, θ_p the plane angle of the proton with respect to the primed coordinate system whose origin is at the center of the ionization stack and P_p is the fitted proton momentum.

In the unprimed system x,y components of $\bar{P}_p$ is given by:

$$P_{p_x} = \bar{P}_p \cdot \bar{i} = u_{\Lambda'x}P''_{p_x} + u_{\Lambda'y}P''_{p_y} + u_{\Lambda'z}P''_{p_z} \qquad (X.6)$$

$$P_{p_y} = \bar{P}_p \cdot \bar{j} = (u_{\Lambda'z}P''_{p_y} - u_{\Lambda'y}P''_{p_z})(u_{\Lambda'y}^2 + u_{\Lambda'z}^2)^{-1/2} \qquad (X.7)$$

These components transform into the c.m.s. system of Λ° as follows:

$$P'_{p_x} = \gamma(P_{p_x} - \beta E_p) \qquad (X.8)$$

and

$$P'_{p_y} = P_{p_y} \qquad (X.9)$$

where

$$\beta = p_{\Lambda^0} / (m^2_{\Lambda^0} + p^2_{\Lambda^0})^{1/2} \quad , \quad \gamma = 1/(1 - \beta^2)^{1/2}$$

and

$$E_p = (m_p^2 + p_p^2)^{1/2} \, .$$

The angle φ is given by :

$$\varphi = \tan^{-1} \frac{p_{p'x}}{p_{p'y}} \qquad (6.20)$$

TABLE I

SOME THEORETICAL VALUES OF THE MAGNETIC MOMENT OF THE Λ^0 HYPERON

Method	Reference	μ_Λ(in n.m.)
Pure SU_3	(33, 34)	-0.73
Pure SU_3(from μ_p)	(35)	-0.93
Pure-connected SU_6	(36)	-0.78
Broken SU_3(depends on f_{8F}/D)	(36)	-0.66
Broken SU_3(photo production amplitudes)	(37)	-0.75
Broken SU_3 (current algebra)	(38)	-0.69
Broken SU_6(ω - φ mixing)	(39)	-0.76
Broken SU_3	(40)	-0.90
Broken SU_3(asymptotic symmetry)[a]	(41)	-0.65±0.03
Broken SU_3(current algebra)	(42)	-0.64
Quark model[a]	(43)	-0.65±0.03
Quark model	(44)	-0.88
Partial symmetry	(45)	-0.68
Isotopy	(46)	0.00
Two triplets of fundamental particles	(47)	-0.57

[a] The "errors" show the effect of varying the parameters within a reasonable range.

TABLE 2

THE LABORATORY VELOCITY, MOMENTA, ENERGY AND ANGLE OF THE Λ^0 PRODUCED IN THE REACTION $\pi^- + p \longrightarrow \Lambda^0 + K^0$ AS A FUNCTION OF THE C.M.S. ANGLE (FOR p_π=1.09 Gev/c)

C.M. ANGLE	β	p(Mev/c)	E (Mev)	θ^0
0	0.667	998.3	1497.1	0.0
10	0.666	994.8	1494.7	2.5
20	0.662	984.4	1487.8	5.0
30	0.655	967.2	1476.3	7.4
40	0.646	943.6	1461.1	9.7
50	0.634	914.0	1442.2	12.0
60	0.619	879.0	1420.3	14.2
70	0.601	839.3	1396.0	16.2
80	0.581	795.6	1370.2	18.0
90	0.557	748.7	1343.5	19.4
100	0.531	699.7	1316.9	20.5
110	0.503	649.7	1291.0	21.1
120	0.474	600.1	1266.8	21.0
130	0.444	552.3	1244.8	20.2
140	0.415	508.2	1225.9	18.5
150	0.388	470.0	1210.6	16.3
160	0.367	440.1	1199.3	13.1
170	0.353	420.8	1192.3	9.9
180	0.348	414.2	1190.0	0.0

TABLE 3

THE LABORATORY MOMENTA AND ANGLES OF THE PROTON AND PION WITH THE DECAY $\Lambda^0 \longrightarrow p + \pi^-$ AS A FUNCTION OF THE CMS ANGLE

(1) For $\beta_{\Lambda^0} = \beta_{max} = 0.667$

CMS ANGLE	θ_p	P_p (Mev/c)	θ^0_π	P_π (Mev/c)
0	0.0	800.9	0.0	247.1
10	1.3	799.2	4.1	245.8
20	2.5	794.2	8.2	242.1
30	3.7	785.9	12.3	235.9
40	4.8	774.6	16.5	227.3
50	5.8	760.6	20.8	216.9
60	6.7	744.2	25.2	204.7
70	7.6	725.7	29.7	191.7
80	8.1	705.7	34.3	177.9
90	8.4	684.6	39.1	163.3
100	8.6	663.2	44.1	148.1
110	8.5	641.9	49.3	132.5
120	8.1	621.5	54.7	116.6
130	7.3	602.7	60.3	100.6
140	6.3	586.1	66.2	85.7
150	5.0	572.3	72.0	72.0
160	3.5	562.1	78.2	59.1
170	1.8	555.7	84.7	47.6
180	0.0	553.5	173.4	0.0

(ii) For $\beta_{\Lambda^0} = \beta_{cm} = 0.743$

C.M. ANGLE	θ_p	p_p (MeV/c)	θ^0_π	p_π (MeV/c)
0	0.0	536.7	0.0	187.9
10	1.9	535.5	5.4	187.1
20	3.7	531.2	10.7	184.5
30	5.5	524.5	16.2	180.3
40	7.2	515.0	21.7	174.5
50	8.8	503.2	27.4	167.9
60	10.2	489.4	33.2	159.0
70	11.3	473.7	39.3	149.1
80	12.5	456.9	45.6	139.9
90	13.3	438.2	52.3	127.0
100	13.7	419.2	59.4	115.0
110	13.7	400.1	67.0	102.6
120	13.0	381.9	75.4	89.9
130	12.1	363.9	84.9	77.9
140	10.7	348.1	95.9	66.9
150	8.6	334.8	107.6	55.3
160	6.1	324.8	125.9	45.0
170	3.1	318.4	150.4	37.4
180	0.0	316.3	180.0	32.5

TABLE 4

THE RESULTS OF SOME OF THE MEASUREMENTS

Event No	θ_p Meas. 1	θ_p Meas. 2	Δ =1-2	δ_p Meas. 1	δ_p Meas. 2	Δ =1-2	σ_p Meas. 1	σ_p Meas. 2	Δ =1-2
1	10°.6	10°.6	0°.0	0°.915	0°.688	0°.227	2.50	2.54	-0.04
2	1°.9	1°.8	0°.1	1°.600	1°.600	0°.000	2.32	2.58	-0.26
3	6°.1	6°.3	-0°.2	0°.688	0°.915	-0°.227	1.40	1.50	-0.10
4	9°.6	9°.6	0°.0	0°.230	0°.457	-0°.227	2.31	2.61	-0.30
5	350°.6	350°.4	0°.2	2°.750	2°.750	0°.000	2.14	2.04	0.10
6	352°.0	352°.0	0°.0	0°.457	0°.688	-0°.231	2.13	2.11	0.02
7	16°.4	16°.0	0°.4	3°.200	3°.650	-0°.450	2.74	2.89	-0.15
8	8°.0	8°.0	-0°.1	0°.915	0°.915	0°.000	2.52	2.55	-0.01

Event No	θ_π Meas. 1	θ_π Meas. 2	Δ =1-2	δ_π Meas. 1	δ_π Meas. 2	Δ =1-2	σ_π Meas. 1	σ_π Meas. 2	Δ =1-2
1	353°.3	353°.8	0°.5	0°.457	0°.457	0°0	1.40	1.43	-0.03
2	159°.3	159°.1	0°.2	26°.30	25°.0	1°.30	Blank	Blank	-
3	20°.0	20°.0	0°.0	12°.00	10°.50	1°.50	Blank	Blank	-
4	343°.4	343°.4	0°.0	1°.84	1°.60	0°.24	2.00	2.19	-0.11
5	20°.0	20°.1	-0°.1	7°.18	7°.45	-0°.27	1.32	1.34	-0.02
6	22°.2	22°.0	0°.2	0°.457	0.227	0°.230	1.06	0.89	0.17
7	216°.0	216°.0	0°.0	8°.25	8°.13	0°.12	1.12	1.47	-0.35
8	352°.8	352°.9	-0°.1	8°.13	7°.18	0°.95	0.81	1.19	-0.38

TABLE 5

THE α-β OXIDATION

DATA

P Bar/a	β	α Runs. 5	α Runs. 6	$\delta\alpha$
450	.334	3.14	3.37	[illegible]
500	.436	2.49	2.45	[illegible]
600	.360	1.99	1.93	[illegible]
700	.615	1.74	1.68	[illegible]
800	.666	1.49	1.50	[illegible]
900	.703	1.36	1.42	[illegible]
	.560	1.30 (Berlam)		[illegible]

TABLE 6

PARAMETERS OF THE FITTED g^2-β CURVES OF THE ISOTHERMS

$\log g^2 = a + b \log \beta + c (\log \beta)^2$

Frequency	a	b	c	χ^2	$\chi^2_{th.}$
3	-0.102	-1.866	-0.559	2.070	4
6	-0.209	-1.467	0.066	9.526	4
3.6	-0.163	-1.643	-0.138	20.742	11

$g^2 = a + b / \beta^c$

Frequency	a	b	c	χ^2	$\chi^2_{th.}$
3	-0.101	0.949	1.364	7.37	4
6	0.071	0.737	1.665	9.196	4
3.6	-0.031	0.823	1.497	22.796	11

$\chi^2_{th.}$ = No. of experimental points - No. of parameters solved for.

TABLE 7

SEED VARIATION IN THE GRAIN COLOUR OF A HEADROW

Plot No	C_a 1st Measurement	C_a 2nd Measurement
140/3	24.60 ± .5	24.09 ± .5
140/4	26.24 ± .5	27.31 ± .5
140/5	25.04 ± .5	26.30 ± .5
140/6	26.33 ± .5	26.90 ± .5
140/5	27.07 ± .5	26.74 ± .5
140/4	27.39 ± .5	26.22 ± .5
140/6	27.71 ± .5	27.76 ± .5

TABLE 8

THE NUMBER OF EVENTS LEFT (IN ARBITRARY UNITS) AFTER EACH CUT ONE

Restriction	No. of events left
$0.05 < x < 0.55$	440
$x^2 < 25$	395
$\lvert x_p \rvert < 24$, $\lvert y_p \rvert < 8$, $\lvert z_p \rvert < 1$	295
$450 < P_{\Lambda^0} < 800$	281
$\sin \psi_p < 0.91$	200

BIBLIOGRAPHY

1. M.A.Preston; Physics of the Nucleus, Addison Wesley,(1962).

2. J.G. Combe; CERN (64-13).

3. Particle Data Group: in Review of Particle Properties, Rev. Mod. Phys. 42, 87 (1970).

4. R.L.Cool et al.; Phys. Rev., 127 B2 35 (1962).

5. S. [illegible] et.al.; Phys. Rev., 129, 870 (1963).

6. J.A. Anderson et.al.; Phys. Rev. Lett., 13, 167 (1964).

7. G.[illegible] et.al.; Nuovo Cimento, 46, A205(1966).

8. D.A. Hill et.al.; Phys. Rev.Lett., 15, 85(1965).

9. M. Goldhaber; Phys.Rev. 101, 1828 (1956).

10. T.D.Lee and C.N. Yang: Phys. Rev., 108, 1645 (1957).

11. L.B.Auerbach et.al.: Nuovo Cimento, 47, 419(1967).

12. W.H.Holland et.al.; Phys.Letters 25, 145 (1967).

13. E.Dahl-Jensen, H.T.Doble: Nucl.Instrum.Methods (To be published).

14. E.Dahl Jensen et.al.: Nucl.Instrum. Methods, 77, 299(1970).

15. E.T. Friedlander et.al.: Nucl.Instrum.Methods, 77,105(1970).

16. E.Dahl-Jensen et.al.: Nuovo Cimento, 3, 41 (1971).

17. L.Van Hove: Proceedings of the 1965. Easter School for Physicists vol III, CERN(65-24), p.2.

18. V.F. Weisskopf: CERN(66-19) p.23.

19. L.C. Biedenharn: CERN(65-41), p.45.

20. T.P.Cheng and H.Pagels : Phys. Rev., 172 1635 (1968).

21. J. Franklin: Phys.Rev., 172, 1807 (1968).

22. J.Schwinger : Phys. Rev. Lett., 18, 923(1967)

23. Particle Data Group: in Review of Particle Properties, Rev. Mod. Phys. 43, 556 (1971).

24. R.Levi Setti: Elementary particles, Univ. of Chicago Press(1963).

25. R.Pondlovitz, E.P.Gasos: Phys.Rev.92, 33(1955).

26. V.Bargmann, L.Michel, V.L.Telegdi: Phys.Rev.Lett.2, 435 (1959).

27. R.Hagedorn: Relativistic Kinematics(New York,1963).

28. Ph.Rosselet: Helv.Phys.Acta, 38, 691 (1965).

29. B.Ronne: Proceedings of the 1964 Easter School for Physicists Vol.1, CERN(64-13), p.92.

30. D.J.Hudson: Statistics Lectures II. CERN(64-18), p.143.

31. M.G.Kendall, A.Stuart: The Advanced Theory of Statistics, Vol.1, Griffin (1959).

32. A.Mood, F.Graybill: Introduction to the theory of statistics, McGraw-Hill (1963)

33. N.Cabibbo and R.Gatto: Nuovo Cimento, 21, 872 (1961).

34. S.Coleman and S.L.Glashow: Phys.Rev.Lett., 6, 423(1961).

35. M.A.Beg and A.Pais: Phys.Rev., 137, B1514(1965).

36. E.Pagels: Phys.Rev., 179, 2979 (1969).

37. V.S.Mathur and L.K.Pandit: Phys.Rev., 147, 965(1966); Phys. Lett. 20, 308(1966).

38. S.Bonini, P.Pasquinelli and S.Sciuto: Nuovo Cimento, 46A, 182(1966).

39. A.L.L.Videira and C.H.Renninger: Phys.Rev., 152, 1250(1967).

40. D.P.Zarotskii and I.O.Ivanter: Yad.Fiz., 5, 804 (1967).

41. P.N.Dobrinescu: Nucl. Phys., 120, 681 (1970).

42. H.Kleinert: Springer Tracts in Modern Physics, 49, 90(1969).

43. R.Davis : Nucl. Phys., B12, 249(1969).

44. T.Sudduth : Phys.Rev., 184, 1780(1969).

45. J.Schwinger: Phys.Rev.Lett., 18, 923(1967).

46. H.Pagels: Nucl. Phys., B3 , 481 (1969).

47. H.Rosenberg: Phys.Rev., 133, B1047 (1964).

48. CERN 2626 Vol.II.

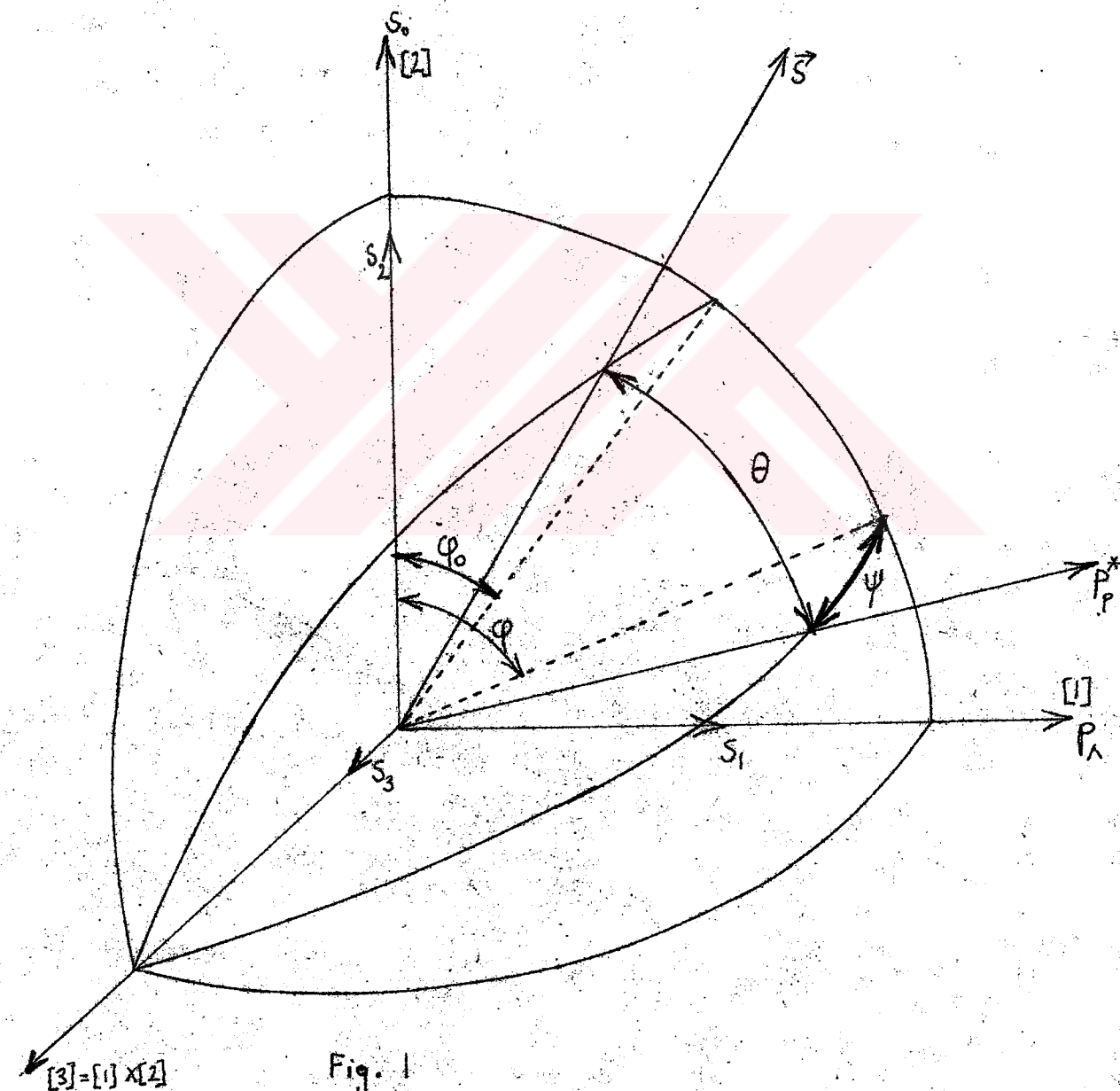

Fig. 1

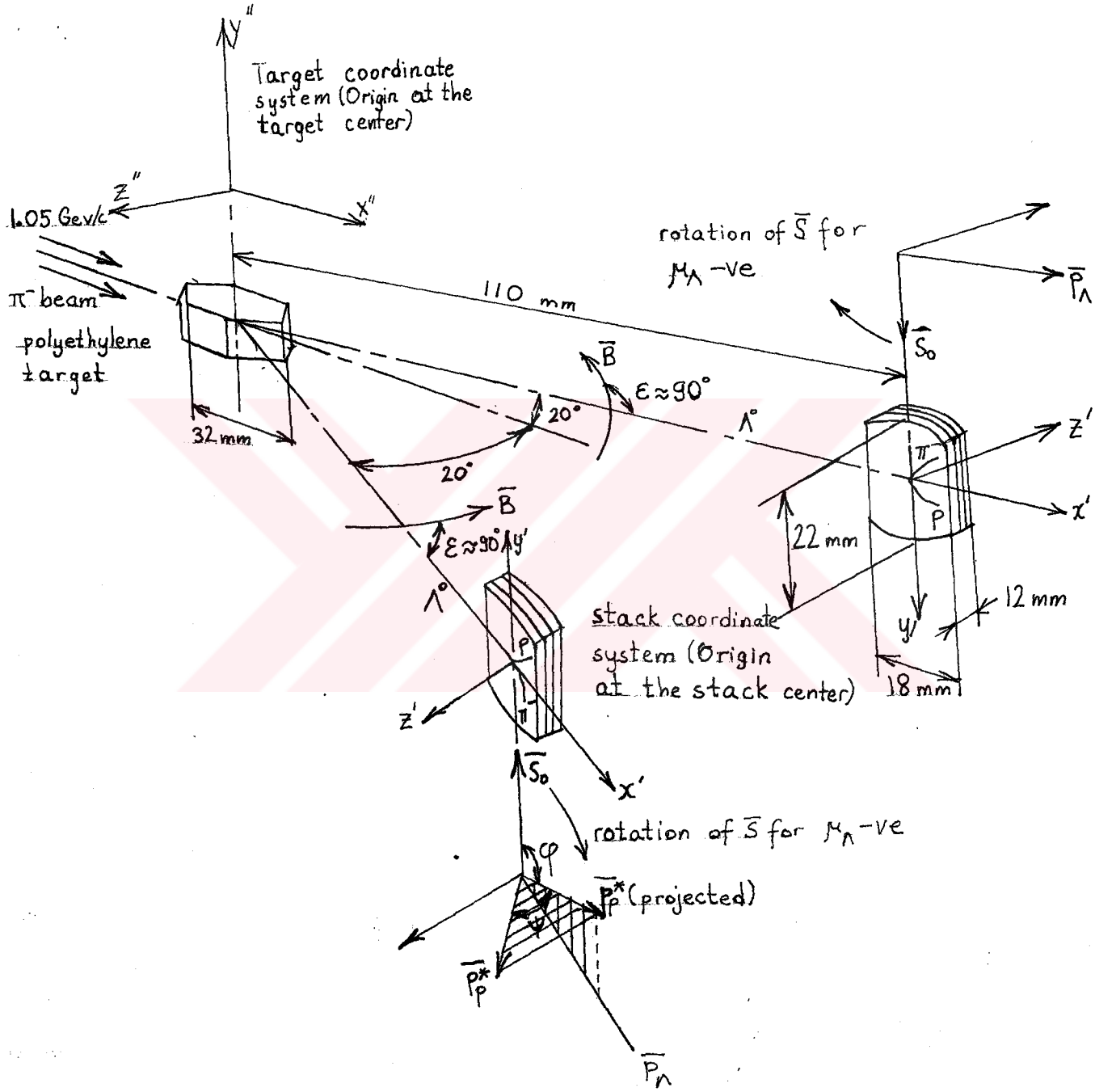
Target coordinate system (Origin at the target center)
y''
z''
x''
1.05 Gev/c
π⁻ beam
polyethylene target
32 mm
110 mm
20°
20°
B
ε≈90°
Λ°
rotation of S for μΛ -ve
P_Λ
S₀
z'
x'
π
P
22 mm
12 mm
y'
18 mm
stack coordinate system (Origin at the stack center)
B
ε≈90°
y'
Λ°
P
π⁻
z'
S₀
x'
rotation of S for μΛ -ve
φ
P*p (projected)
P*p
P_Λ

Fig. 2

1:1

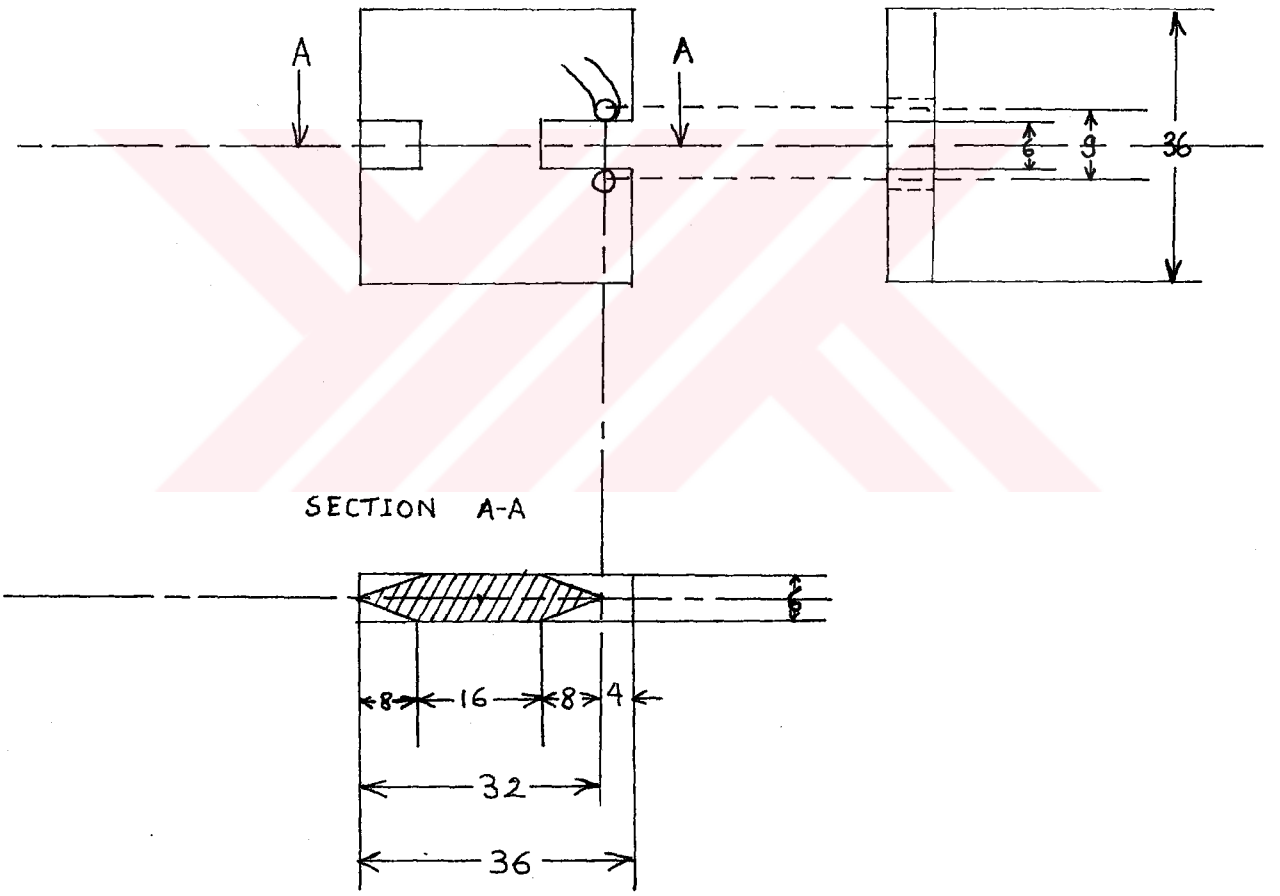

Fig. 3

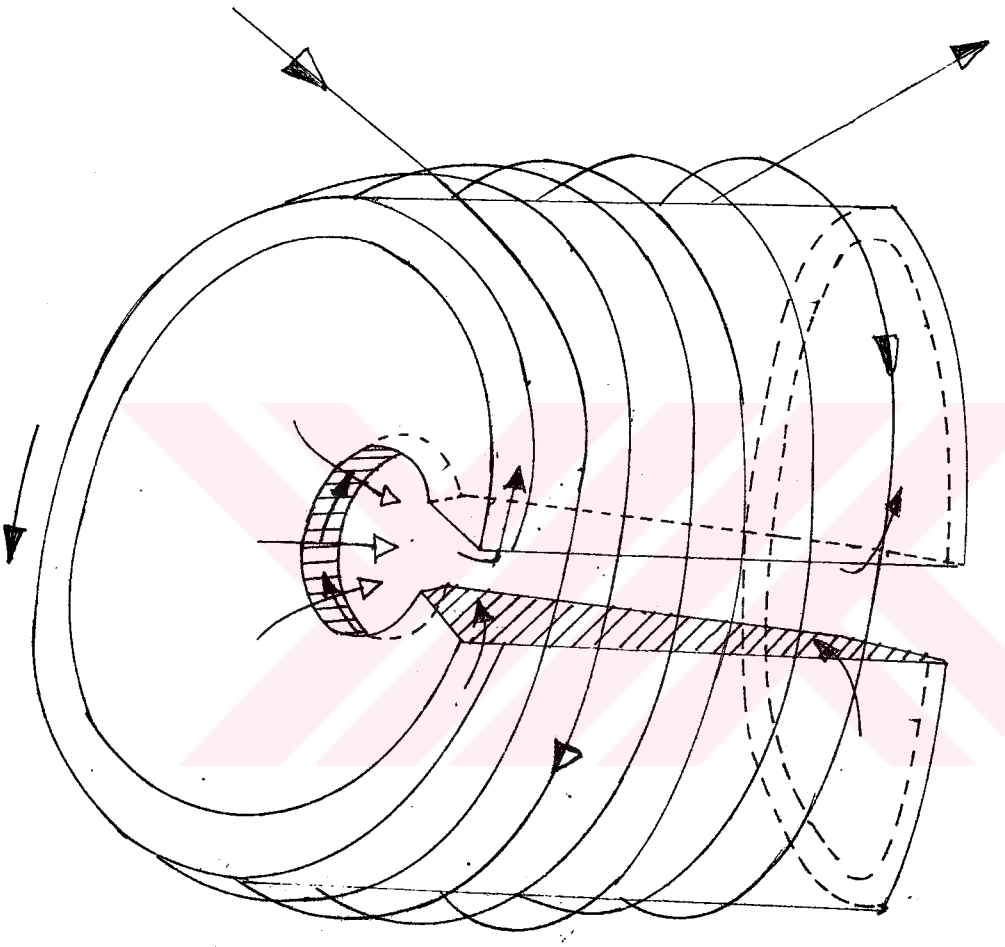

Primary Current

Secondary Current

Magnetic field

Fig. 4

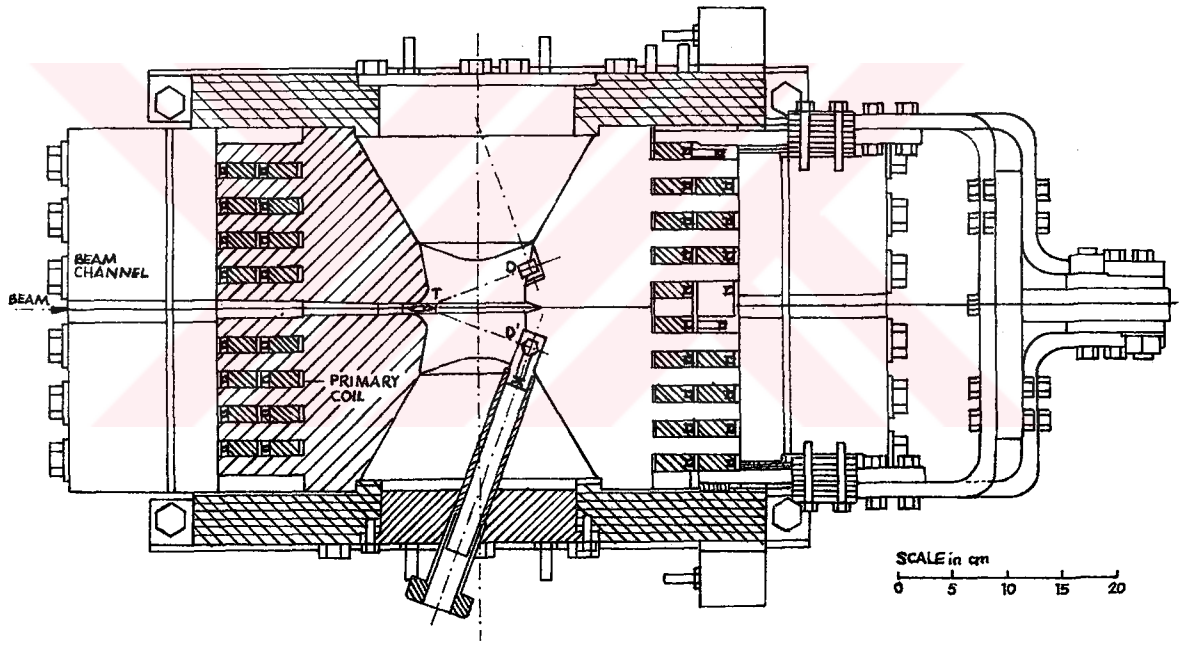

SECTION A-A

Fig. 5

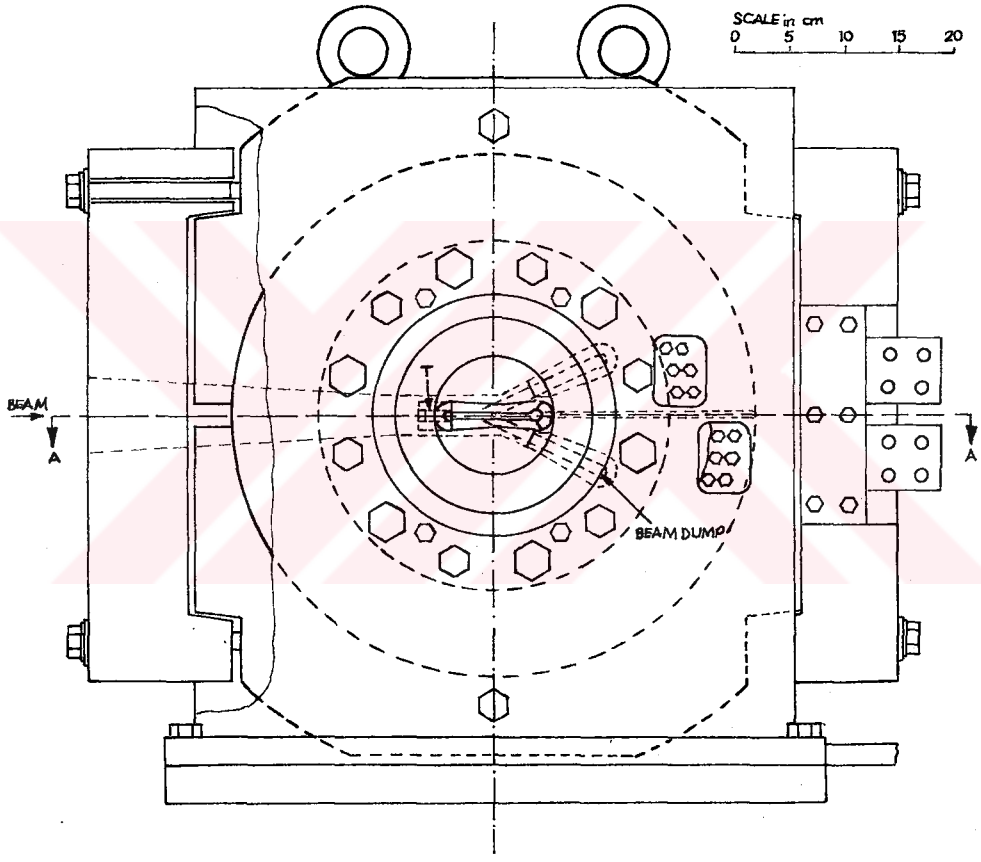

Fig. 6

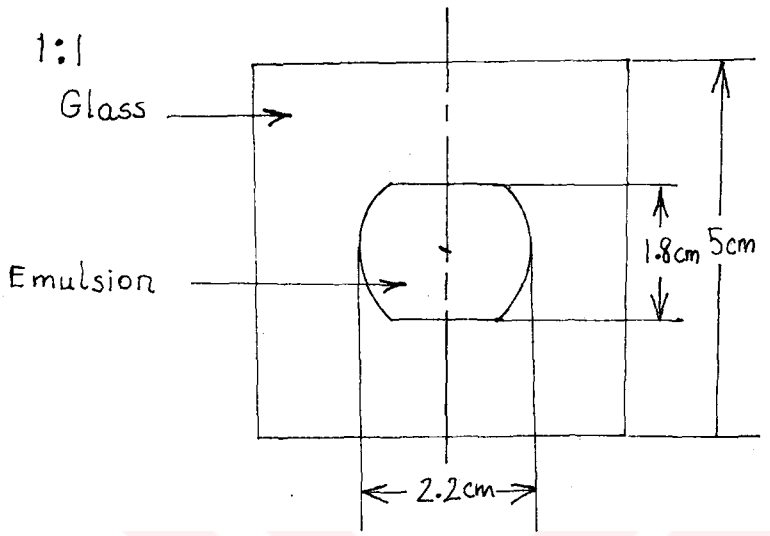
1:1
Glass
Emulsion
1.8cm
5cm
2.2cm

Fig. 7

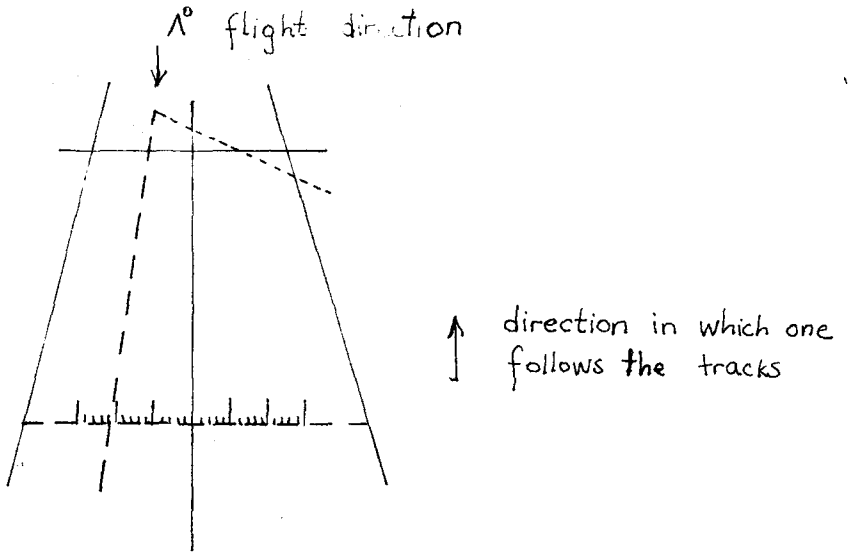
flight direction
direction in which one follows the tracks

Fig. 8

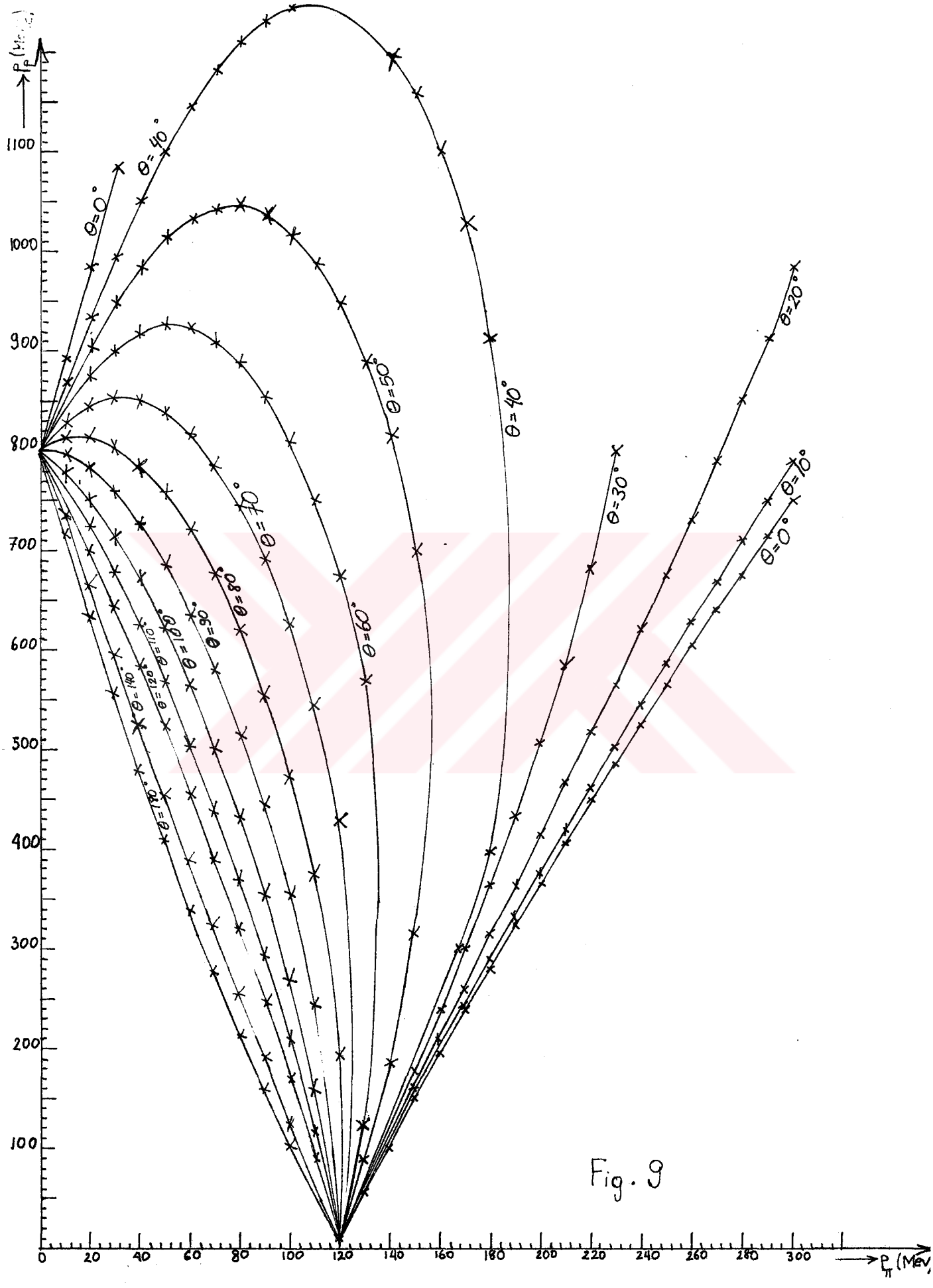
p_p (MeV/c)
1100
1000
900
800
700
600
500
400
300
200
100
θ=0°
θ=10°
θ=20°
θ=30°
θ=40°
θ=50°
θ=60°
θ=70°
θ=80°
θ=90°
θ=120°
θ=150°
θ=180°
0
20
40
60
80
100
120
140
160
180
200
220
240
260
280
300
p_π (MeV/c)

Fig. 9

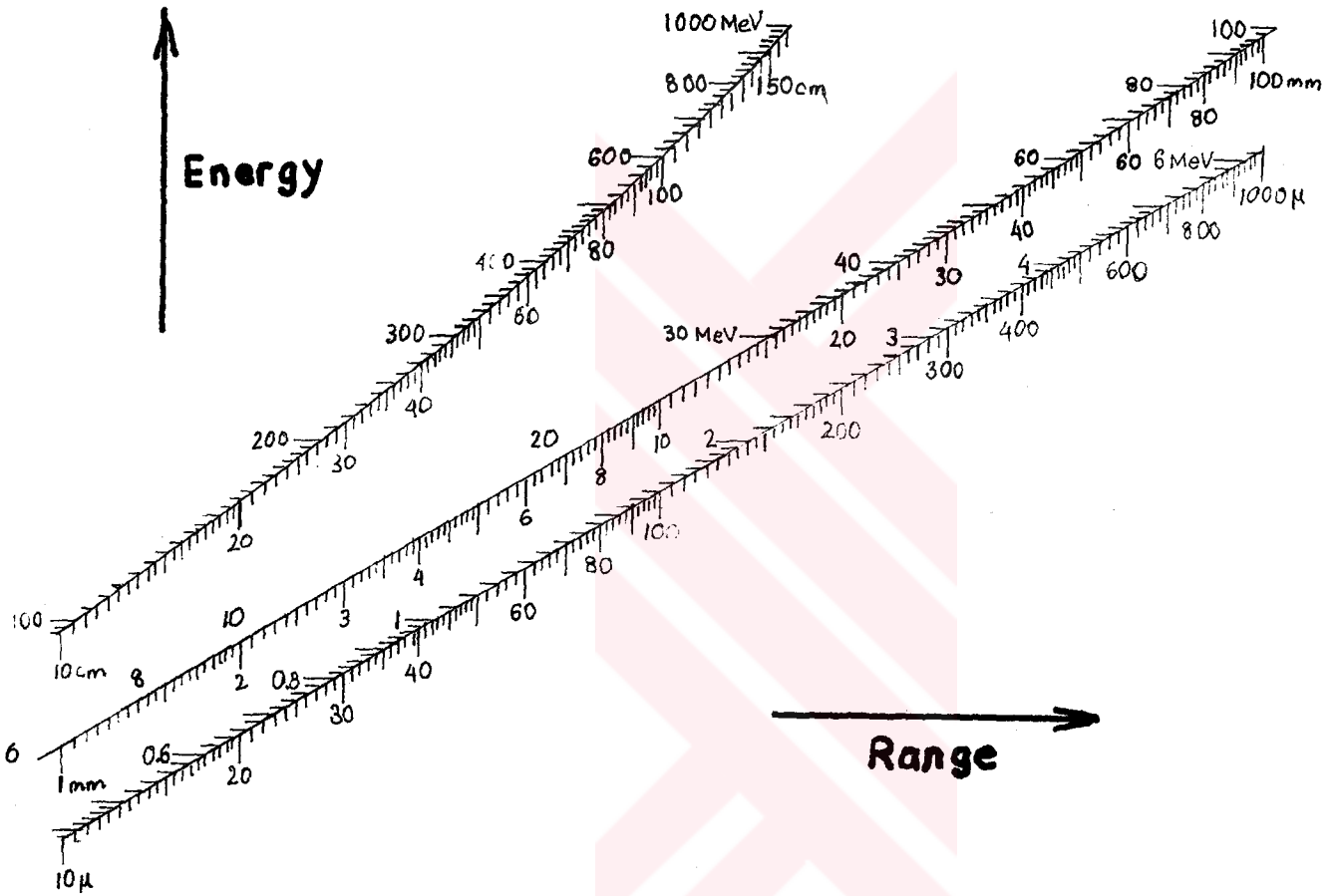
Energy
Range
1000 MeV
800
150cm
600
100
400
80
60
300
40
200
30
20
100
10cm
8
6
1mm
0.6
10μ
30 MeV
20
10
8
6
4
3
2
0.8
1
100
80
60
40
30
20
6 MeV
100mm
80
60
40
30
20
1000μ
800
600
400
300
200
100

Fig. 10

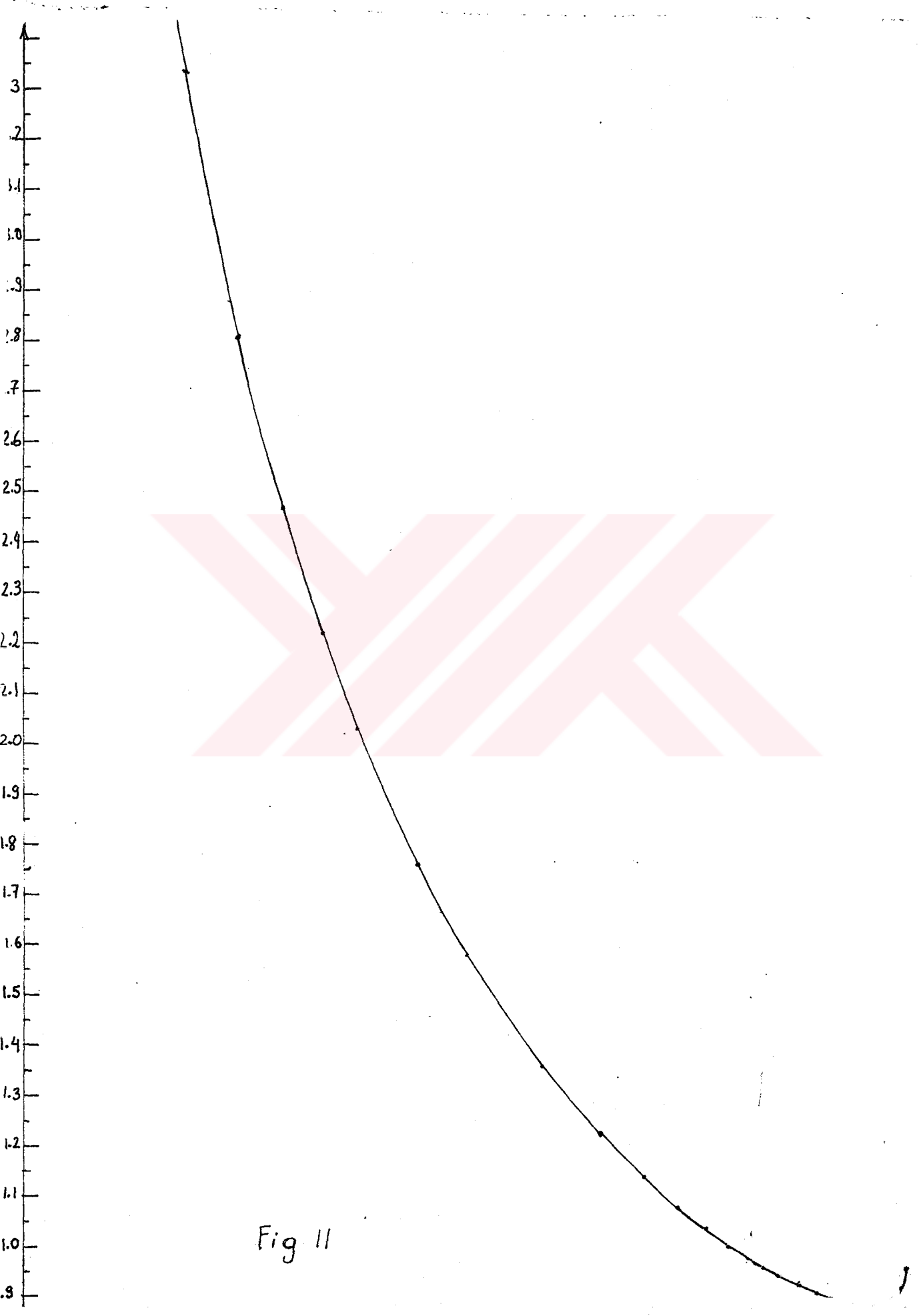

Fig 11

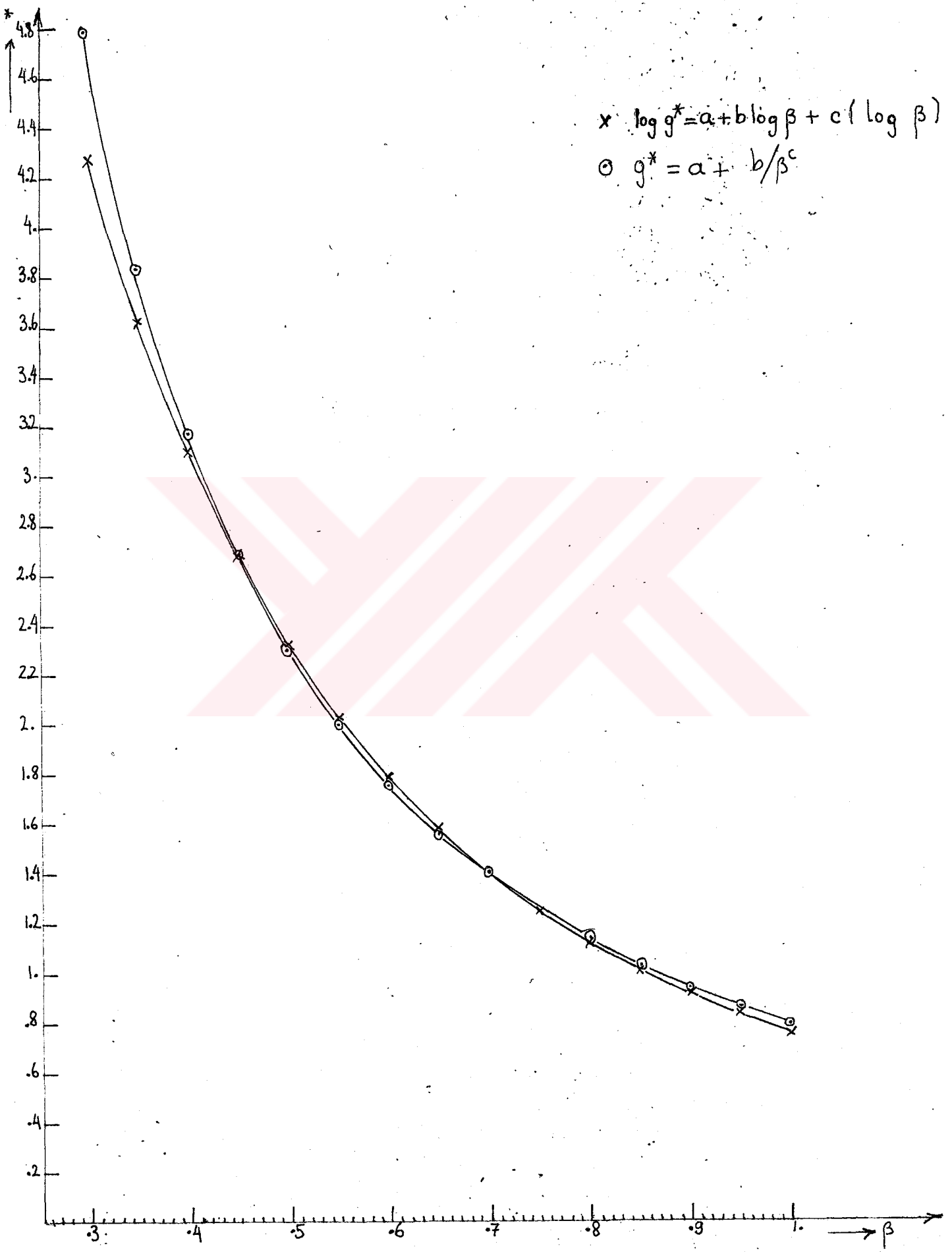
g*
4.8
4.6
4.4
4.2
4.
3.8
3.6
3.4
3.2
3.
2.8
2.6
2.4
2.2
2.
1.8
1.6
1.4
1.2
1.
.8
.6
.4
.2
.3
.4
.5
.6
.7
.8
.9
1.
β
× log g* = a + b log β + c (log β)
⊙ g* = a + b/β^c

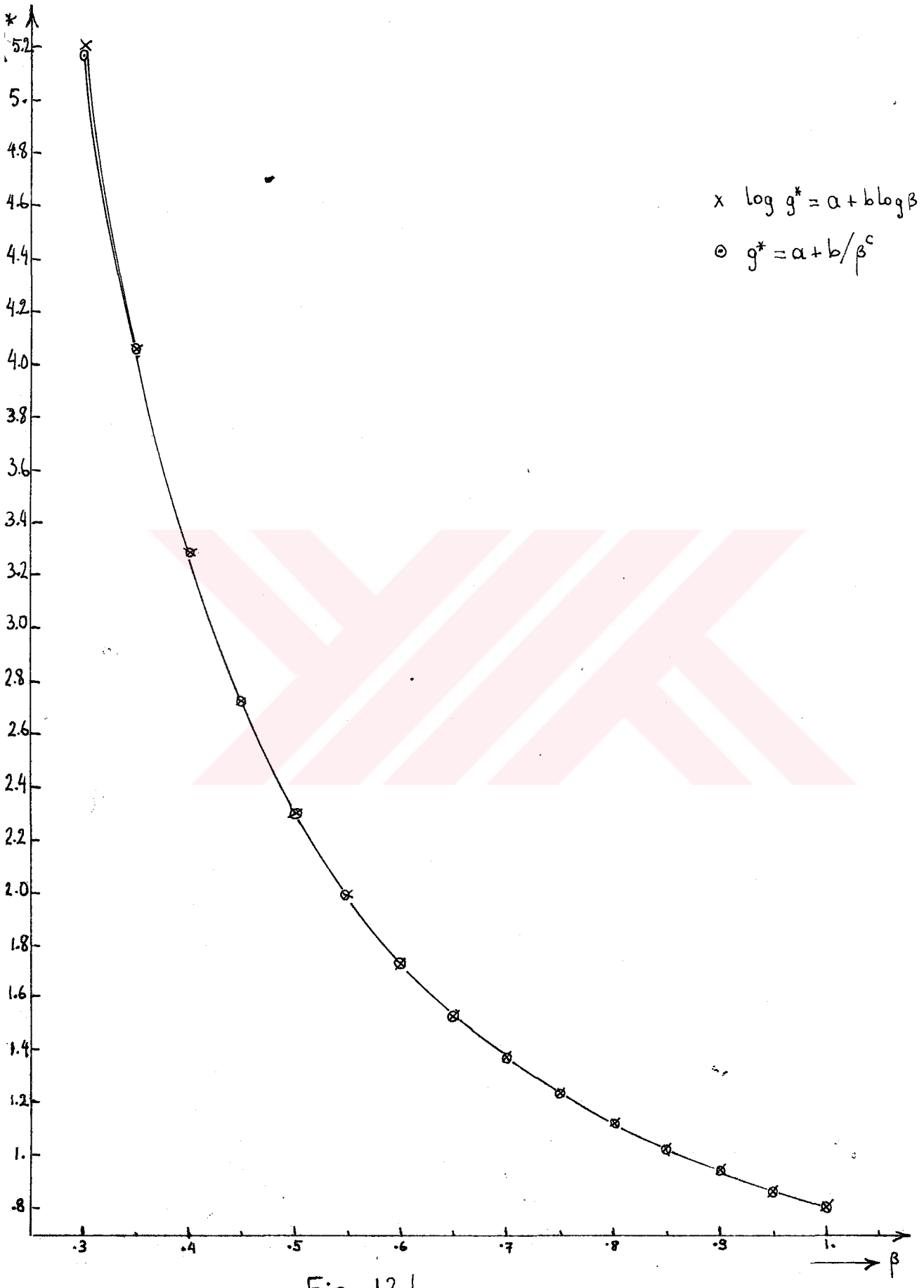
g*
5.2
5.
4.8
4.6
4.4
4.2
4.0
3.8
3.6
3.4
3.2
3.0
2.8
2.6
2.4
2.2
2.0
1.8
1.6
1.4
1.2
1.
.8
.3
.4
.5
.6
.7
.8
.9
1.
β
x log g* = a + b log β + c (log β
⊙ g* = a + b/β^c

Fig 12 b

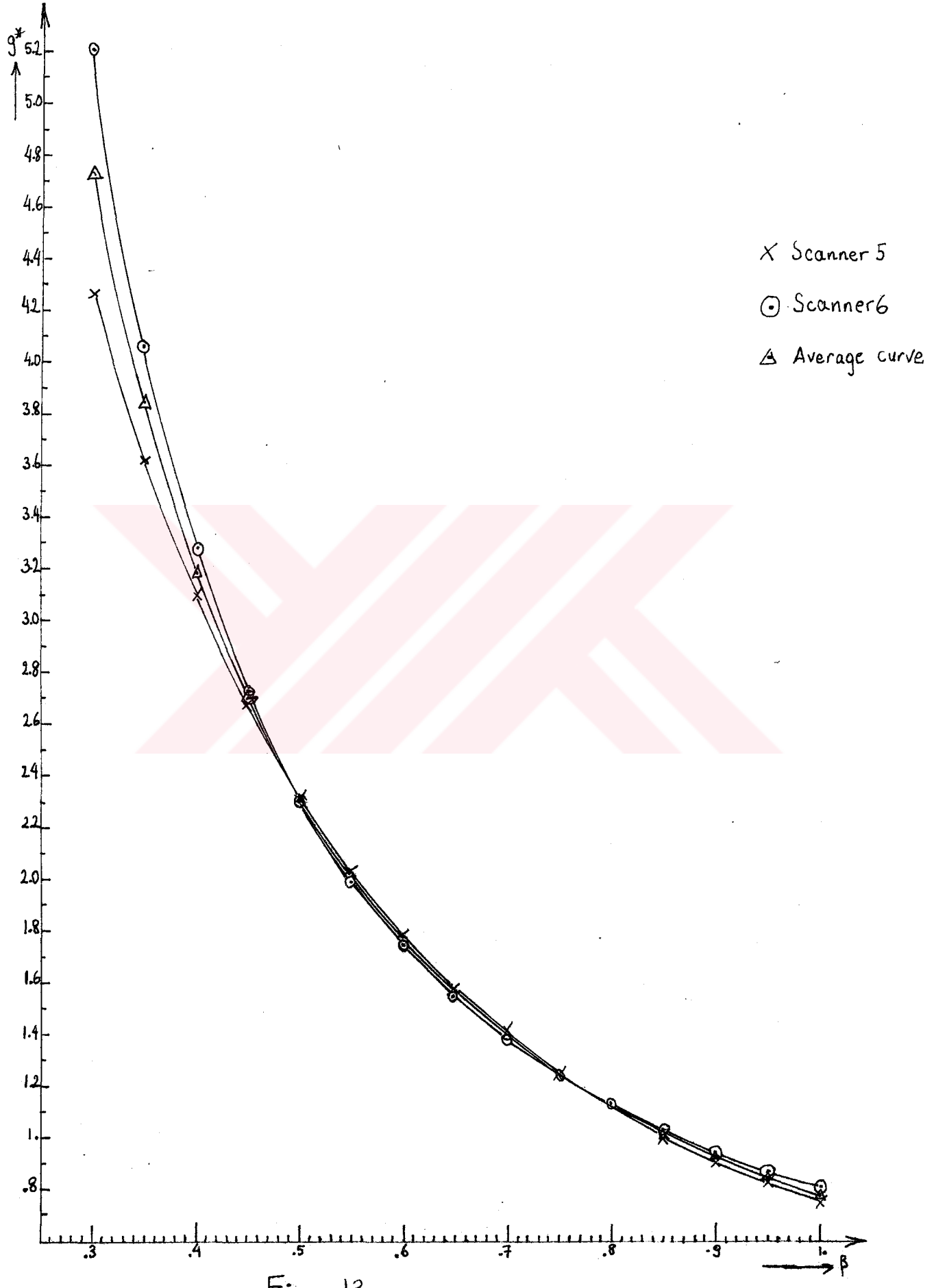
g*
5.2
5.0
4.8
4.6
4.4
4.2
4.0
3.8
3.6
3.4
3.2
3.0
2.8
2.6
2.4
2.2
2.0
1.8
1.6
1.4
1.2
1.
.8
.3
.4
.5
.6
.7
.8
.9
1.
β
X Scanner 5
⊙ Scanner6
△ Average curve

Fig. 13

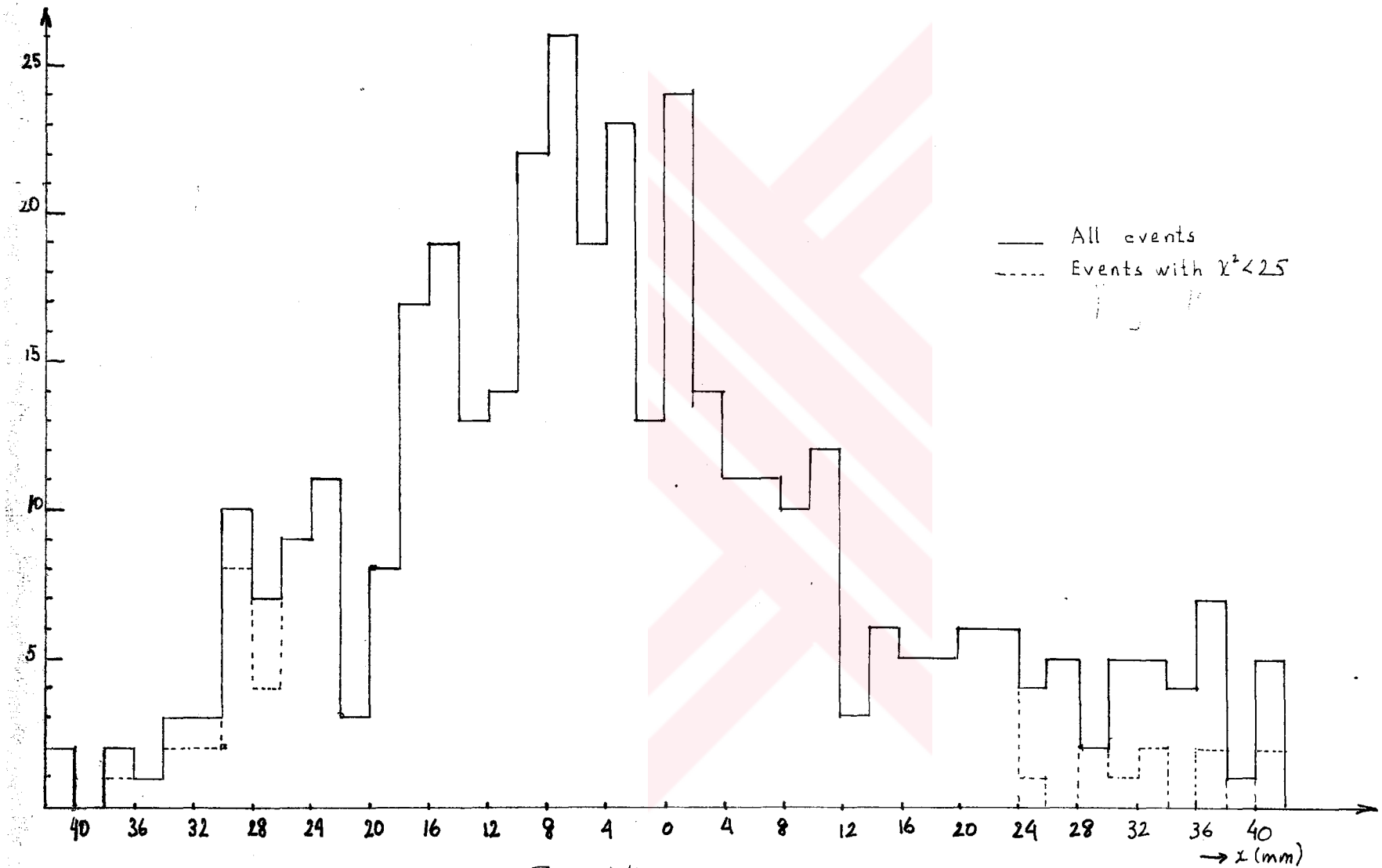
25
20
15
10
5
All events
Events with $\chi^2 < 2.5$
40 36 32 28 24 20 16 12 8 4 0 4 8 12 16 20 24 28 32 36 40
→ x (mm)

Fig. 14

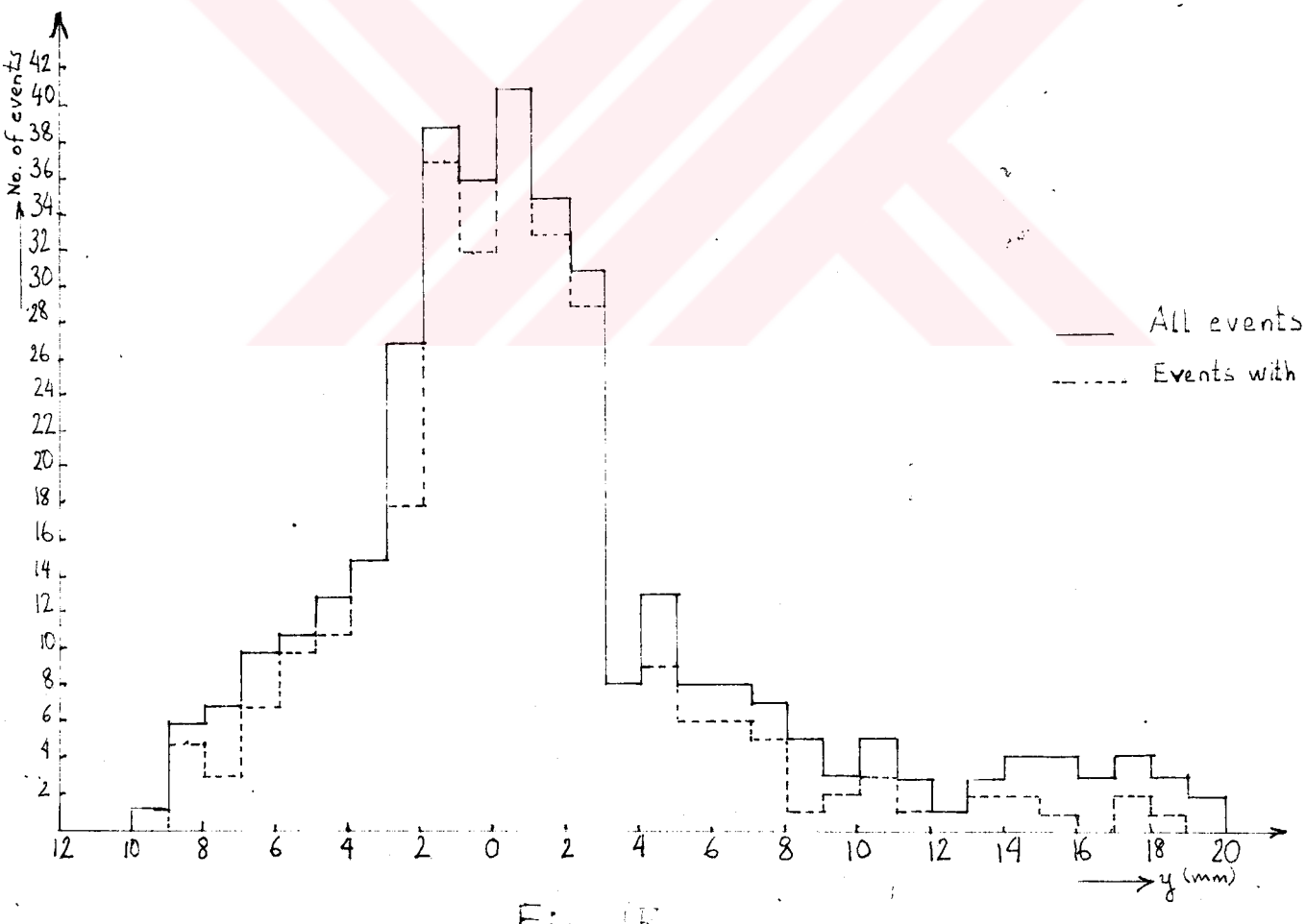
No. of events
42
40
38
36
34
32
30
28
26
24
22
20
18
16
14
12
10
8
6
4
2
12
10
8
6
4
2
0
2
4
6
8
10
12
14
16
18
20
y (mm)
All events
Events with χ^2

Fig. 15

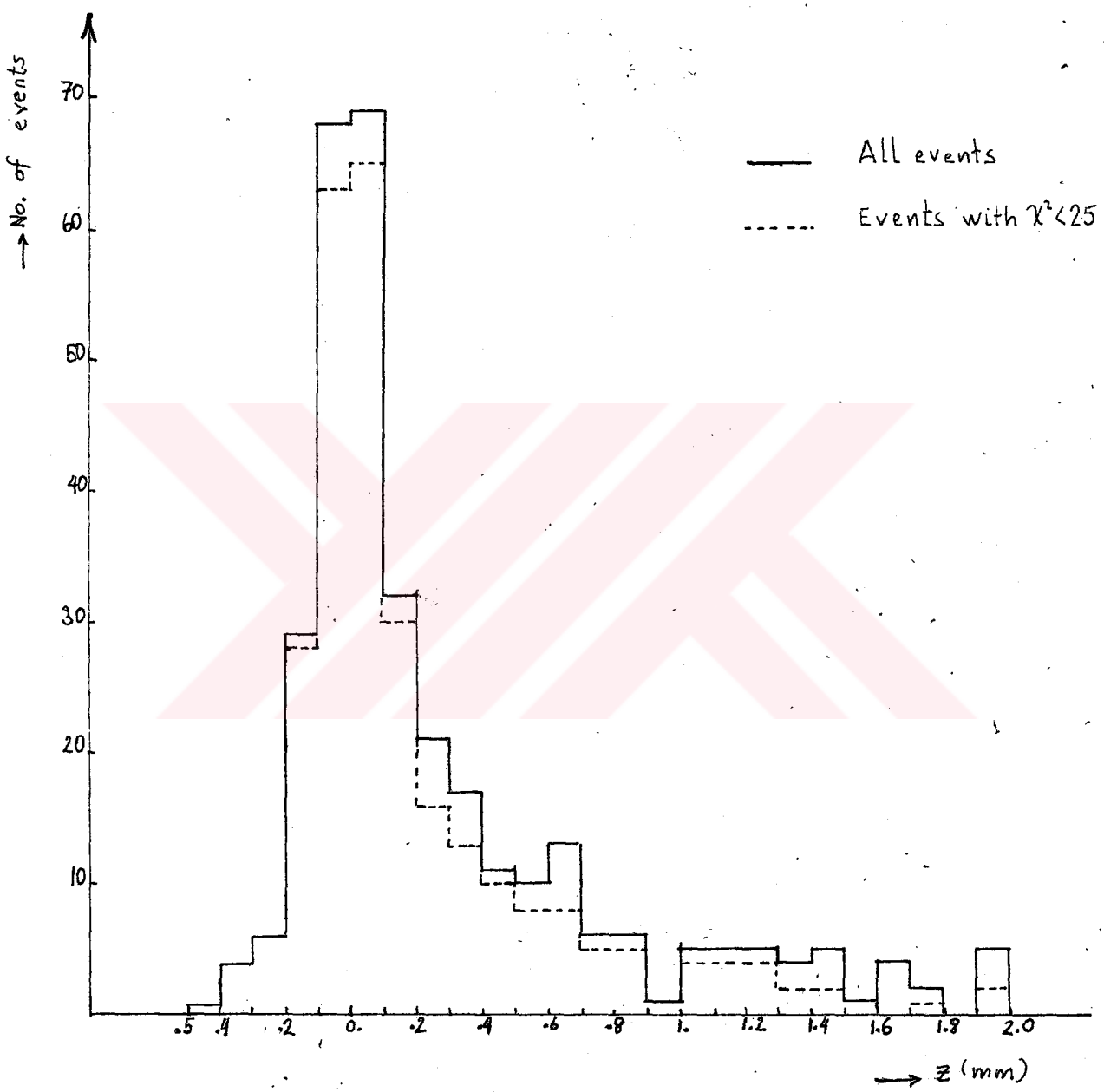
No. of events
70
60
50
40
30
20
10
All events
Events with $\chi^2<25$
.5
.4
.2
0.
.2
.4
.6
.8
1.
1.2
1.4
1.6
1.8
2.0
z (mm)

Fig. 16

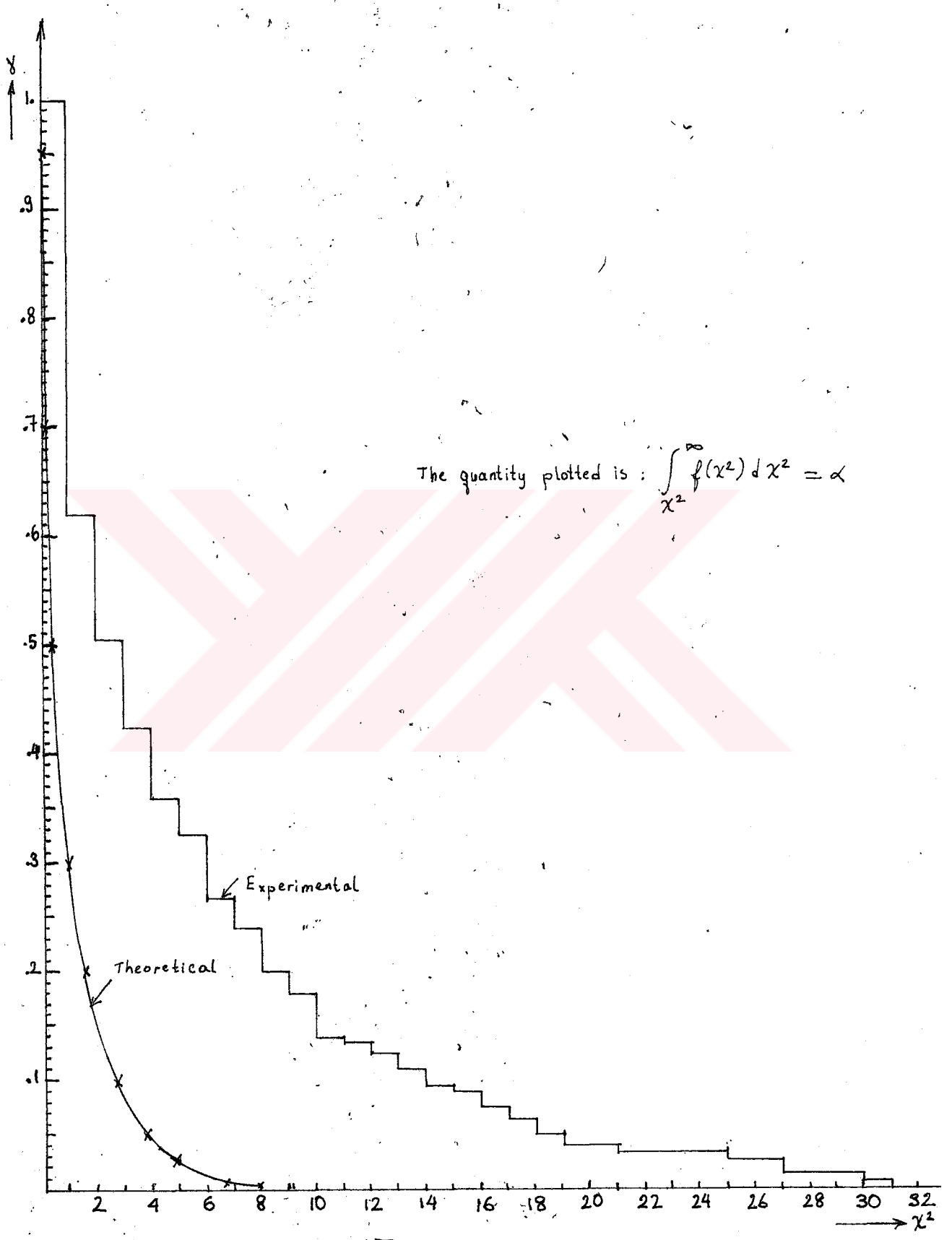
γ
1.
.9
.8
.7
.6
.5
.4
.3
.2
.1
The quantity plotted is : $\int_{\chi^2}^{\infty} f(\chi^2)\, d\chi^2 = \alpha$
Experimental
Theoretical
2
4
6
8
10
12
14
16
18
20
22
24
26
28
30
32
χ^2

Fig. 17

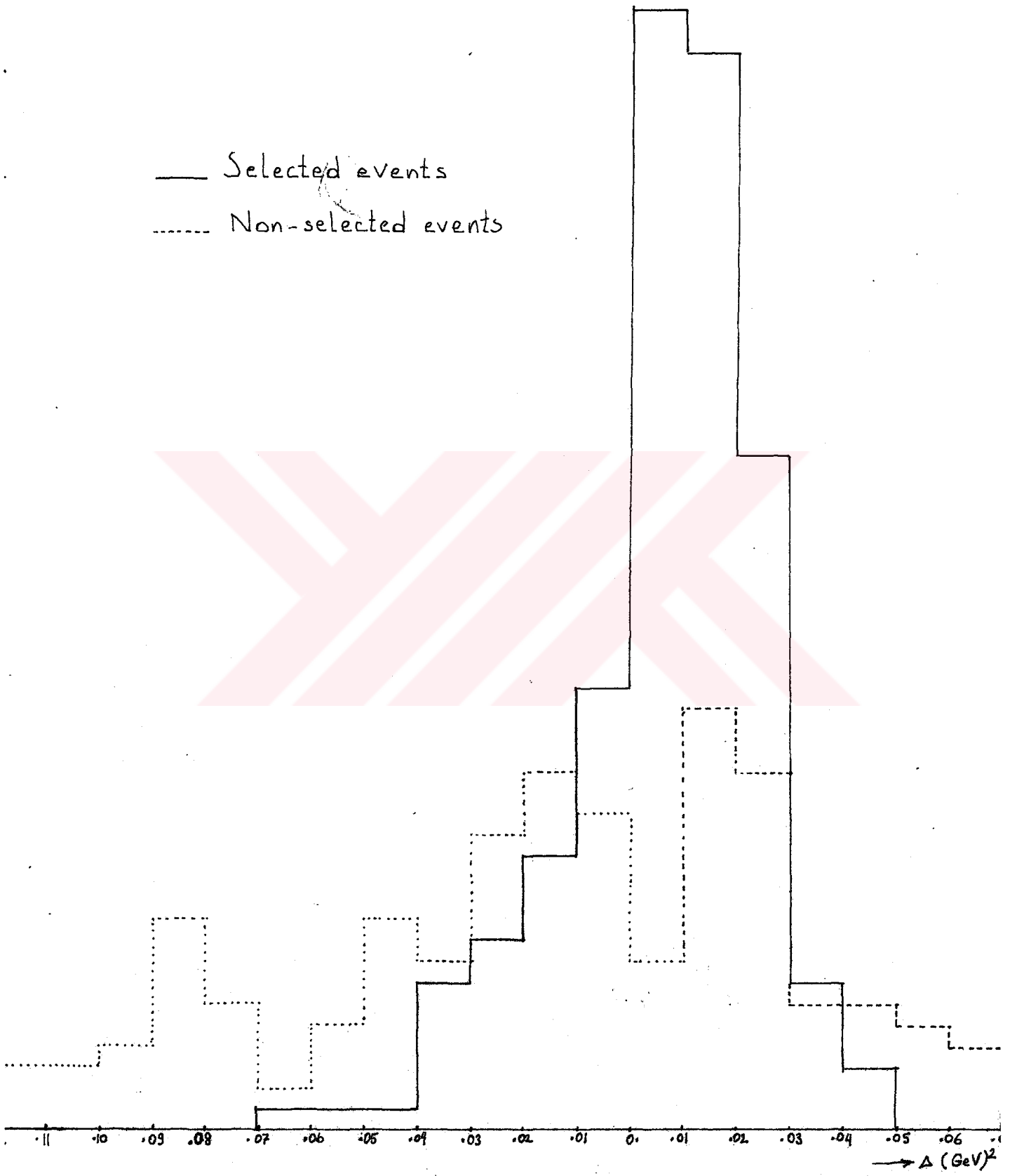
Selected events
Non-selected events
·11
·10
·09
·08
·07
·06
·05
·04
·03
·02
·01
0·
·01
·02
·03
·04
·05
·06
Δ (GeV)²

Fig. 18

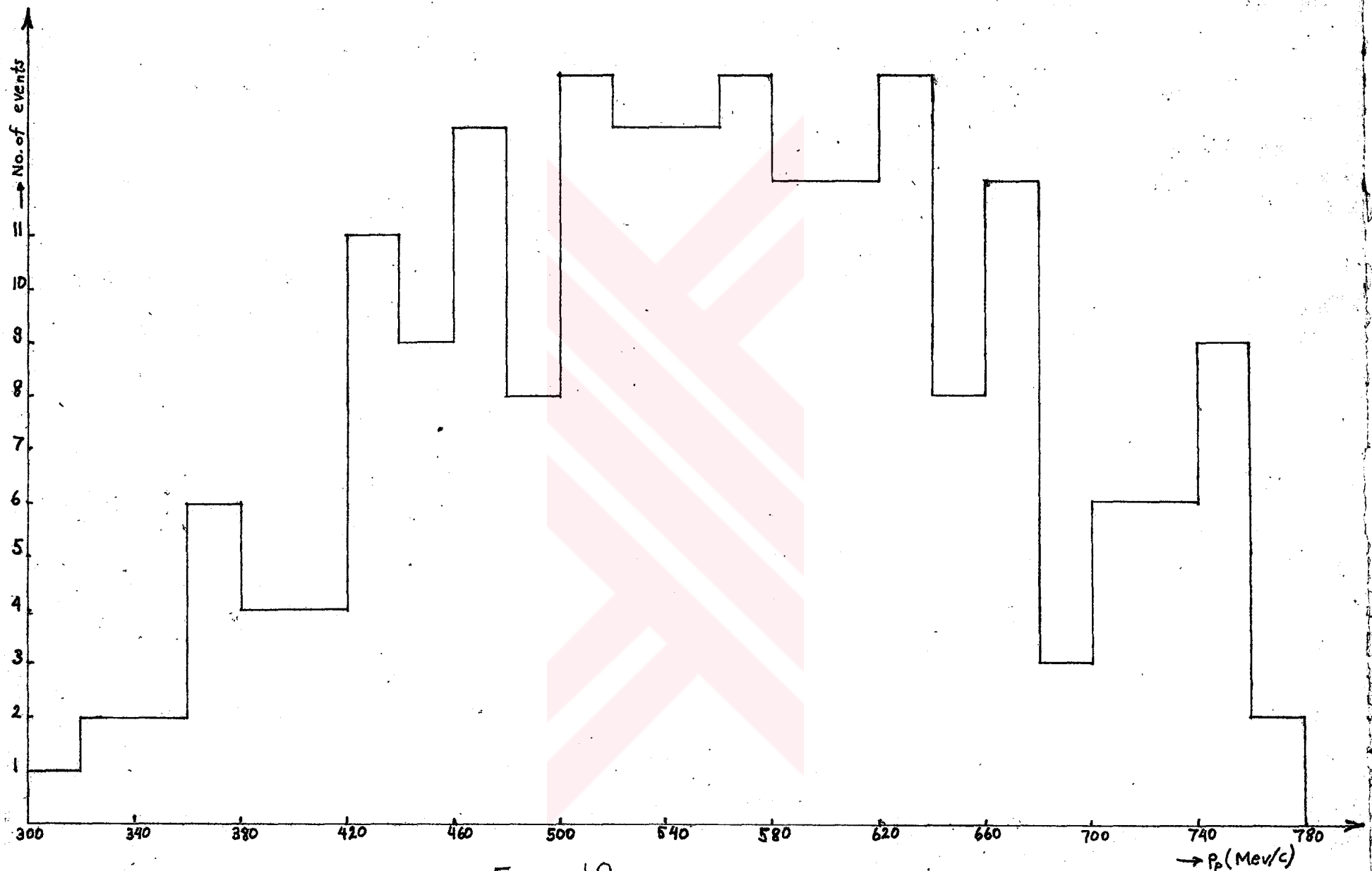
No. of events
1
2
3
4
5
6
7
8
9
10
11
300
340
380
420
460
500
540
580
620
660
700
740
780
P_p (Mev/c)

Fig. 19

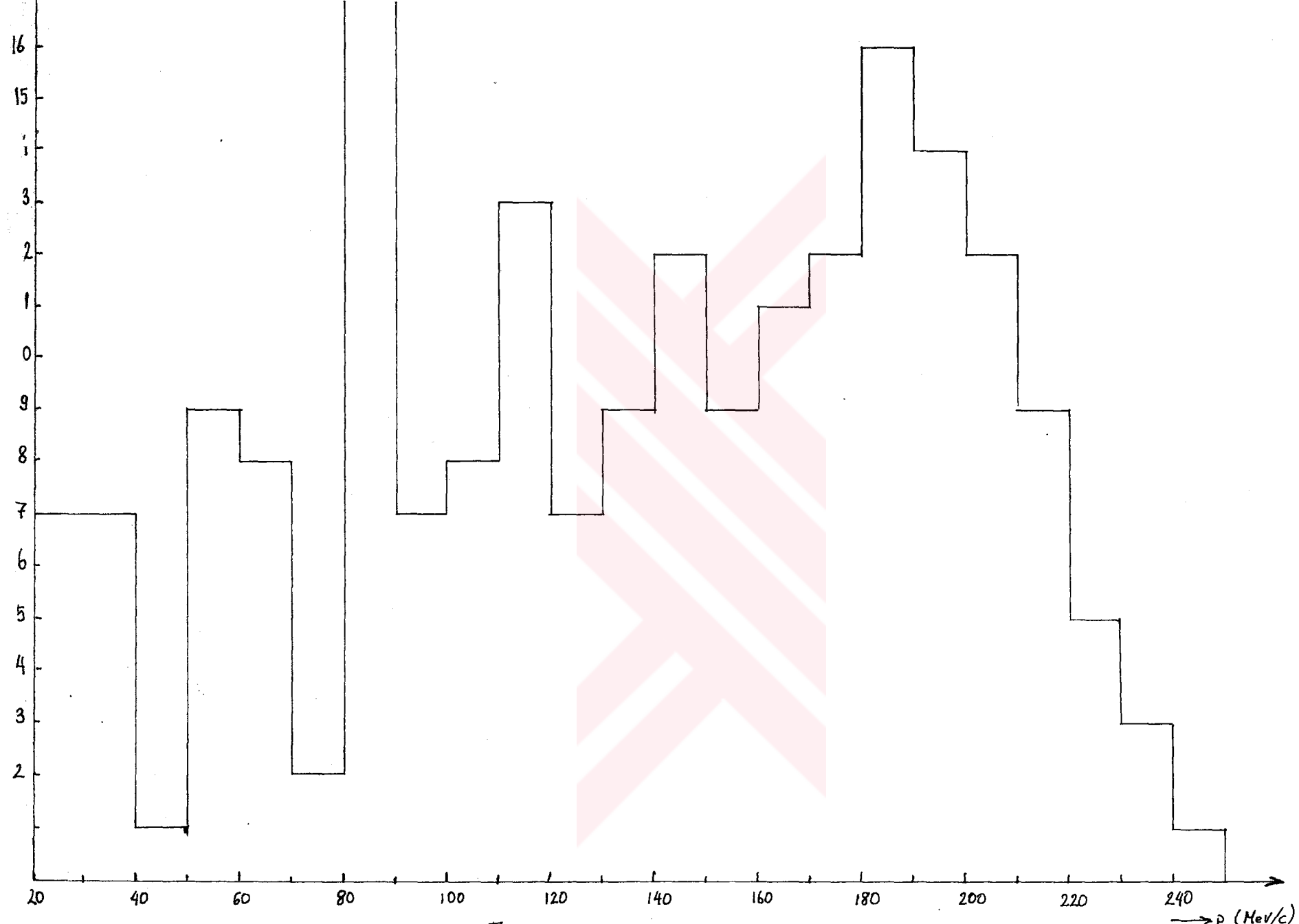
16
15
3
2
1
0
9
8
7
6
5
4
3
2
20
40
60
80
100
120
140
160
180
200
220
240
P_π (Mev/c)

Fig. 20

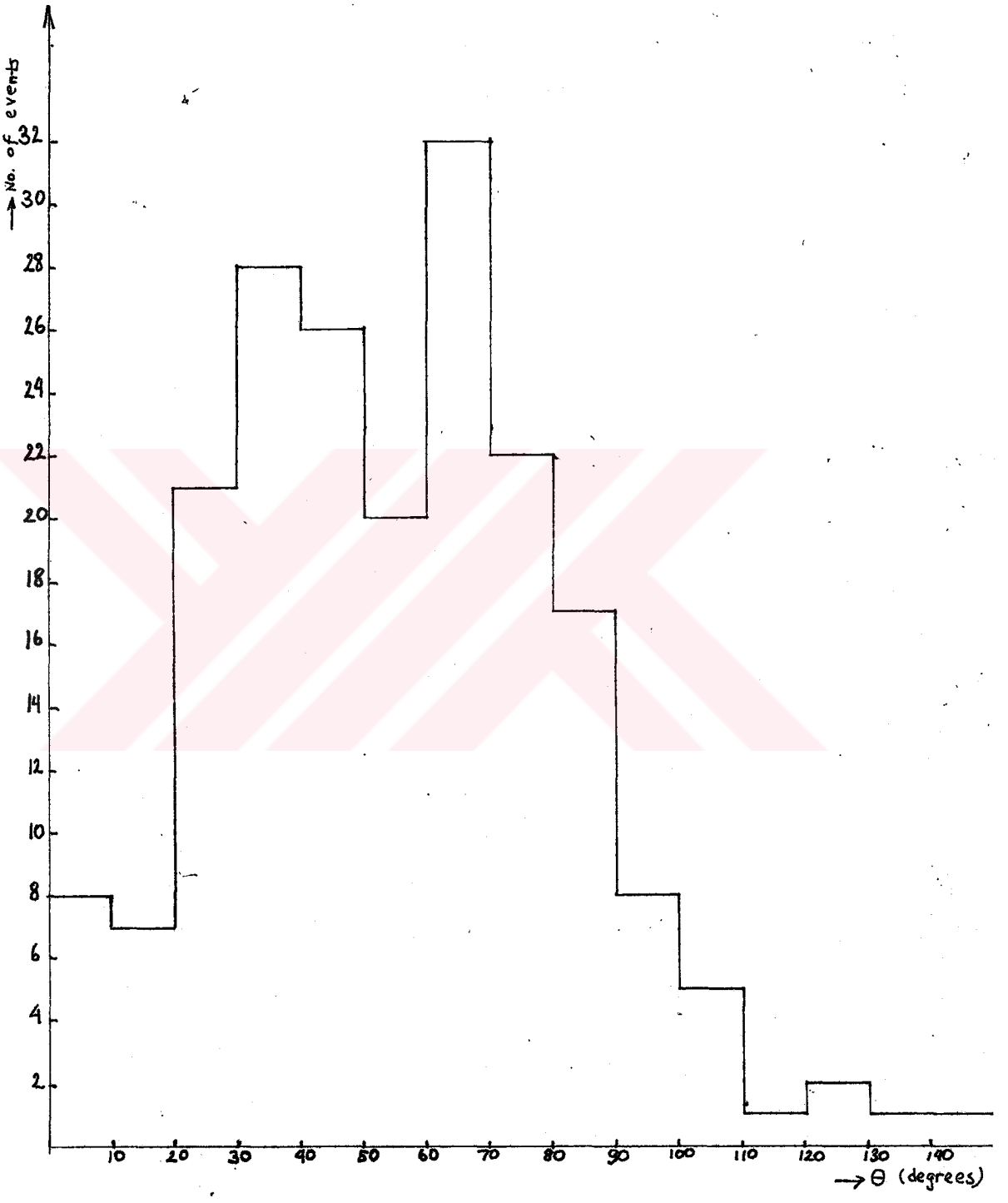
No. of events
32
30
28
26
24
22
20
18
16
14
12
10
8
6
4
2
10
20
30
40
50
60
70
80
90
100
110
120
130
140
θ (degrees)

Fig. 21

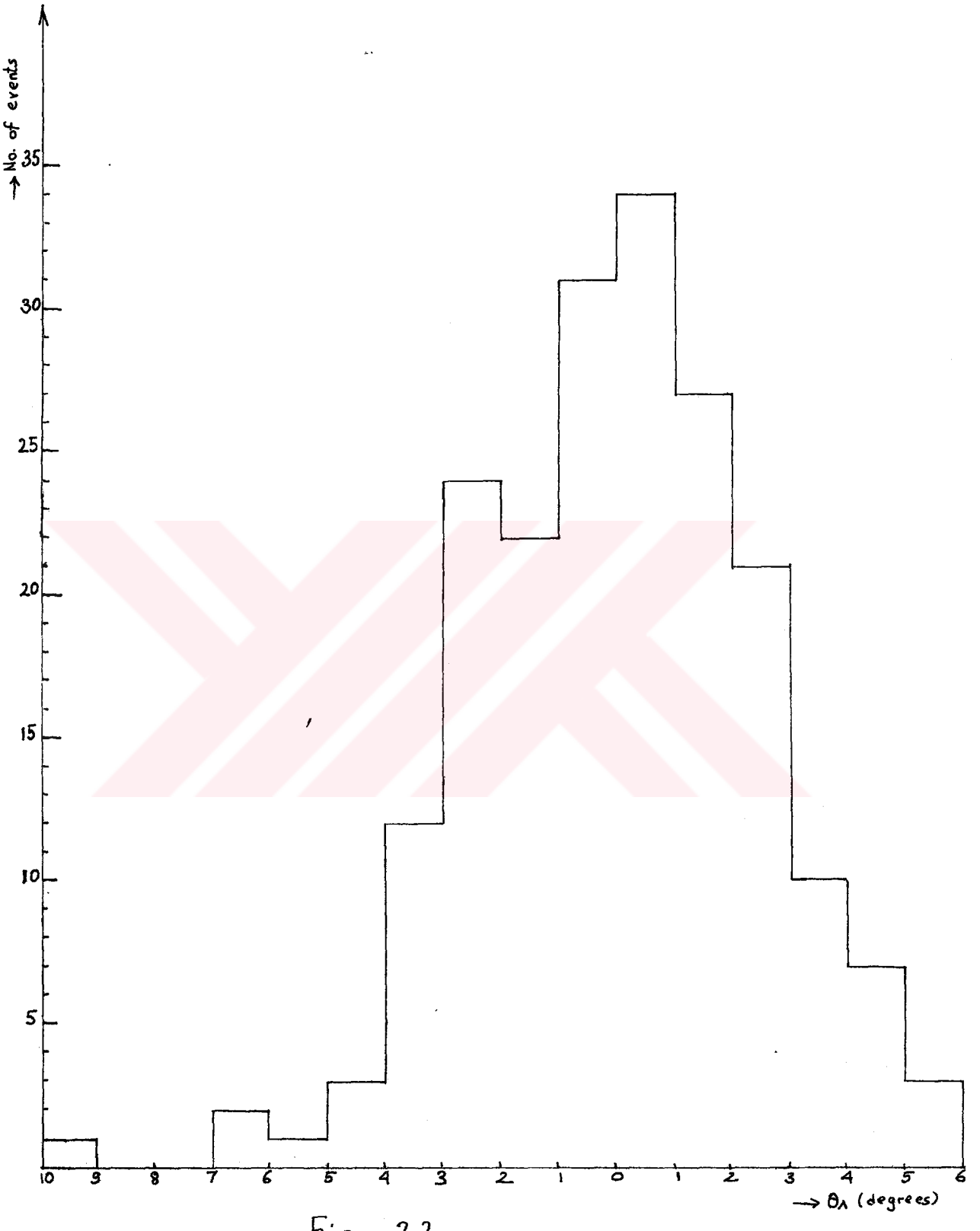
→ No. of events
35
30
25
20
15
10
5
10
9
8
7
6
5
4
3
2
1
0
1
2
3
4
5
6
→ θΛ (degrees)

Fig. 22

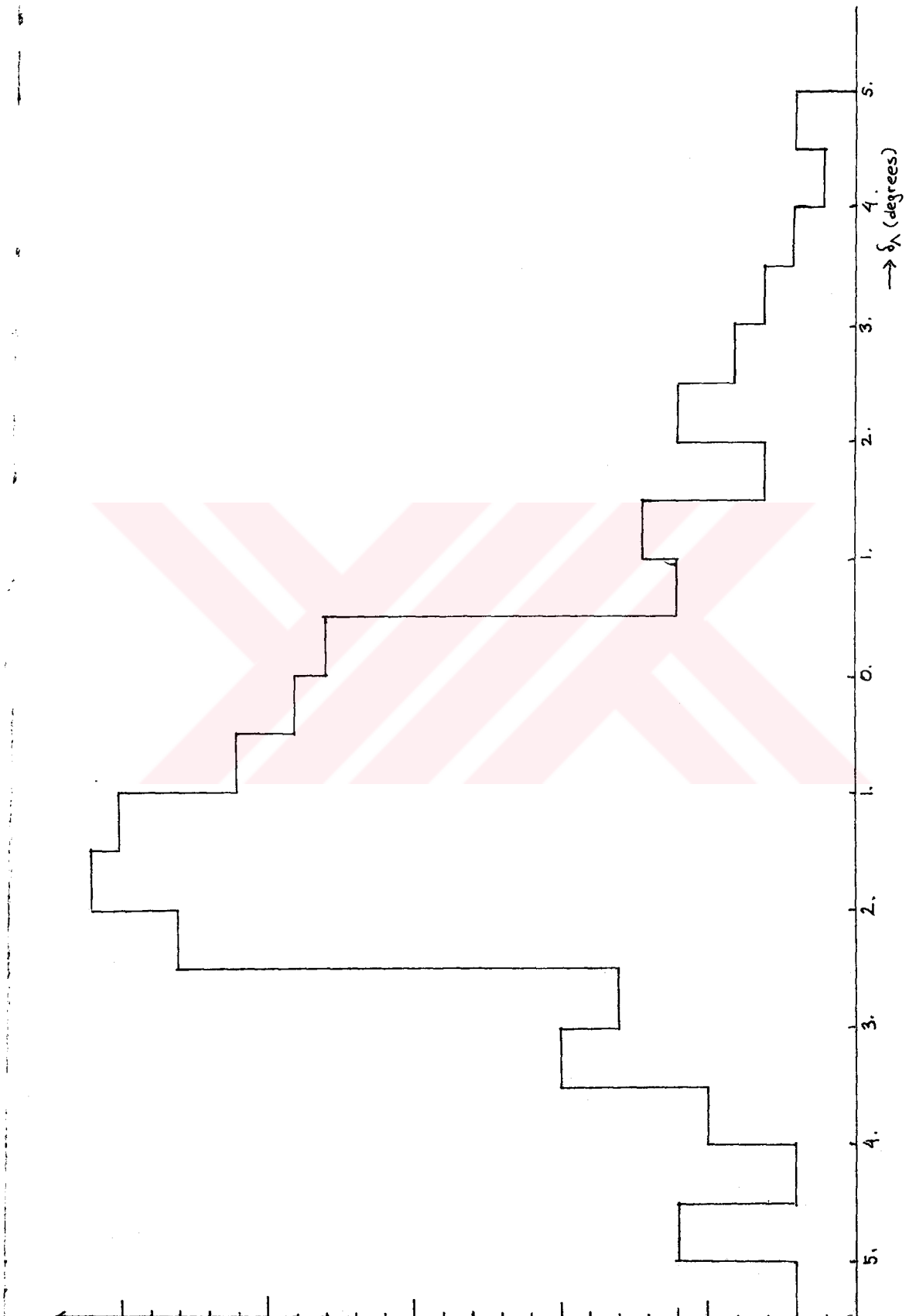

Fig. 23

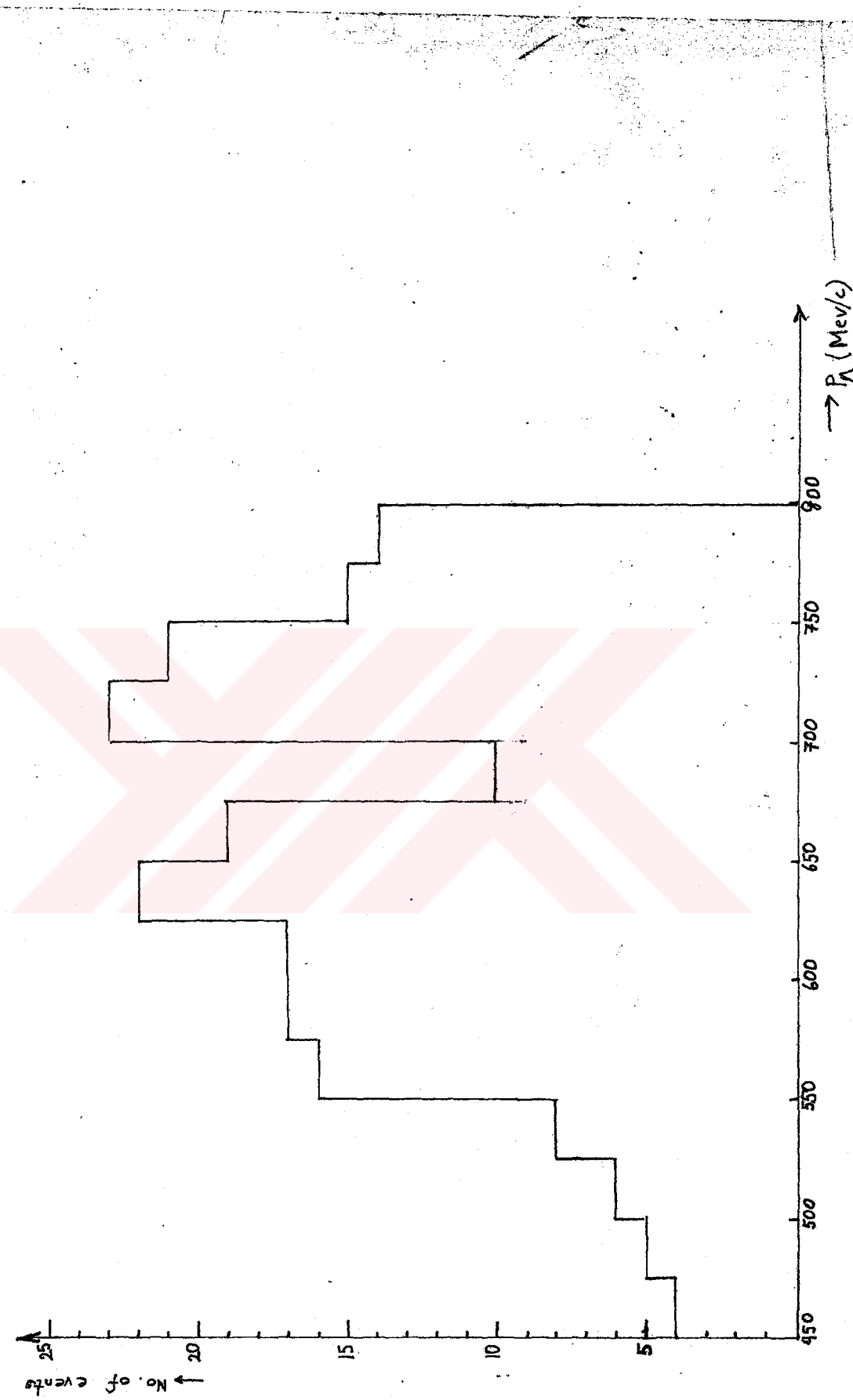
No. of events
25
20
15
10
5
450
500
550
600
650
700
750
800
P_Λ (Mev/c)

Fig. 24

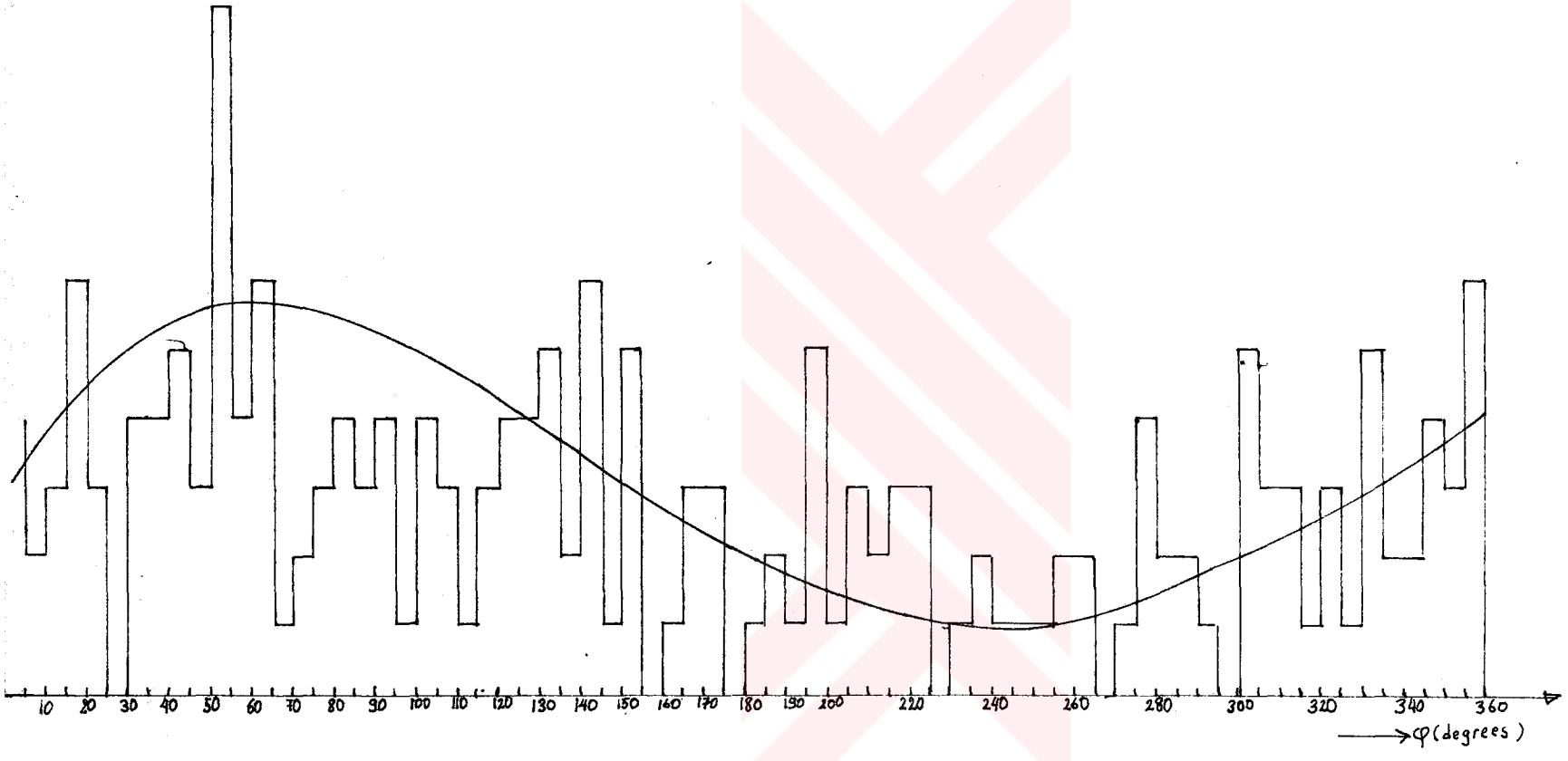
10 20 30 40 50 60 70 80 90 100 110 120 130 140 150 160 170 180 190 200 220 240 260 280 300 320 340 360
φ (degrees)

Fig. 25

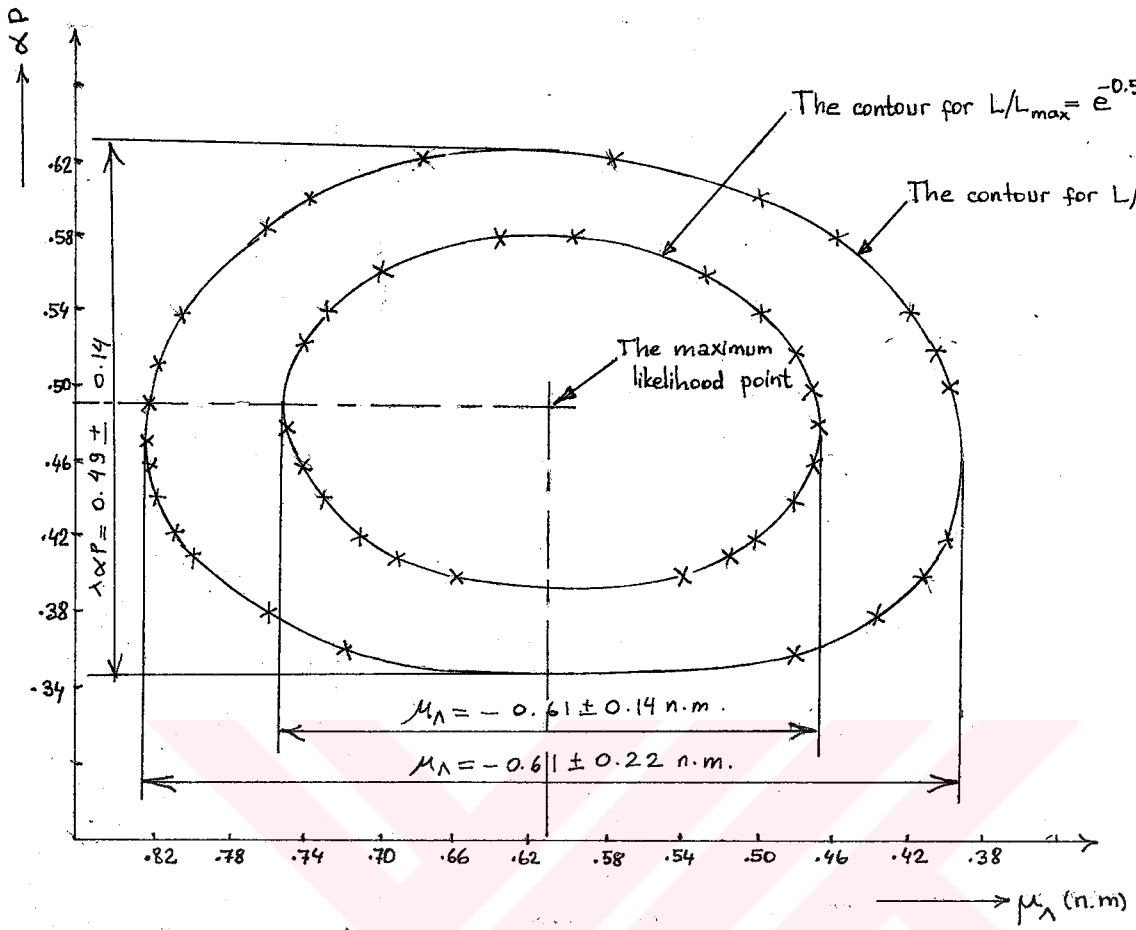

Fig. 26 a

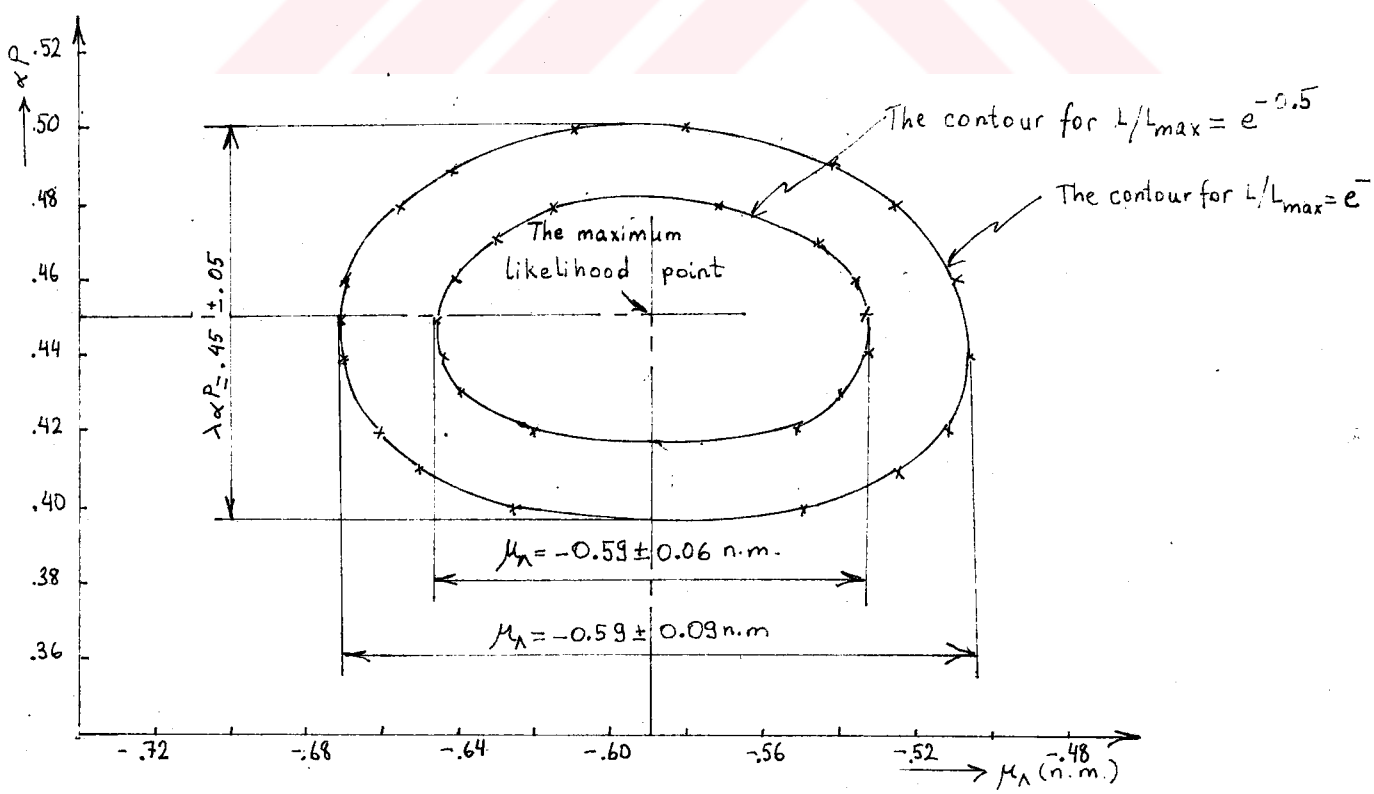

Fig: 26 b

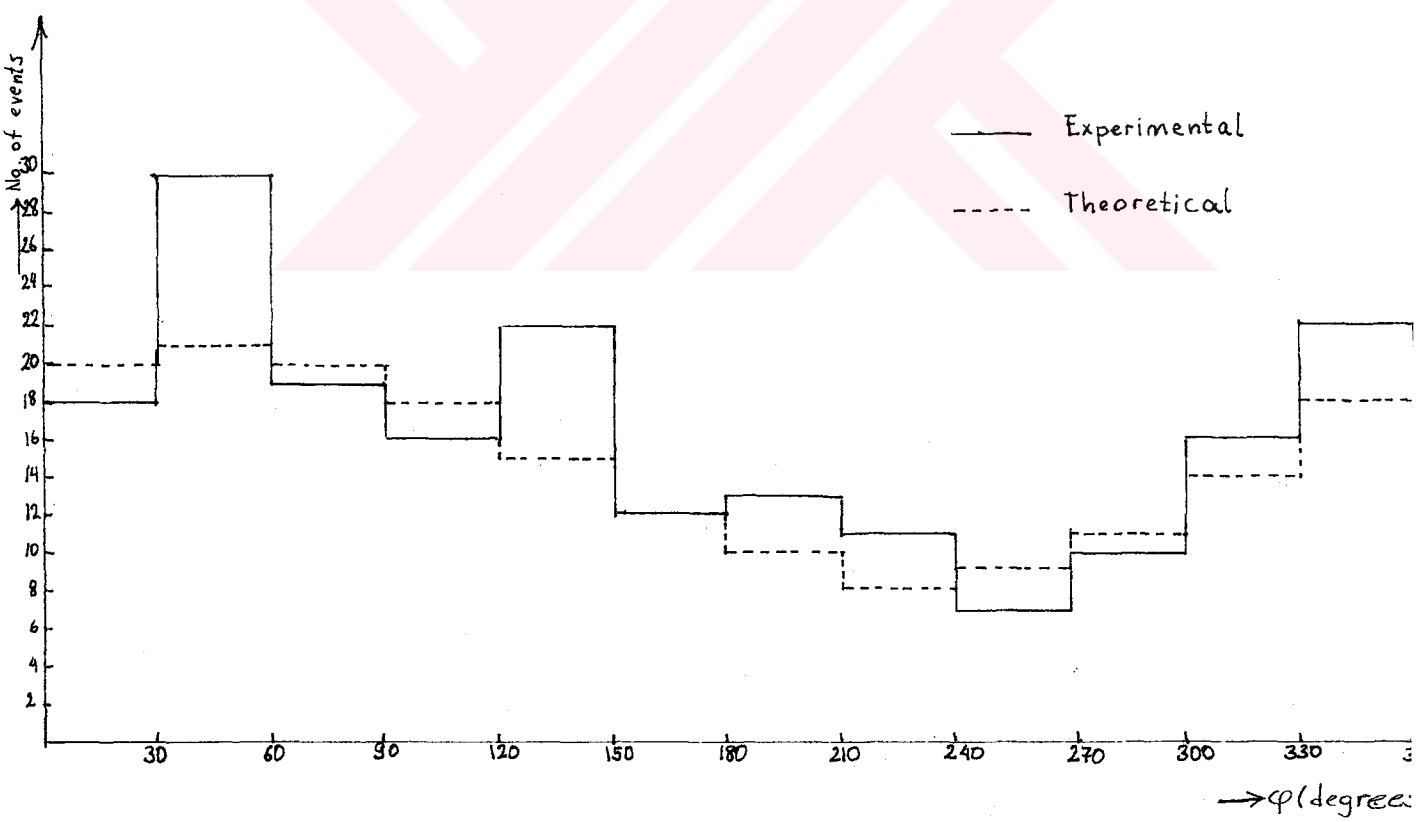
No. of events
Experimental
Theoretical
2
4
6
8
10
12
14
16
18
20
22
24
26
28
30
30
60
90
120
150
180
210
240
270
300
330
φ (degree

Fig. 27

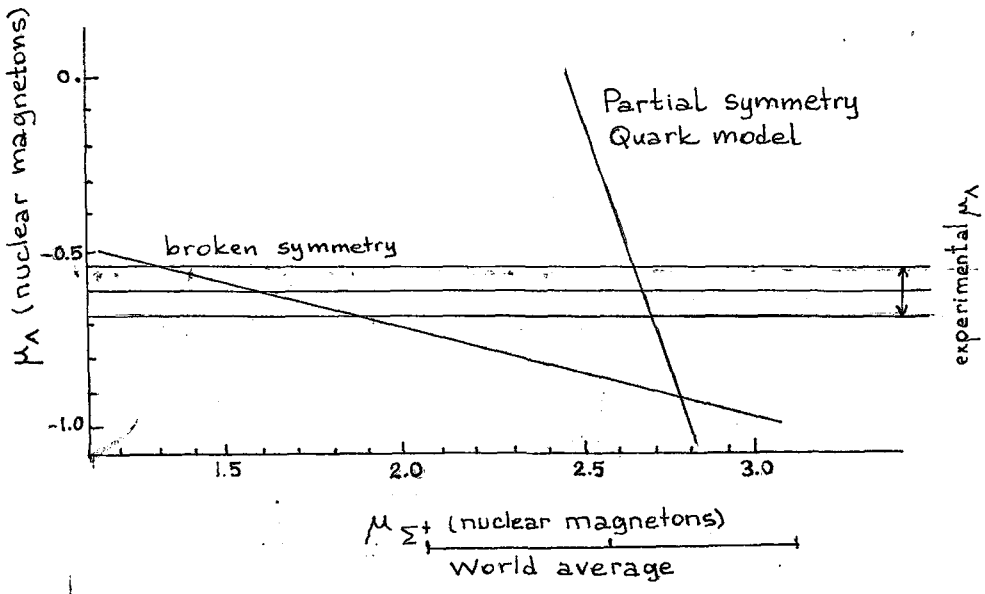
μ_Λ (nuclear magnetons)
0.
-0.5
-1.0
Partial symmetry
Quark model
broken symmetry
experimental μ_Λ
1.5
2.0
2.5
3.0
μ_{Σ^+} (nuclear magnetons)
World average

Fig. 28

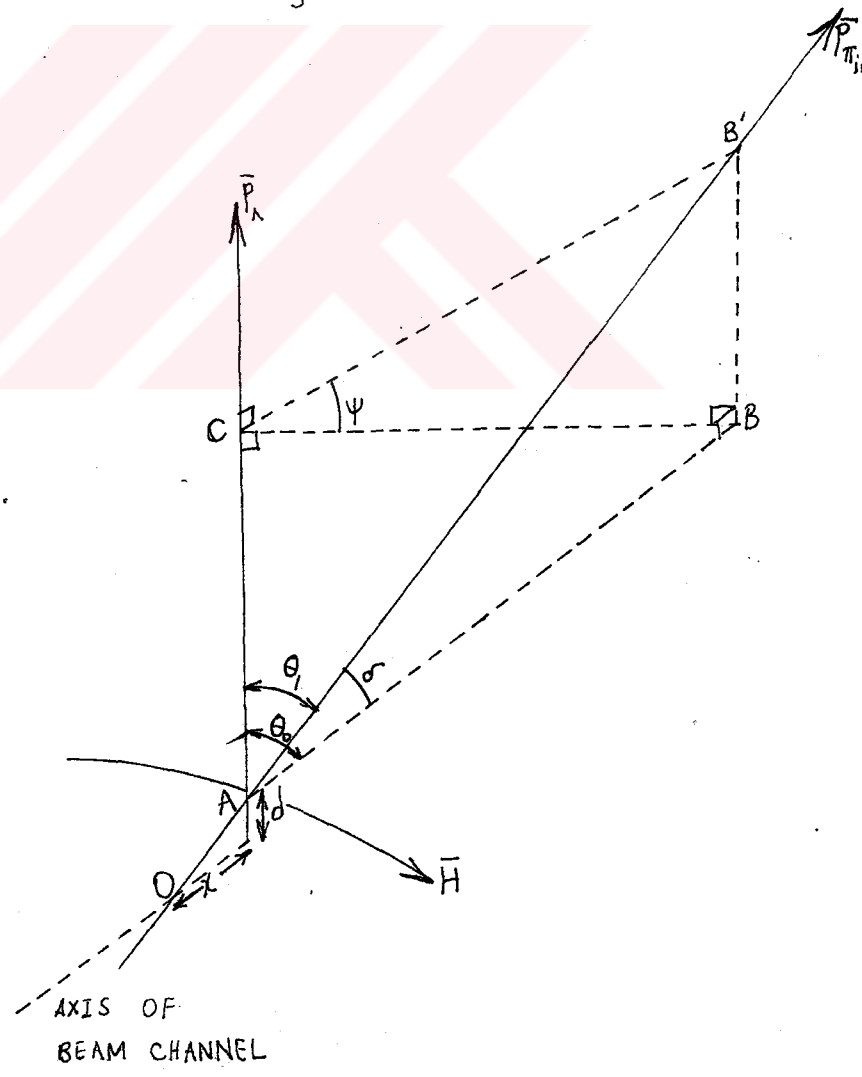
$\bar{P}_{\pi_{in}}$
B'
$\bar{P}_\Lambda$
C
Ψ
B
θ_1
σ
θ_0
A
d
O
$\bar{H}$
AXIS OF
BEAM CHANNEL

Fig. 29

```
' 360N-FO-479 3-6          MAINPGM          DATE    21/05/72      TIME     23.

      DIMENSION SA(25),X(19),Y(19),APS(3),ORD(3),TITLE(20)
     1,Z(19)
    6 READ(1,4) SF,BL
    4 FORMAT (2F5.2)
      DO 3 K=1,20
    3 SA(K)=0.
    1 READ(1,2) ID,J,JA,JB,KO,GA,LO,MO,KA,IKA,IZO,ND,IGA,IGB,IGC,IA,ZJ,
     1ZA8M
    2 FORMAT(I3,I2,2I1,I2,F2.0,I4,I2,I3,I4,4X,I3,I4,4I2,2F3.0,I1)
      J=J+100
      IF (IA) 35,35,50
   50 IF (IA-4) 10,10,51
   51 IF (IA-7) 11,11,52
   52 IF(IA-10) 12,12,53
   53 IF (IA-13) 13,13,54
   54 IF (IA-16) 14,14,55
   55 IF (IA-19) 15,15,56
   56 IF (IA-22) 16,16,57
   57 IF (IA-25) 17,17,58
   58 IF (IA-28) 18,18,59
   59 IF (IA-31) 19,19,60
   60 IF (IA-34) 20,20,61
   61 IF (IA-37) 21,21,62
   62 IF (IA-40) 22,22,63
   63 IF (IA-43) 23,23,64
   64 IF (IA-46) 24,24,65
   65 IF (IA-49) 25,25,66
   66 IF (IA-52) 26,26,67
   67 IF (IA-55) 27,27,28
   10 SA(1)=SA(1)+1.
      GO TO 1
   11 SA(2)=SA(2)+1.
      GO TO 1
   12 SA(3)=SA(3)+1.
      GO TO 1
   13 SA(4)=SA(4)+1.
      GO TO 1
    4 SA(5)=SA(5)+1.
      GO TO 1
    5 SA(6)=SA(6)+1.
      GO TO 1
   16 SA(7)=SA(7)+1.
      GO TO 1
   17 SA(8)=SA(8)+1.
      GO TO 1
   18 SA(9)=SA(9)+1.
      GO TO 1
   19 SA(10)=SA(10)+1.
      GO TO 1
   20 SA(11)=SA(11)+1.
      GO TO 1
   21 SA(12)=SA(12)+1.
      GO TO 1
   22 SA(13)=SA(13)+1.
```

```
    GO TO 1
 23 SA(14)=SA(14)+1.
    GO TO 1
 24 SA(15)=SA(15)+1.
    GO TO 1
 25 SA(16)=SA(16)+1.
    GO TO 1
 26 SA(17)=SA(17)+1.
    GO TO 1
 27 SA(18)=SA(18)+1.
    GO TO 1
 28 SA(19)=SA(19)+1.
    GO TO 1
 35 WRITE(3,7) J
  7 FORMAT (//8H  STACK=,I3)
 36 WRITE(3,8) JA
  8 FORMAT (/8H  PLATE=,I2)
 37 WRITE(3,9) JB
  9 FORMAT (/11H  TRAVERSE=,I2)
    XZ=3.
    DO 40 I=1,19
    X(I)=SA(I)
    Y(I)=XZ
    Z(I)=PLUS
 40 XZ=XZ+3.
    I=JA
    N=19
    NL=19
    NS=1
    IYFORM=1
    IYRGHT=3
    IXFORM=1
    IXRGTH=3
    READ(1,41) ORD,APS,TITLE
 41 FORMAT(2(3A4/),20A4)
    CALL GRAPH(X,Y,Z,N,ORD,APS,TITLE,I,NL,NS,IYFORM,IYRGHT,IXFORM,IXRG
   1HT)
    GO TO 6
 70 STOP
    DATA PLUS /'+'/
    END
```

PROG.2


```
      DIMENSION DA(19),X(19),Y(19),APS(3),ORD(3),TITLE(20)
     1,Z(19)
    6 READ(1,4) SF,BL
    4 FORMAT(2F5.2)
      DO 3 K=1,20
    3 DA(K)=0.
    1 READ(1,2) ID,J,JA,JB,KO,GA,LO,MO,KA,IKA,IZO,NO,IGA,IGB,IGC,IA,ZU,
     1ZA,M
    2 FORMAT(I3,I2,2I1,I2,F2.0,I4,I2,I3,I4,4X,I3,I4,4I2,2F3.0,I1)
      J=J+100
      IF(ZU-ZA) 91,90,90
   91 D=ATAN((ZU-ZA)*SF/BL)
      GO TO 92
   90 D=-ATAN((ZA-ZU)*SF/BL)
   92 D=D*180./3.1416
      IF (IA) 30,30,50
   50 IF (D+26.) 10,10,51
   51 IF (D+23.) 11,11,52
   52 IF (D+20.) 12,12,53
   53 IF (D+17.) 13,13,54
   54 IF (D+14.) 14,14,55
   55 IF (D+11.) 15,15,56
   56 IF (D+8.)  16,16,57
   57 IF (D+5.)  17,17,58
   58 IF (D+2.)  18,18,59
   59 IF (D-1.)  19,19,60
   60 IF (D-4.)  20,20,61
   61 IF (D-7.)  21,21,62
   62 IF (D-10.) 22,22,63
   63 IF (D-13.) 23,23,64
   64 IF (D-16.) 24,24,65
   65 IF (D-19.) 25,25,66
   66 IF (D-22.) 26,26,67
   67 IF (D-25.) 27,27,28
   10 DA(1)=DA(1)+1.
      GO TO 1
   11 DA(2)=DA(2)+1.
      GO TO 1
   12 DA(3)=DA(3)+1.
      GO TO 1
   13 DA(4)=DA(4)+1.
      GO TO 1
   14 DA(5)=DA(5)+1.
      GO TO 1
   15 DA(6)=DA(6)+1.
      GO TO 1
   16 DA(7)=DA(7)+1.
      GO TO 1
   17 DA(8)=DA(8)
      GO TO 1
   18 DA(9)=DA(9)
      GO TO 1
   19 DA(10)=DA(10)
      GO TO 1
```

```
   20 DA(11)=DA(11)
      GO TO 1
   21 DA(12)=DA(12)
      GO TO 1
   22 DA(13)=DA(13)
      GO TO 1
   23 DA(14)=DA(14)
      GO TO 1
   24 DA(15)=DA(15)
      GO TO 1
   25 DA(16)=DA(16)
      GO TO 1
   26 DA(17)=DA(17)
      GO TO 1
   27 DA(18)=DA(18)
      GO TO 1
   28 DA(19)=DA(19)+1.
      GO TO 1
   30 WRITE(3,7) J
    7 FORMAT (//8H  STAVK=,I3)
   36 WRITE(3,8) JA
    8 FORMAT (/8H  PLATE=,I2)
   37 WRITE (3,9) JB
    9 FORMAT(/11H  TRAVERSE=,I2)
      XZ=-27.
      DO 40 I=1,19
      X(I)=DA(I)
      Y(I)=XZ
      Z(I)=PLUS
   40 XZ=XZ+3.
      I=JA
      N=19
      NS=1
      NL=19
      READ(1,41) ORD,APS,TITLE
      IYFORM=1
      IYRGHT=3
      IXFORM=1
      IXRGHT=3
   41 FORMAT(2(3A4/),20A4)
      CALL GRAPH(X,Y,Z,N,ORD,APS,TITLE,I,NL,NS,IYFORM,IYRGHT,IXFORM,IXRG
     1HT)
      GO TO 6
   70 STOP
      DATA PLUS /'+'/
      END
```

```
/ 360N-FO-479 3-6          MAINPGM          DATE    21/06/72      TIME     23.

      DIMENSION DI(25),X(25),Y(25)
     1,Z(19)
    6 READ(1,4) SF,BL
    4 FORMAT(2F5.2)
      DO 3 K=1,20
    3 DI(K)=0.
    1 READ(1,2) JO,J,JA,JB,KO,GA,LO,MO,KA,IKA,IZO,NO,IGA,IGB,IGC,IA,ZU,
     ZA,M
    2 FORMAT(I3,I2,2I1,I2,F2.0,I4,I2,I3,I4,4X,I3,I4,4I2,2F3.0,I1)
      J=J+100
      GB=GA*BL
      IF (IA) 35,35,50
   50 IF(IGA-47) 10,10,51
   51 IF(IGA-50) 11,11,52
   52 IF(IGA-53) 12,12,53
   53 IF(IGA-56) 13,13,54
   54 IF(IGA-59) 14,14,55
   55 IF(IGA-62) 15,15,56
   56 IF(IGA-65) 16,16,57
   57 IF(IGA-68) 17,17,58
   58 IF(IGA-71) 18,18,59
   59 IF(IGA-74) 19,19,60
   60 IF(IGA-77) 20,20,61
   61 IF(IGA-80) 21,21,62
   62 IF(IGA-83) 22,22,63
   63 IF(IGA-86) 23,23,64
   64 IF(IGA-89) 24,24,65
   65 IF(IGA-92) 25,25,66
   66 IF(IGA-95) 26,26,67
   67 IF(IGA-98) 27,27,28
   10 DI(1)=DI(1)+1.
      GO TO 1
   11 DI(2)=DI(2)+1.
      GO TO 1
   12 DI(3)=DI(3)+1.
      GO TO 1
   13 DI(4)=DI(4)+1.
      GO TO 1
   14 DI(5)=DI(5)+1.
      GO TO 1
   15 DI(6)=DI(6)+1.
      GO TO 1
   16 DI(7)=DI(7)+1.
      GO TO 1
   17 DI(8)=DI(8)+1.
   18 DI(9)=DI(9)+1.
      GO TO 1
   19 DI(10)=DI(10)+1.
      GO TO 1
   20 DI(11)=DI(11)+1.
      GO TO 1
   21 DI(12)=DI(12)+1.
      GO TO 1
   22 DI(13)=DI(13)+1.
```

```
      GO TO 1
   23 DI(14)=DI(14)+1.
      GO TO 1
   24 DI(15)=DI(15)+1.
      GO TO 1
   25 DI(16)=DI(16)+1.
      GO TO 1
   26 DI(17)=DI(17)+1.
      GO TO 1
   27 DI(18)=DI(18)+1.
      GO TO 1
   28 DI(19)=DI(19)+1.
      GO TO 1
   35 WRITE(3,7) J
    7 FORMAT(//8H  STACK=,I3)
   36 WRITE(3,8) JA
    8 FORMAT (/8H  PLATE=,I2)
   37 WRITE(3,9) JB
    9 FORMAT (/11H  TRAVERSE=,I2)
   38 WRITE(3,43) GA
   43 FORMAT (//9H  G MIN =,F3.0)
   39 WRITE(3,44) GB
   44 FORMAT (/12H  G MIN/BOX=,F3.0)
      XZ=46.
      DO 40 I=1,19
      Y(I)=XZ
      X(I)=DI(I)
      Z(I)=PLUS
   40 XZ=XZ+3.
      I=JA
      N=19
      NL= 9
      NS=1
      IYFORM=1
      IYRGHT=3
      IXFORM=1
      IXRGHT=3
      READ(1,41) ORD,APS,TITLE
   41 FORMAT(2(3A4/),20A4)
      CALL GRAPH(X,Y,Z,N,ORD,APS,TITLE,I,NL,NS,IYFORM,IYRGHT,IXFORM,IXRG
     1HT)
      GO TO 6
   70 STOP
      DATA PLUS /'+'/
      END
```

```
      DIMENSION G(50), V(50), DG(50)
    1 READ 2,A,N
    2 FORMAT (F5.3,I4)
      PRINT 3
    3 FORMAT (//12H        INPUT)
      DO 5 I=1,N
      READ 4,V(I),G(I),DG(I)
    4 FORMAT (3F5.3)
      PRINT 14,V(I),G(I),DG(I)
   14 FORMAT (3F8.3)
    5 CONTINUE
      PRINT 21
   21 FORMAT(//51H        C          B          B          A          CHI)
      IT=1
    6 S1=0.
      S2=0.
      S3=0.
      S4=0.
      S5=0.
      DO 10 I=1,N
      Y=G(I)-A
      ELY=ALOG(Y)
      RDY=Y*Y/(DG(I)*DG(I))
      ELV=ALOG(V(I))
      S1=S1+ELV*RDY
      S2=S2+ELV*ELV*RDY
      S3=S3+RDY
      S4=S4+ELY*ELV*RDY
   10 S5=S5+ELY*RDY
      DET=S1*S1-S2*S3
      ELB=(S4*S1-S2*S5)/DET
      B1=EXP(ELB)
      C=(S4*S3-S5*S1)/DET
      S6=0.
      S7=0.
      S8=0.
      S9=0.
      S10=0.
      DO 20 I=1,N
      VC=V(I)**C
      RDG=1./(DG(I)*DG(I))
      R=1./(DG(I)*DG(I)*VC)
      S6=S6+R/VC
      S7=S7+RDG
      S8=S8+R
      S9=S9+G(I)*RDG
   20 S10=S10+G(I)*R
      DET=S6*S7-S8*S8
      A=(S6*S9-S8*S10)/DET
      B2=(S7*S10-S8*S9)/DET
      S11=0.
      DO 30 I=1,N
      T=G(I)-A-B2/(V(I)**C)
      RDG=1./(DG(I)*DG(I))
```

```
      T=T*T*RDG
   30 S11=S11+T
      PRINT 40,C,B1,B2,A,S11
   40 FORMAT (//4F10.3,5X,F10.3)
      IT=IT+1
      IF (IT-15) 6,6,15
   15 PRINT 55
   55 FORMAT (//24H                FITTED CURVE)
      V(1)=.3
      DO 50 I=1,15
      GF=A+B2/(V(I)**C)
      ELV=ALOG(V(I))
      ELG=ALOG(GF)
      RGM=SQRT(1.-V(I)*V(I))
      IF (RGM) 51,52,51
   51 PP=938.21*V(I)/RGM
      GO TO 54
   52 PP=9999.
   54 PRINT 56, V(I),GF,ELV,ELG,PP
   56 FORMAT (2F10.3,2F10.4,F10.0)
   50 V(I+1)=V(I)+.05
      GO TO 1
      END
```

```
      DIMENSION G(50), V(50), DG(50)
    1 READ 2, EX, N
    2 FORMAT (F5.3,I4)
      PRINT 3
    3 FORMAT (//12H          INPUT)
      DO 5 I=1,N
      READ 4,V(I),G(I),DG(I)
    4 FORMAT (3F5.3)
      ELV=ALOG(V(I))
      ELG=ALOG(G(I))
      PRINT 14,V(I),G(I),DG(I),ELV,ELG
   14 FORMAT (5F8.3)
    5 CONTINUE
    6 S1=0.
      S2=0.
      S3=0.
      S4=0.
      S5=0.
      S6=0.
      S7=0.
      S8=0.
      DO 10 I=1,N
      ELG=ALOG(G(I))
      ELV=ALOG(V(I))
      ELV2=ELV*ELV
      RDG=G(I)*G(I)/(DG(I)*DG(I))
      S1=S1+RDG
      S2=S2+ELV*RDG
      S3=S3+ELV2*RDG
      S4=S4+ELV*ELV2*RDG
      S5=S5+ELV2*ELV2*RDG
      S6=S6+ELG*RDG
      S7=S7+ELG*ELV*RDG
   10 S8=S8+ELG*ELV2*RDG
      DET=S1*S3*S5-S1*S4*S4+S2*S4*S3-S2*S2*S5+S3*S2*S4-S3*S3*S3
      A=S6*S3*S5-S6*S4*S4+S2*S4*S8-S2*S7*S5+S3*S7*S4-S3*S3*S8
      B=S1*S7*S5-S1*S4*S8+S6*S4*S3-S6*S2*S5+S3*S2*S8-S3*S7*S3
      C=S1*S3*S8-S1*S7*S4+S2*S7*S3-S2*S2*S8+S6*S2*S4-S6*S3*S3
      A=A/DET
      B=B/DET
      C=C/DET
      S10=0.
      DO 20 I=1,N
      ELG=ALOG(G(I))
      ELV=ALOG(V(I))
      RDG=G(I)*G(I)/(DG(I)*DG(I))
      X=ELG-A-B*ELV-C*ELV*ELV
   20 S10=S10+X*X*RDG
      PRINT 21
   21 FORMAT(//38H          A          B          C          CHI)
      PRINT 30,A,B,C,S10
   30 FORMAT (//4F10.3,5X,E10.0)
      PRINT 55
   55 FORMAT (//24H                FITTED CURVE)
```

```
      V(1)=.3
      DO 50  I=1,15
      ELV=ALOG(V(I))
      ELG=A+B*ELV+C*ELV*ELV
      GF=EXP(ELG)
      RGM=SQRT(1.-V(I)*V(I))
      IF (RGM) 51,52,51
   51 PP=938.21*V(I)/RGM
      GO TO 54
   52 PP=9999.
   54 PRINT 56,V(I),GF,ELV,ELG,PP
   56 FORMAT (2F10.3,2F10.4,F10.0)
   50 V(I+1)=V(I)+.05
      GO TO 1
      END
```

PROG.6

```
JOB H26106 GULSEN ONENGUT
EXEC FFORTRAN
   IMPLICIT REAL*8 (A-H,O-Z)
   DIMENSION EP(10),EPI(10),PP(11),PPI(11),TETA(11),B(10),C(10),
  1D(10),DELPPI(10),DELPP(10),E(10),DELT(10),ALPHA(11),SKI(11),
  2A(10),AA(10),AB(10),AC(10),SA(11),SB(11),SC(11),SD(11),CT(10),
  3ST(10),TE(10),TET(11)
12 READ(1,1) W,K,S,P,Y,X,Z,L,M,V,T,EG,PAP,PAPI,DELXP,DELZP2,PG,PGZ,
  1DELXPI,DEZPI2,PIG,PIGZ,RAN,EN
 1 FORMAT (A1,I1,F3.0,F1.0,2F3.1,F3.3,I1,I1,F4.0,F3.0,F4.2,2F4.1,
  1F3.0,3F4.0,F3.0,3F4.0,F5.0,F9.0)
   IF(Z-0.05) 12,901,901
01 IF(Z-0.95) 902,902,12
02 IF(K-5) 80,80,12
41 READ(1,144) W,K,S,P,Y,X,Z,L,M,V,T8,EG8,PAP8,PAPI8,DELXP8,DELZP8,PG
  18,PGZ8,ELXPI8,ELZPI8,PIG8,PIGZ8,RAN,EN
44 FORMAT(A1,I1,F3.0,F1.0,2F3.1,F3.3,I1,I1,F4.0,F3.0,F4.2,2F4.1,F3.0,
  13F4.0,F3.0,3F4.0,F5.0,F9.0)
   IF(K-5) 146,80,80
46 T=T8
   EG=EG8
   PAP=PAP8
   PAPI=PAPI8
   DELXP=DELXP8
   DELZP2=DELZP8
   PG=PG8
   PGZ=PGZ8
   DELXPI=ELXPI8
   DEZPI2=ELZPI8
   PIG=PIG8
   PIGZ=PIGZ8
80 IF (PAP-PAPI) 2,2,3
 2 ALPH=PAPI-PAP
   GO TO 311
 3 ALPH=PAP-PAPI
11 IF(180.0-ALPH) 50,50,51
50 ALP=(360.0-ALPH)*3.1416/180.
   GO TO 15
51 ALP=ALPH*3.1416/180.
15 SHRFAC=1260./T
   CALP=DCOS(ALP)
   SALP=DSIN(ALP)
   DELZP=DELZP2*SHRFAC
   DELZPI=DEZPI2*SHRFAC
   IF(DELZP) 25,26,26
25 DIVP=DABS(DELZP/DELXP)
   DELP=DATAN(DIVP)
   SIP=-DSIN(DELP)
   GO TO 24
26 DELP=DATAN(DELZP/DELXP)
   SIP=DSIN(DELP)
24 IF(DELZPI) 27,28,28
27 DIVPI=DABS(DELZPI/DELXPI)
   DELPI=DATAN(DIVPI)
   SIPI=-DSIN(DELPI)
   GO TO 30
E  1
```

```
28 DELPI=DATAN(DELZPI/DELXPI)
   SIPI=DSIN(DELPI)
30 RA=SIP*SIPI
   COPI=DCOS(DELPI)
   COP=DCOS(DELP)
   RAB=RA+COPI*COP*CALP
   IF(RAB) 31,32,32
31 ABSRA=DABS(RAB)
   TETAZ=3.1416-DARCOS(ABSRA)
   GO TO 34
32 TETAZ=DARCOS(RAB)
34 GP=COP*PG/(PGZ*(EG/100.))
59 AL=DLOG(GP)
   ALBP=-(2.157-DSQRT(2.157*2.157+4.*0.554*(-0.311-AL)))/(2.*0.554)
   BP=DEXP(ALBP)
   PPZ=938.3*BP/(DSQRT(1.-BP*BP))
   AS=(1115.58*1115.58-938.256*938.256-139.579*139.579)/2.
   PP(1)=PPZ
   TETA(1)=TETAZ
64 ERGP=1./PG+1./(100.*EG)
66 ERBP=ERGP/((-2.157-1.108*DLOG(BP))*(-2.157-1.108*DLOG(BP)))
   ERP=ERBP/((1.-BP*BP)*(1.-BP*BP))
   ERP=ERP*PPZ*PPZ
   ERX=(2./126.)*(2./126.)
   ERZP=(4./DELZP)*(4./DELZP)
   YP=DELXP*DELXP+DELZP*DELZP
   YPNA=DELXP*DELXP*DELXP*DELXP*DELZP*DELZP
   YPNB=DELP*DELP*COP*COP
   YPNC=YP*YP*YP
   ERDELP=YPNA*(ERZP+ERX)/(YPNC*YPNB)
   ERZPI=(4./DELZPI)*(4./DELZPI)
   YPI=DELXPI*DELXPI+DELZPI*DELZPI
   YPINA=DELXPI*DELXPI*DELXPI*DELXPI*DELZPI*DELZPI
   YPINC=YPI*YPI*YPI
   YPINB=DELPI*DELPI*COPI*COPI
   ERDEPI=YPINA*(ERZPI+ERX)/(YPINC*YPINB)
   ERA=(0.1*3.1416/180.)/ALP
   ERAL=ERA*ERA
   ABA=SIP*COPI*CALP-COP*SIPI
   IF(TETAZ-3.1416/2.) 35,35,36
35 SITEZ=DSIN(TETAZ)
   GO TO 37
36 SITEZ=DSIN(3.1416-TETAZ)
37 A1=DELP*ABA/(TETAZ*SITEZ)
   ACA=COP*SIPI*CALP-SIP*COPI
   A2=DELPI*ACA/(TETAZ*SITEZ)
   ADA=ALP*COP*COPI*SALP
   A3=ADA/(TETAZ*SITEZ)
   IF(K-5) 176,151,715
76 IF(PIG) 12,141,161
51 GPI8=COPI*PIG8/(PIGZ8*(EG8/100.))
   GPI=(GPI*PIGZ+GPI8*PIGZ8)/(PIGZ+PIGZ8)
   GO TO 162
61 GPI=COPI*PIG/(PIGZ*(EG/100.))
62 APL=DLOG(GPI)
   ALBI=-(2.157-DSQRT(2.157*2.157+4.*0.554*(-.311-APL)))/(2.*.554)
E  2
```

```
    BPI=DEXP(ALBI)
    IF(1.-BPI*BPI) 12,12,13
13  PPIZ=139.58*BPI/(DSQRT(1.-BPI*BPI))
    C2=-2.157-1.108*DLOG(BPI)
    IF(K-5) 168,167,12
67  ERGPI=1./(PIG+PIG8)+1./(100.*EG)
    GO TO 169
68  ERGPI=1./PIG+1./(100.*EG)
69  ERBPI=ERGPI/(C2*C2)
    ERPI=ERBPI/((1.-BPI*BPI)*(1.-BPI*BPI))
    ERPI=ERPI*PPIZ*PPIZ
    GO TO 720
15  ARAN=DLOG10(RAN)
    EV=0.58*ARAN-0.947
    ENER=10.**EV
    PPIZS=ENER*(ENER+2.*139.579)
    PPIZ=DSQRT(PPIZS)
    ERR=(1./63.)*(1./63.)
    ERRO=0.58*(ENER+139.579)/PPIZS
    ERPI=ERRO*ERRO*ERR
20  ERT=A1*A1*ERDELP+A2*A2*ERDEPI+A3*A3*ERAL
    ERT=ERT*TETAZ*TETAZ
    PPI(1)=PPIZ
    DO 8 I=1,10
    EP(I)=DSQRT((PP(I))*(PP(I))+938.256*938.256)
    EPI(I)=DSQRT((PPI(I))*(PPI(I))+139.579*139.579)
    CT(I)=DCOS(TETA(I))
    ST(I)=DSIN(TETA(I))
    B(I)=(PPI(I))*(CT(I))-(PP(I))*(EPI(I))/EP(I)
    C(I)=(PP(I))*(CT(I))-(PPI(I))*EP(I)/EPI(I)
    D(I)=(PP(I))*(PPI(I))
20  DELPPI(I)=PPIZ-PPI(I)
    DELPP(I)=PPZ-PP(I)
    DELT(I)=TETAZ-TETA(I)
22  E(I)=(EP(I))*(EPI(I))
    A(I)=AS+(D(I))*(CT(I))-E(I)+(B(I))*(DELPP(I))
    AA(I)=(C(I))*(DELPPI(I))-(D(I))*(ST(I))*(DELT(I))
    AB(I)=(B(I))*(B(I))*ERP+(C(I))*(C(I))*ERPI
    AC(I)=(D(I))*(D(I))*(ST(I))*(ST(I))*ERT
    ALPHA(I+1)=(A(I)+AA(I))/(AB(I)+AC(I))
    PP(I+1)=PPZ-ERP*(ALPHA(I+1))*(B(I))
    PPI(I+1)=PPIZ-ERPI*(ALPHA(I+1))*(C(I))
    TETA(I+1)=TETAZ+ERT*(D(I))*(ST(I))*(ALPHA(I+1))
    TET(I+1)=(TETA(I+1))*180./3.1416
    SA(I+1)=(PP(I+1)-PPZ)*(PP(I+1)-PPZ)/ERP
    SB(I+1)=(PPI(I+1)-PPIZ)*(PPI(I+1)-PPIZ)/ERPI
    SC(I+1)=(TETA(I+1)-TETAZ)*(TETA(I+1)-TETAZ)/ERT
    SD(I+1)=2.*(ALPHA(I+1))*(AS+(D(I))*(CT(I))-E(I))
 8  SKI(I+1)=SA(I+1)+SB(I+1)+SC(I+1)
    PPIP=COPI*PPI(11)
    PPP=(PP(11))*COP
    DETPLP=PPIP*PPIP+PPP*PPP+2*PPIP*PPP*CALP
    PLP=DSQRT(DETPLP)
    PAPI2=3.1416*PAPI/180.
    PAP2=3.1416*PAP/180.
    CPAPI=DCOS(PAPI2)
;E  3
```

```
      SPAPI=DSIN(PAPI2)
      SPAP=DSIN(PAP2)
      CPAP=DCOS(PAP2)
      PX=PPP*CPAP+PPIP*CPAPI
      PY=PPP*SPAP+PPIP*SPAPI
      J=Y
      YI=J
      PIT=(YI-90.)*3.1416/180.
      CTEL=PX/PLP
      IF(CTEL-1.) 181,182,182
181   TELI=DARCOS(CTEL)
      GO TO 183
182   TELI=0.
183   IF(PY) 180,185,185
180   TEL=PIT-TELI
      GO TO 190
185   TEL=PIT+TELI
190   DETPL=(PPI(11))*(PPI(11))+(PP(11))*(PP(11))
      DETPL=DETPL+2.*(PPI(11))*(PP(11))*(CT(10))
      PL=DSQRT(DETPL)
      SDELL=((PP(11))*SIP+(PPI(11))*SIPI)/PL
      TW=20.*3.1416/180.
      CTW=DCOS(TW)
      STW=DSIN(TW)
      DELL=DARSIN(SDELL)
      CDELL=DCOS(DELL)
      CTEL=DCOS(TEL)
      STEL=DSIN(TEL)
      ULX=CDELL*CTEL*CTW-SDELL*STW
      ULY=CDELL*STEL
      ULZ=SDELL*CTW+CDELL*CTEL*STW
      ZZ=(P-5.5+Z)*1.26
      XZA=110.+2.*(X-55.)
      XZ=XZA*CTW-ZZ*STW
      YZ=(Y-90.)*(3.1416/180.)*XZA
      ZZ=ZZ*CTW+XZA*STW
      BCD=ULZ*ZZ+ULY*YZ
      BC=ULY*ULY+ULZ*ULZ
      XF=XZ-ULX*BCD/BC
      YF=YZ-ULY*BCD/BC
      ZF=ZZ-ULZ*BCD/BC
      TEL=TEL*180./3.1416
      DELL=DELL*180./3.1416
      IF(PIT) 200,205,205
200   PIT=-PIT
      CPIT=DCOS(PIT)
      SPIT=-DSIN(PIT)
      GO TO 210
205   CPIT=DCOS(PIT)
      SPIT=DSIN(PIT)
210   COP2=CPIT*CPAP-SPIT*SPAP
      SIP2=CPIT*SPAP+SPIT*CPAP
      PX=(COP2*COP*CTW-SIP*STW)*(PP(11))
      PY=COP*SIP2*(PP(11))
      PZ=(SIP*CTW+COP2*COP*STW)*(PP(11))
      PXP=ULX*PX+ULY*PY+ULZ*PZ
E     4
```

```
      PPD=ULZ*ULZ+ULY*ULY
      PPD=DSQRT(PPD)
      PYP=(PY*ULZ-PZ*ULY)/PPD
      PZP=-PX*PPD+(PY*ULX*ULY+PZ*ULX*ULZ)/PPD
      EPS=(PP(11))*(PP(11))+938.256*938.256
      EP2=DSQRT(EPS)
      ELS=PL*PL+1115.58*1115.58
      EL=DSQRT(ELS)
      BEL=PL/EL
      GALDS=1.-BEL*BEL
      GALD=DSQRT(GALDS)
      GAL=1./GALD
      PXP=GAL*(PXP-BEL*EP2)
      CPP=PXP*PXP+PYP*PYP+PZP*PZP
      CPP=DSQRT(CPP)
      SSI=PZP/CPP
      SSI=DABS(SSI)
      TT=PXP/PYP
      IF(TT) 230,235,235
230   IF(PYP) 240,245,245
240   TCM=3.1416-DATAN(-TT)
      GO TO 250
245   TCM=2.*3.1416-DATAN(-TT)
      GO TO 250
235   IF(PYP) 255,260,260
255   TCM=3.1416+DATAN(TT)
      GO TO 250
260   TCM=DATAN(TT)
250   TCM=TCM*180./3.1416
      EI=1050.*1050.+139.579*139.579
      EI=DSQRT(EI)
      DE2=EI+938.256-EL
      DE2=DE2*DE2
      P4=1050.-PL*ULX
      P5=P4*P4+PL*PL*(ULY*ULY+ULZ*ULZ)
      DEL=DE2-P5-497.87*497.87
504   IF(SKI(11)-25.) 501,142,142
501   YF=DABS(YF)
      ZF=DABS(ZF)
      XF=DABS(XF)
      IF(XF-24.) 506,142,142
506   IF(YF-8.) 502,142,142
502   IF(ZF-1.) 503,142,142
503   IF(PL-450.) 142,505,505
505   IF(800.-PL) 142,561,561
561   IF(SSI-0.91) 562,562,142
562   D7=0.1*BCD/BC
      P7=20.*4.80298*D7/(BEL*938.256*1.6021)
      WRITE(2,7) S,X,Y,Z,P7,TCM,EN
    7 FORMAT(F5.0,2F5.1,F6.3,F8.4,F10.4,F5.0)
142   IF(PIG-400.) 141,12,12
      END
ID OF DATA
E  5
```

PROG.7

/ 360N-FO-479 3-0 MAINPGM DATE 07/06/71 TIME 09.

```
      READ(1,1) N
    1 FORMAT(I4)
      DIMENSION S(1360),P7(1360),TCM(1360),FLE(1360),FLO(1360),A(45),
     1FL(1360),C(55),C2(55)
      DO 5 I=1,N
      READ(1,3) S(I),P7(I),TCM(I)
    3 FORMAT(F5.0,16X,F8.4,F10.4)
    5 TCM(I)=TCM(I)*3.1416/180.
      A(1)=0.40
      C(1)=0.40
      DO 20 J=1,40
      WRITE(3,6) A(J)
    6 FORMAT(8H     AP=,F5.2,20H      MU          LLF   )
      DO 19 K=1,50
      FFLLE=0.
      FFLLO=0.
      DO 18 I=1,N
   22 C2(K)=C(K)*P7(I)
      L=S(I)/2.
      P=S(I)/2.
      E=L
      IF(P-E) 11,11,12
   11 FL(I)=1.+A(J)*COS(TCM(I)+C2(K))
      FLE(I)=FL(I)/(2.*3.1416)
      FFLLE=FFLLE+ALOG(FLE(I))
      GO TO 18
   12 FL(I)=1.+A(J)*COS(TCM(I)-C2(K))
   21 FLO(I)=FL(I)/(2.*3.1416)
      FFLLO=FFLLO+ALOG(FLO(I))
   18 CONTINUE
      FFLL=FFLLE+FFLLO
      WRITE(3,15) C(K),FFLLO,FFLLE,FFLL
   15 FORMAT(10X,F6.2,5X,F12.4,5X,F12.4,5X,F12.4)
   19 C(K+1)=C(K)+.01
   20 A(J+1)=A(J)+.01
      STOP
      END
```

PROG. 8

```
IBM FORTRAN IV G1 RELEASE 2.0   MAINPGM   DATE 30/03/72   TIME 09.43.
      DIMENSION ALPHA(182),TETA(181),PLLAB(181),ELLAB(181),BETAL(18
     1 1),GAMA(181)
      AKM=497.76
      ALM=1115.6
      PM=938.259
      PIP=1050.
      PIM=139.579
      PIE=PIP*PIP+PIM*PIM
      PIE=SQRT(PIE)
      BETA=PIP/(PIE+PM)
      BETAS=BETA*BETA
      BETAS=1.-BETAS
      BETAS=SQRT(BETAS)
      GAMMA=1./BETAS
      CMSE=GAMMA*(PIE+PM-BETA*PIP)
      CMSES=CMSE*CMSE
      AKMS=AKM*AKM
      ALMS=ALM*ALM
      ELCMS=(CMSES+ALMS-AKMS)/(2.*CMSE)
      PLCMS=SQRT(ELCMS*ELCMS-ALMS)
      WRITE(3,1) BETA,GAMMA,CMSE
    1 FORMAT(1X,5HBETA=,F5.3,3X,6HGAMMA=,F6.3,3X,11HCMS ENERGY=,F8.3)
      WRITE(3,2) ELCMS,PLCMS
    2 FORMAT (/1X,15HLAMBDA CMS EN.=,F8.3,3X,16HLAMBDA CMS MOM.=,F7.3)
      ALPHA(1)=0.
      DO 3 I=1,181
      CA=COS(ALPHA(I))
      SA=SIN(ALPHA(I))
      PLCMSY=PLCMS*SA
      PLCMSX=GAMMA*(PLCMS*CA+BETA*ELCMS)
      TANT=PLCMSY/PLCMSX
      TETA(I)=ATAN(TANT)
      CT=COS(TETA(I))
      PLLAB(I)=PLCMSX/CT
      PLLABS=PLLAB(I)*PLLAB(I)
      ELLAB(I)=SQRT(ALMS+PLLABS)
      BETAL(I)=PLLAB(I)/ELLAB(I)
      BETS=BETAL(I)*BETAL(I)
      BETS=SQRT(1.-BETS)
      GAMA(I)=1./BETS
    3 ALPHA(I+1)=ALPHA(I)+3.1416/180.
      WRITE(3,4)
    4 FORMAT(/62H  ALPHA      TETA  LAMBDA MOMENTUM  LAMBDA ENERGY  BETA
     1  GAMMA)
      DO 5 I=1,181
      TETA(I)=TETA(I)*180./3.1416
      ALPHA(I)=ALPHA(I)*180./3.1416
      WRITE(3,6) ALPHA(I),TETA(I),PLLAB(I),ELLAB(I),BETAL(I),GAMA(I)
    6 FORMAT(2X,F7.3,5X,F7.3,2X,F8.3,2X,F8.3,2X,F5.3,3X,F6.3)
      WRITE(2,6) ALPHA(I),TETA(I),PLLAB(I),ELLAB(I),BETAL(I),GAMA(I)
    5 CONTINUE
      END
```

```
      DIMENSION ALPHA(182),TETAP(181),PPLAB(181),TETAPI(181),PPILAB(181)
      ALM=1115.6
      PM=938.259
      PIM=139.579
      ALMS=ALM*ALM
      PMS=PM*PM
      PIMS=PIM*PIM
      EPCM=(ALMS+PMS-PIMS)/(2.*ALM)
      EPICM=ALM-EPCM
      EPCMS=EPCM*EPCM
      EPICMS=EPICM*EPICM
      PPCMS=EPCMS-PMS
      PPCM=SQRT(PPCMS)
      PPICMS=EPICMS-PIMS
      PPICM=SQRT(PPICMS)
      WRITE(3,2) EPCM,EPICM,PPCM,PPICM
    2 FORMAT(1X,18HPROTON CMS ENERGY=,F6.2,2X,16HPION CMS ENERGY=,F6.2,2
     1X,15HPROTON CMS MOM=,F6.2,2X,13HPION CMS MOM=,F6.2)
      WRITE(3,5)
    5 FORMAT(/69H    ALPHA        PR. ANG.        PR. MOM.        PI. ANG.
     1       PI. MOM )
    8 READ(1,1) GAMMA,BETA
    1 FORMAT(1X,F5.3,1X,F5.3)
      ALPHA(1)=0.
      DO 4 I=1,181
      CA=COS(ALPHA(I))
      SA=SIN(ALPHA(I))
      PPCMY=PPCM*SA
      PPCMX=GAMMA*(PPCM*CA+BETA*EPCM)
      TANTP=PPCMY/PPCMX
      TETAP(I)=ATAN(TANTP)
      CTP=COS(TETAP(I))
      PPLAB(I)=PPCMX/CTP
      PPICMY=PPICM*SA
      PPICMX=GAMMA*(PPICM*CA+BETA*EPICM)
      TANTPI=PPICMY/PPICMX
      IF (PPICMY) 3,3,20
   20 IF (PPICMX) 6,6,9
    9 TETAPI(I)=ATAN(TANTPI)
      GO TO 10
    6 TANTPI=-TANTPI
      TETAPI(I)=3.1416-ATAN(TANTPI)
      GO TO 10
    3 IF(PPICMX) 11,11,12
   11 TETAPI(I)=3.1416+ATAN(TANTPI)
      GO TO 10
   12 TANTPI=-TANTPI
      TETAPI(I)=2.*3.1416-ATAN(TANTPI)
   10 CTPI=COS(TETAPI(I))
      PPILAB(I)=PPICMX/CTPI
      TETAP(I)=TETAP(I)*180./3.1416
      TETAPI(I)=TETAPI(I)*180./3.1416
      ALPHA(I)=ALPHA(I)*180./3.1416
      WRITE(3,7) ALPHA(I),TETAP(I),PPLAB(I),TETAPI(I),PPILAB(I)
```

```
  7 FORMAT(4X,F5.1,7X,F7.3,8X,F8.3,7X,F7.3,7X,F8.3)
  4 ALPHA(I+1)=(ALPHA(I)+1.)*3.1416/180.
    GO TO 8
    END
```